ISBN 978-82-471-1828-3 (printed ver.)
ISBN 978-82-471-1829-0 (electronic ver.)
ISSN 1503-8181

Doctoral theses at NTNU, 2009:213

Jianying He

NANOMECHANICS OF POLYMER AND COMPOSITE PARTICLES

Jianying He
Doctoral Thesis

NTNU
Norwegian University of
Science and Technology
Thesis for the degree of
philosophiae doctor
Faculty of Engineering Sciences and Technology
Department of Structural Engineering
NTNU Nanomechanical Lab

Doctoral theses at NTNU, 2009:213

NTNU

NTNU
Norwegian University of
Science and Technology

NTNU
Norwegian University of
Science and Technology

Jianying He

NANOMECHANICS OF POLYMER AND COMPOSITE PARTICLES

Thesis for the degree of philosophiae doctor

Trondheim, November 2009

Norwegian University of
Science and Technology
Faculty of Engineering Sciences and Technology
Department of Structural Engineering
NTNU Nanomechanical Lab

NTNU
Norwegian University of
Science and Technology

NTNU
Norwegian University of Science and Technology

Thesis for the degree of philosophiae doctor

Faculty of Engineering Sciences and Technology
Department of Structural Engineering

©Jianying He

ISBN 978-82-471-1828-3 (printed ver.)
ISBN 978-82-471-1829-0 (electronic ver.)
ISSN 1503-8181

Doctoral Theses at NTNU, 2009:213

Printed by Tapir Uttrykk

NANOMECHANICS OF POLYMER AND COMPOSITE PARTICLES

Jianying He

Norwegian University of Science and Technology

Faculty of Engineering Sciences and Technology

Department of Structural Engineering

NTNU Nanomechanical Lab

Trondheim, Norway

PREFACE

This doctoral thesis is submitted to the Norwegian University of Science and Technology (NTNU) for the degree of Philosophiae Doctor.

The thesis comprises an introductory section and five published journal papers.

The PhD work was carried out at NTNU Nanomechanical Lab, Department of Structural Engineering, NTNU, and was initiated in April 2006, under supervision of Prof. Zhiliang Zhang (Department of Structural Engineering, NTNU, Trondheim, Norway) and Dr. Helge Kristiansen (Conpart AS, Skjetten, Norway). The research was performed within the NANOMAT KMB project "Nanostructured Polymer and Composite Particles: Mechanical Properties (NanoPCP)", financially supported by the Research Council of Norway, industry partners Conpart AS and Invitrogen Dynal AS.

ABSTRACT

This thesis concerns the nanomechanics of micron-sized polymer and composite particles used in electronic packaging technology. The aim of this PhD study is to develop a scientific methodology for characterizing the mechanical properties of single micron-sized particles produced by the well-known Ugelstad method. This includes pure polymer particles as well as metal coated polymer particles.

Such particles have recently been exploited for new applications in microelectronics and microsystems. The mechanical properties of the particles are of crucial importance for these applications. However, due to the inherent complexity of the spherical geometry, mechanical characterization of single particles possesses great challenges. Because of large surface to volume ratio and in most cases lack of surfactants, the polymer particles tested in this work usually occur in a state of clusters. Accordingly, a particle dispersion procedure has been first developed to obtain individual particles suitable for testing. Thereafter a nanoindentation-based flat punch method for measuring the mechanical properties of single particles has been established. A diamond flat punch is specially designed for characterizing single particles, instead of the common sharp tip used for nanohardness measurements.

Both polymer and metal-coated composite particles with various chemical compositions, crosslink densities, sizes and loading conditions have been studied using the nanoindentation-based flat punch methodology. All the polymers have been of an amorphous type. The contact load-displacement relationship of single micron-sized particles has been recorded and the stress-strain behavior has been determined. It has been shown that the slightly crosslinked polystyrene particles display a yielding behavior, and smaller surface cracks have been observed after deformation. However, the strongly crosslinked acrylic and polystyrene particles show a brittle fracture behavior. A striking particle size effect on the mechanical properties has been discovered for the first time. The results show that for the slightly crosslinked polystyrene particles the smaller the particle diameter is, the harder the particle behaves. The corresponding mechanisms of the particle size effect have been analyzed and are mainly contributed by a possible “core-shell” microstructure of this type of polymer particles. The effect of loading rate on the stress-strain behavior and the failure mechanism for both polymer particles and metal coated polymer particles has been investigated. The results indicate that the mechanical behavior of both particles is strongly dependent on the loading rate. The influence of the nanoscale metal coating has been revealed through comparing the mechanical properties of metal

coated polymer particles with that of identical size, but uncoated ones. It has been found that within a range of relatively small deformations the metal coating plays a significant strengthening effect on the mechanical properties of the particles.

The original findings in this PhD work have been presented in 6 international journal articles and 3 international conference papers. 5 published journal articles are attached in this thesis.

ACKNOWLEDGEMENTS

When doing a PhD, there are many people involved in different ways. I would like to extend my acknowledgements for their contributions.

First I want to express my sincerest thanks to my main supervisor, Prof. Zhiliang Zhang, for his enduring guidance throughout this research, his constructive feedback on papers and thesis, and our fruitful discussions. His encouraging nature, his continuous enthusiasm, and his outstanding knowledge are truly a great inspiration to me. I would also extend my deepest gratitude to my co-supervisor, Dr. Helge Kristiansen, for his constant support and everlasting assistance on the experimental work, analyses and proofreading. His remarkable patience, his academic skills and his numerous suggestions are greatly appreciated. This thesis would not have been possible without their professional inputs, as well as the strength of a team work.

Dr. Keith Redford at Conpart AS, Dr. Geir Fonnum and Dr. Grete Modahl at Invitrogen Dynal AS have been very important for the work presented in this thesis. They have been always helpful whenever I need discussion and analyses. Their positive cooperation has been an immense help and prominent stimulation for me.

I appreciate the assistance provided by Dr. Yingda Yu and Dr. Tor Nilsen at the EM Lab, Department of Materials Science and Engineering, NTNU with the operation of Scanning Electron Microscope.

I have been fortunate to be surrounded by supportive and inspirational colleagues at NTNU Nanomechanical Lab and Department of Structural Engineering, NTNU. I am also grateful to all of my colleagues for the pleasant atmosphere at work, especially to Hallvard Tyldum, Dr. Junhua Zhao and Dr. Shijo Nagao for their useful discussion about the polymer particle research.

Special thanks are also directed to three master students Mari Midttun, Tore Helland and Jon Arne Habostad for their company and cooperation, who were under my co-supervision during their project study and master thesis work.

The Research Council of Norway, Conpart AS and Invitrogen Dynal AS are highly appreciated for the financial support.

At last but not least, I would like to thank my family and my friends for their support, encouragement and faith in me during all these years.

TABLE OF CONTENTS

ABBREVIATIONS

AC	—	Acrylic Crosslinked with Diacrylic
ACA	—	Anisotropic Conductive Adhesive
BGA	—	Ball Grid Array
CV	—	The Coefficient of Variance
FEM	—	Finite Element Method
Au	—	Gold
IC	—	Integrated Circuit
μm	—	Micrometer
μN	—	MicroNewton
nm	—	Nanometer
Ni	—	Nickel
PS-DVB	—	Polystyrene Crosslinked with Divinylbenzene
SEM	—	Scanning Electron Microscope

Chapter 1

INTRODUCTION

In this introductory chapter, the background and the objective for this PhD study are described, followed by a short summary of the achievements made in this work and a discussion of the thesis structure.

1.1 Background

This study represents the main part of the NANOMAT KMB project [1] titled "Nanostructured Polymer and Composite Particles: Mechanical Properties (NanoPCP)". The project has been supported by the Research Council of Norway [2], Conpart AS [3] and Invitrogen Dynal AS [4]. The duration of the project has been from April 2006 to November 2009.

There has been developed a unique competence to produce highly monodisperse, micron-sized polymer particles in Norway, based on the so-called Ugelstad technology [5]-[7] invented by the late Professor John Ugelstad [8] at the Norwegian Institute of Technology (now NTNU). The technology has been successfully used for industrial applications for around 30 years. So far these particles have been widely used in pharmaceutical, chemical and biological industries [9]-[13]. Recently there is a renewed interest in exploiting this polymer particle technology toward applications in the manufacturing of microelectronics and microsystems.

One example of the use of micron-sized polymer particles has been in the development and manufacturing of Liquid Crystal Display (LCD). Here one of the major concerns has been to obtain a reliable electrical contact between the electronics and the display. To cope with this challenge, Anisotropic Conductive Adhesive (ACA) was introduced in the late 70s by Sony [14]. A few years later, Hitachi Chemical [15] for the first time replaced the solid Ni-particles with Ni and Au plated polymer beads, which significantly improved the reliability of the contacts [16][17]. The composite particle usually consists of a polymer core with a typically diameter of 3 to 30 micrometer, depending on the type of display. The

compliant polymer core dramatically improves the contact stability during thermal cycling and ingress of moisture. A 30-50nm thick Ni layer is first applied to the polymer core to obtain electrical conductivity and improve the adhesion to the polymer core. Thereafter a 15-30nm Au outer layer is added to protect the inner layer from oxidation and hence improve contact reliability and electrical conduction [18][19]. The ACA technology is also very interesting as a replacement technology for solder as it can contribute to reduced package size, lower assembly temperature, environmentally friendly manufacturing and reliable performance.

In the ACA application, some unique properties are required of the conductive particles to obtain a reliable interconnection. This includes uniform particle size, homogeneous microstructure and fit mechanical property. Using the Ugelstad two-step seeded polymerization method, polymer particles with the extremely narrow size distribution and a wide variety of chemical composition can be synthesized. The possibility to tailor-make mechanical properties as well as the narrow size distribution has been the main motivation to extending the Ugelstad technology into ACA applications through metallizing the polymer particles.

A schematic plot of an ACA assembly is shown in Figure 1.1. The conductive particles are dispersed in an adhesive matrix which is placed to form the electrical interconnections between an integrated circuit (IC) and a glass panel or a flex-circuit. These connections are made to be anisotropic such that the current can only travel through the thickness of the adhesive but do not short-circuit between adjacent joints. The bonding of the ACA assembly is a thermal-mechanical process, in which the conductive particles are highly deformed to create a sufficient contact area for achieving a low resistance connection. Therefore, the mechanical behavior of individual particles under such large deformation is a key issue in the ACA application. In order to understand the mechanics of micron-sized polymer and composite particles, such as deformation behaviors and fracture properties, the demand for mechanical characterization of single particles is raised [17].

In a previous study [23] it has been found that the fracture of the micron-sized conductive particles under compression takes place with different fracture patterns, as shown in Figure 1.2. The appearance of particle failure is expected to bring a crucial impact on the electrical properties, in particular the reliability of the ACA assembly. A significant amount of work has been dedicated to understand the phenomena of electrical contact resistance within the particles due to the concern of the electronics industry [20]. However, the mechanical properties of the particles have not been subjected to a thorough scientific investigation. A reliable and quantitative testing method for determining the mechanical properties of nanostructured polymer and composite particles has clearly been missing. This thesis represents as such a significant contribution to the scientific understanding of the mechanics of the micron-sized polymer and composite particle.

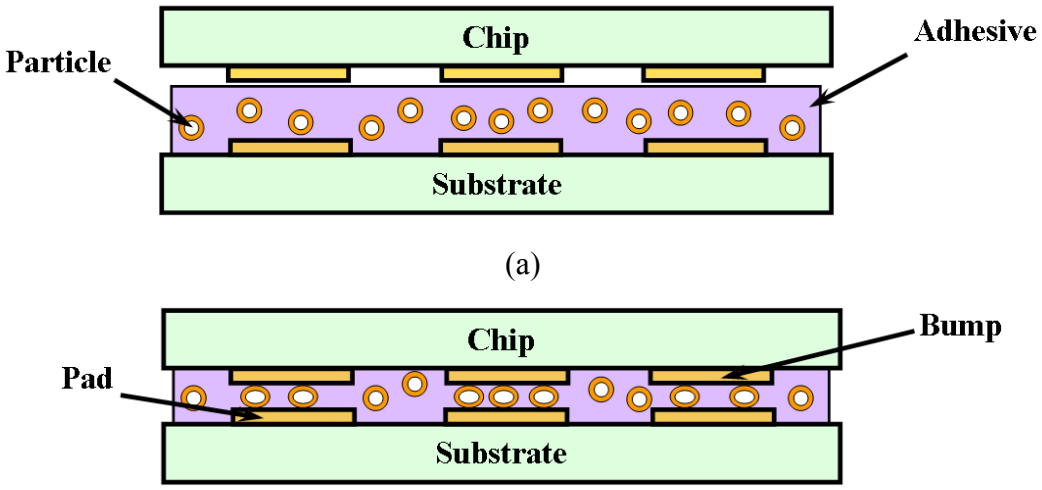

Figure 1.1 A typical ACA assembly [21][22].

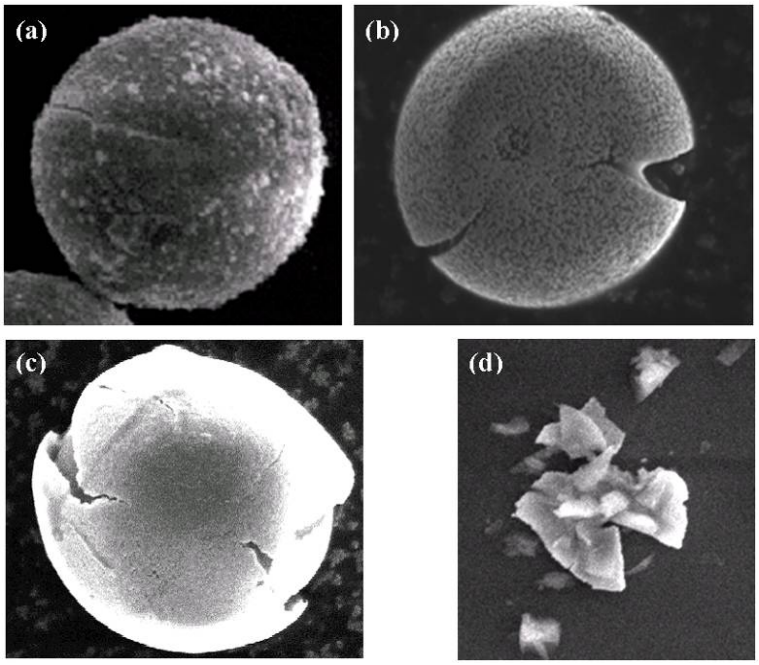

Figure 1.2 Different fracture patterns of conductive particles: (a) minor cracking of metal coating; (b) rift behavior; (c) cracking and delamination of metal coating; and (d) completely crushed particle [23].

This thesis will focus on the mechanical characterization of both polymer and metallized polymer particles. From an experimental point of view it is very important that the particles produced by the Ugelstad technology shows very uniform properties from particle to particle. This fact is critical to be able to verify that the procedure developed for mechanical characterization is reliable and consistent. To simulate the particle behavior in

the ACA assembly, a novel technique, based on Nanoindentation using a flat punch has been developed to investigate individual particles. The thesis represents a systematic study on the mechanical properties of single micron-sized particles. The results of this work have been very important in the design and industrialization of the particle technology for electronic packaging applications.

1.2 Objectives

This thesis is dedicated to develop fundamental understanding and knowledge of mechanical properties of nanostructured polymer and composite particles aimed for electronic packaging technology. The focus has been on quantitative analysis, characterization and control of mechanical properties. Three interrelated objectives have been included in this work, schematically shown in Figure 1.3. These are development of methodology for mechanical characterization, determination of constitutive properties and the relationship between mechanical properties and particle "design", including particle size, chemical composition, crosslink density, and so on.

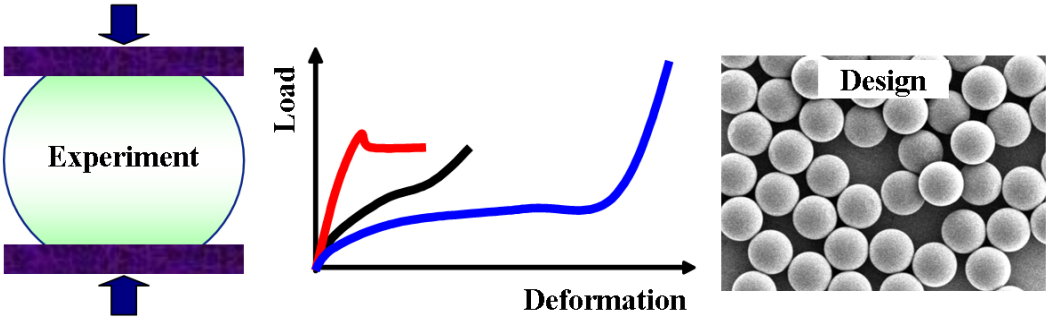

Figure 1.3 The three interrelated objectives in this work.

- Develop a nanoindentation based methodology for characterizing mechanical properties of individual particles.

  The particles used in ACA assembly are typically sized from around 3μm to 30μm in diameter. Due to small volume, spherical geometry, composite structure and large deformation involved in ACA application, the mechanical characterization of single particles is full of complexities and challenges. Previous studies on the ACA particles have typically focused on the aggregate properties of the monolayer of multiple particles, normally several hundred particles compressed between two flat surfaces [22][23]. It is very important to develop a suitable technique for measuring single particles.

Nanoindentation with highly sensitive transducers for force and displacement measurements is the state-of-the-art nanomechanical testing method for determining mechanical properties of small volume materials. This technique has widely been applied to thin films, nanobelts, carbon nanotubes and so on. The fine resolution of nanoindentation is perfectly fit for the study of mechanical properties of the relevant particles. However, the current nanoindentation method is based on the contact theory of a rigid sharp tip against a deformable and initially flat surface of material. Obviously the traditional nanoindentation directly on free standing polymer particles is not relevant. Thus the first objective of this study was to modify the conventional nanoindentation technique and develop a new method to characterize single particles.

- Determine the constitutive properties of single particles and systematically study the sensitivity of mechanical properties to different factors such as chemical composition and crosslinking.

  For industrial applications in the microelectronics industry it is a very important competence to be able to characterize mechanical properties of single particles and determine the constitutive properties of the commercial particles delivered by our industrial partners. The existing contact models used to describe the deformation of macroscopic spheres as a function of applied load are usually limited to small deformations and ignore time dependent behaviors [24]-[26]. They are therefore inapplicable to describe particle behavior with large deformation. It is therefore a strong need to understand large deformation behaviors of the present particles and extend the knowledge to the particle design and manufacturing.

- Establish a link between the mechanical properties and processing parameters of selected particles, and extend knowledge to design particles with unique properties.

  Once the experimental method is established, the work will change focus towards the relations between the mechanical properties and manufacturing parameters of the particles. Together with the Ugelstad technology, the results will be further utilized to design particles with unique properties for different applications. The variation of the chemical composition, the type of monomers, the type of crosslinking, the crosslink density and the glass transition temperature will be considered to optimize the mechanical properties of particles. This task has been carried out in collaboration with the industrial partner Conpart AS.

1.3 Original Techniques and Findings

This work represents a first quantitative and systematic study on the nanomechanics of single micron-sized polymer particles and metal coated polymer particles. A methodology has been established for mechanical characterization of single particles. The mechanical properties of particles have been investigated, including the effect of various factors on the

large deformation behavior, the fracture process as well as other failure mechanisms observed in the particles.

A novel experimental design to characterize the mechanical properties of the single micron-sized particles has been developed in this work. Procedures including the dispersion of particles and the nanoindentation-based flat punch test have been established. Due to a small volume and the lack of surfactants, particles possess large surface energy so that dry particles usually occur in a state of clusters. How to disperse these clusters and obtain single particles is an important precondition for the mechanical measurement. The selection of the dispersing medium and the sample substrate is crucial for obtaining single particles, keeping the particles fixed on the substrate, and minimizing their influences on particle properties. Through trying with different organic solvent and sample substrate, finally a dispersion process with the use of 96% industrial ethanol and a silicon chip as a substrate has been demonstrated and qualified.

Based on the conventional nanoindentation technique, the flat punch test has been specially designed for compressing single particles. A diamond flat punch has been manufactured to deform single particles, instead of the commonly used sharp tip. The tip-particle contact can be considered as an inverse indentation with a rigid plate against a soft sphere. A polished indium sample has been used to calibrate the relative position between the optics and the indenter, and also chosen as the standard for the co-planarity calibration of the flat punch to the silicon substrate. The load-displacement relationship under compression of single particles under large deformation has been established. The method has been applied to measure the mechanical response of single particles with different experimental conditions, and with a very high reproducibility. The influence of different factors during particles synthesis and mechanical testing on the mechanical behavior has been determined using the nanoindentation-based flat punch method.

A previously unreported particle size effect on the stress-strain behavior has been found and the corresponding mechanisms have been analyzed. In a series of particles with identical chemistry but different size in micron scale, this size effect is manifested that the smaller the diameter is, the harder the particle behaves. An inhomogeneity of chemistry induced core-shell microstructure has been presumed to be the dominate mechanism for the particle size effect. The finding has important implications for the scientific research on micron- and nano- mechanical testing of materials.

The fracture process and failure mechanisms of metal coated polymer particles have been published for the first time. The cracking and delamination of the metal coating from the polymer core have been documented in detail. A three-stage deformation process has been identified. The results provide understanding of deformation and fracture of metal coated polymer particles, which offers theoretical support to designing conductive particles and manufacturing ACA assemblies.

So far, this work has been published in five international journal articles [27]-[31] and three international conference papers [32]-[34]. Besides, one journal article has been submitted [35] and some papers are under preparation.

1.4 Organization of the Thesis

The thesis contains an introductory section and five separate papers. The introductory section is organized in 6 chapters. The introduction to this study is presented in Chapter 1 and outlines the background and objectives. The original findings in this PhD work are also given in this chapter.

A literature review on development of micron-sized polymer particles is presented in Chapter 2. The conventional nanoindentation technology is briefly introduced here. The Ugelstad technology and applications are elaborated to illustrate the synthesis of polymer particles. The history of mechanical characterization of particles is also reviewed here. The main challenges of this study are finally pointed out in the last section.

Chapter 3 introduces general knowledge of the particles used in this study. The preparation of the particle sample is explained in detail.

The details of the experimental method, including the used flat punch, the co-planarity calibration and the measurement procedures, are described in Chapter 4.

In Chapter 5 a summary of the five published journal papers produced in this PhD study are presented and the scientific papers are attached. In addition, the results presented at international conferences are listed.

Finally concluding remarks are presented and suggestions for further work are discussed in Chapter 6.

Chapter 2

LITERATURE SURVEY

The goal of this chapter is to present the background for the work performed in this thesis. This includes an introduction of the conventional nanoindentation method together with an overview of the particle technology including synthesis and application, and the review of the previous research about ACA including electrical performance of ACA assembly and mechanical characterization of the polymer particles. In the last part the main challenges involved in this work are offered.

2.1 Nanoindentation

During the last two decades, the development of nanoindentation techniques have been motivated by the progress made in nanocomposite and thin film materials and their application in the miniaturization of engineering and electronic components. The scope of mechanical testing was extended down to the nano range by newly available methods for measuring mechanical properties in a small volume. This has been achieved mainly through the development of instruments capable of continuously measuring load and displacement with a very high resolution, so-called nanoidentation [36]. Today, nanoindentation has become a well-known method used for probing the mechanical properties at the micro- and nano- scale [37][38]. During nanoindentation test, the contact load and displacement are simultaneously monitored and the obtained load-displacement relationship during this test contains a wealth of information. From the load-displacement data, the mechanical properties, such as, nanohardness and reduced elastic modulus can be directly determined according to the renowned Oliver and Pharr's theory [39][40]. Due to the extremely high sensitivity of the load and displacement transducers used for these measurements, the technique satisfies a wide range of applications. Besides the two most commonly measured properties, hardness and elastic modulus [41][42], nanoindentation can also provide information on cracking, creep, strain-hardening, phase-transformation, fracture toughness and energy absorption, etc. [43]-[47]. Since the measurement scale is very small, nanoindentation is also applicable to thin films or coating systems [48]-[52].

2.1.1 Nanoindentation Theory

Nowadays a well-established nanoindentation theory is used and based on Oliver and Pharr's analyses [39]. The two main mechanical properties measured by nanoindentation are the hardness H and elastic modulus E. During the nanoindentation, the contact load-displacement curve is recorded, and both elastic and plastic deformation will normally occur. However, at the initial stage when the indenter starts to withdraw, only the elastic portion of the displacement is recovered. Therefore an elastic solution in modelling the contact process can be obtained at this point, which can be used to calculate the elastic modulus.

Figure 2.1 (a) plots the configuration during and after nanoindentation. The indenter first penetrates into material surface until the pre-defined peak load; then withdraws from the specimen and leaves a residual indent on the material. A typical contact load-displacement curve obtained during nanoindentation is shown in Figure 2.1 (b). Here $h_{\max}$ represents the penetration depth at the peak load $P_{\max}$, h_c is defined as the contact depth and calculated by the recovery displacement after indentation, and h_f is the final displacement after unloading. According to the normal definition, the hardness H is expressed as the contact load $P_{\max}$ divided by the projected contact area A and represents the mean pressure that a material can support under a certain load

$$H = \frac{P_{\max}}{A} \tag{2.1}$$

The projected contact area A is expressed as a function of the contact depth h_c and can be obtained by a tip-shape calibration on a standard fused quartz sample (see section 2.1.2).

Through taking the assumption that Young's modulus of elasticity is constant and independent of indentation depth, the initial unloading contact stiffness $S = dP/Dh$ which is the slope of the initial portion of the unloading curve, is employed to calculate the elastic modulus. Based on the relationship for the indentation of an elastic half space by a punch, which can be described as a solid of revolution of a smooth function, a geometry-independent relation involving the contact stiffness S, contact area A and reduced elastic modulus E_r can be derived as

$$S = \frac{dP}{dh} = \frac{2}{\sqrt{\pi}} E_r \sqrt{A} \tag{2.2}$$

Rearranging eq. (2.2):

$$A = \frac{\pi}{4}\left(\frac{S}{E_r}\right)^2 \tag{2.3}$$

$$\frac{1}{E_r} = \frac{1-\nu_S^2}{E_S} + \frac{1-\nu_T^2}{E_T} \tag{2.4}$$

where E and ν are the elastic modulus and Poisson's ratio for the sample (subscript S) and the tip (subscript T), respectively. For a diamond tip, $E_T = 1140GPa$ and $\nu_T = 0.07$. The reduced elastic modulus E_r accounts for the fact that the measured displacement includes contribution from both the specimen and the indenter.

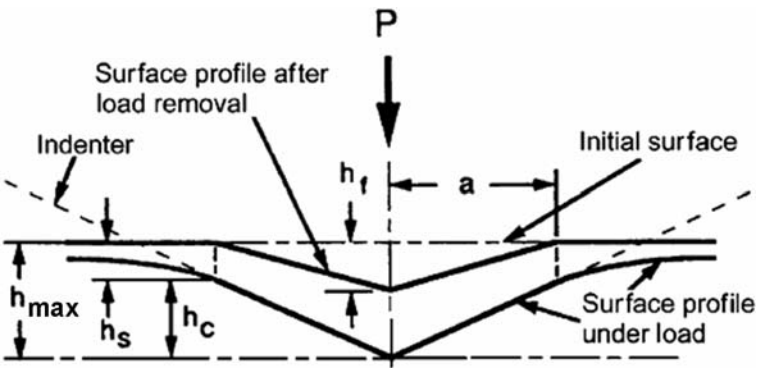

(a)

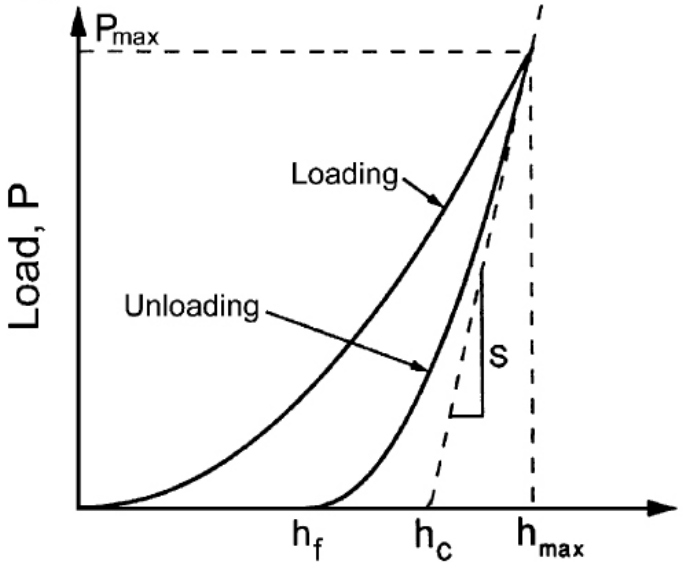

(b)

Figure 2.1 Schematic plots of (a) the indentation pattern of an elastic-plastic material and (b) a typical load-displacement curve [39].

In the calculation, the contact stiffness can be calculated from the contact load-displacement curve, while the projected contact area to the contact depth function has to be determined on the standard fused quartz sample beforehand. Moreover the hardness and the

reduced elastic modulus are deduced from the above equations based on the elastic solution. It should be noted that the Oliver-Pharr theory neglects a pile-up (movement of the material around the tip above the original surface plane) or sink-in (the material surface after measurement around the tip below the initial surface) during the penetration of the indenter into the material surface, as shown in Figure 2.2. It will therefore underestimate the true contact area at the presence of a pile-up, and overestimate this area when a sink-in occurs. It influences the results of the hardness and reduced elastic modulus. Besides, this theory does not consider the time-dependent behavior of materials, so that the modification of the calculation is required when testing viscoelastic materials, such as polymers [53]-[55].

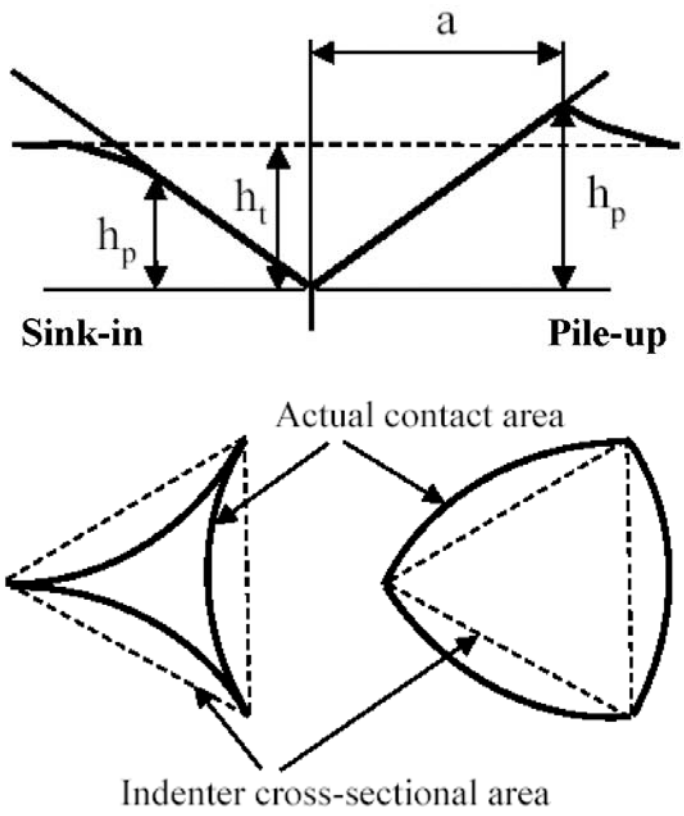

Figure 2.2 Schematic plots of nanoindentation pile-up and sink-in.

2.1.2 Indenters

Diamond is the most generally used material for the indentation tip due to its large hardness and elastic modulus which minimize the contribution of the indenter itself to the measurement. There are many geometric configurations available for the indenter tip for use in the nanoindentation testing. The geometrical accuracy of the tip becomes more critical as the indenter volume is reduced. The commonly used tips for nanoindentation measurement are shown in Figure 2.3.

Three sided pyramid tips, such as the Berkovich tip and the Cube Corner tip, are commonly used for the measurement of hardness and reduced elastic modulus at small scales. The Berkovich tip includes a total peak angel of 142.3° with a half angle of 65.35° which makes a very flat tip, as shown in Figure 2.3 (a). The average radius of curvature for a Berkovich tip is typically between 100 and 200nm. The Berkovich tip is used as the standard indenter for nanoindentation measurement. The Cube Corner tip includes a right angle, which makes the shape same as a corner of a cube, as shown in Figure 2.3 (b). The sharper angle and a higher aspect ratio of the Cube Corner tip allow the radius of curvature to be much smaller than that for a Berkovich tip. There are three classes of the Cube Corner tip depending on the radius of curvature: less than 40nm, 40-60nm and 60-100nm. The smaller the radius of curvature of the tip, the thinner films can be measured accurately, but it is easier to chip or break the tip.

The other commonly used tip is the conical tip with a spherical end, as shown in Figure 2.3 (c) and (d). Due to the limitation of tip geometry, it is very difficult or impossible for the conical tip to get the radius of curvature at the end as small as that for the three-sided pyramidal tip. The radius of curvature for the conical tip is usually larger than 1μm. This tip is frequently used for wear and scratch testing on hard materials because of the non-directional geometry. Besides, this tip would also work well with soft materials such as polymer which is too soft to image with the Berkovich tip.

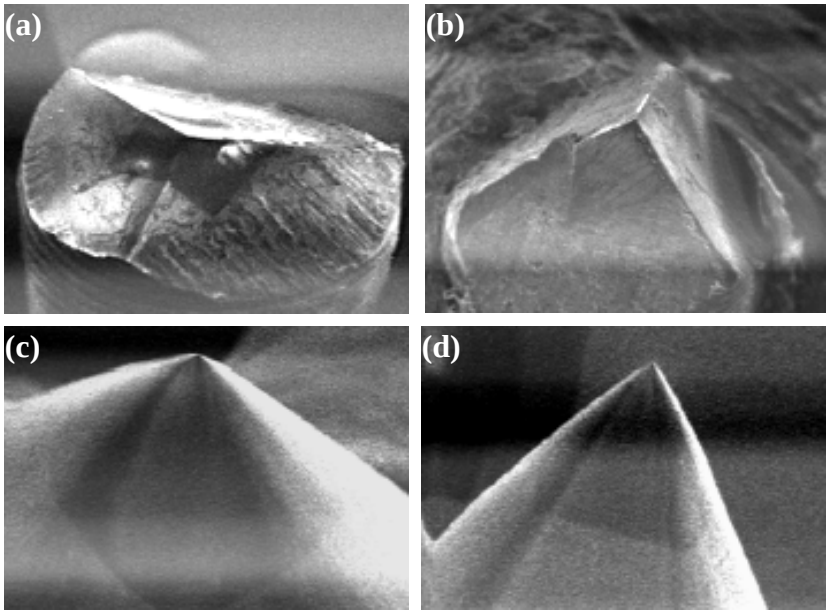

Figure 2.3 Commonly used nanoindentation tips [56]: (a) Berkovich; (b) Cube Corner; (c) conical tip with radius 3μm; and (d) conical tip with radius 1μm.

Before nanoindentation test, the tip-shape calibration is necessary to determine the area function of the indenter. This calibration is based on the assumption that the Young's modulus of the standard material is constant and independent of the indentation depth. Fused quartz with Young's modulus of 72GPa is usually used for this purpose. Through making a number of indentations with different contact depth on the fused quartz and then fitting with the computed area as a function of the contact depth, the area function of indenter is expressed as a sixth order polynomial of the form:

$$A = C_0 h_c^2 + C_1 h_c + C_2 h_c^{1/2} + C_3 h_c^{1/4} + C_4 h_c^{1/8} + C_5 h_c^{1/16} \quad (2.5)$$

where C_0 for a Berkovich tip is 24.5 while for a cube corner (90°) tip is 2.598. For an ideal Berkovich tip, the projected contact area $A = 24.5 h_c^2$.

However, while these tips are working well on an initially flat surface, they are not suitable for a curvy surface unless the radius of curvature of the surface is much larger than the indentation depth. This is certainly not the case when trying to measure large deformation of a micron-sized spherical particle. Therefore a new geometry of the indenter is required for the particle characterization in this study.

2.1.3 Instruments

There are several commercially available nanoindentation instruments with different designs. The device used in this work is the Triboindenter® (Hysitron, MN, USA) (Figure 2.4 (a)). The central part of Triboindenter is the patented design of the transducer, which includes a three-plate capacitive sensor for load and displacement measurements, as shown in Figure 2.4 (b). This transducer design provides a high sensitivity of 1nN and 0.004nm for load and displacement, respectively. The tip is mounted to the capacitive plate in the center, which is suspended in springs and free to move in the normal direction. By modulating the electrical potential applied to this center plate with respect to the top and bottom plates an electrostatic actuated force is applied to the center plate and hence drives the indenter tip. The force applied to the indenter tip is therefore the sum of the electrostatic applied force and the force introduced by the deformation (displacement) of the spring. The displacement is calculated from capacitance between the center plate and the top/bottom plate respectively. Due to the high resolution and the low drift during measurements, the Triboindenter is suitable for mechanical testing of materials and the material responses at a very small scale. Thus the Triboindenter with a specially designed tip was chosen to characterize the single micron-sized particles in this study.

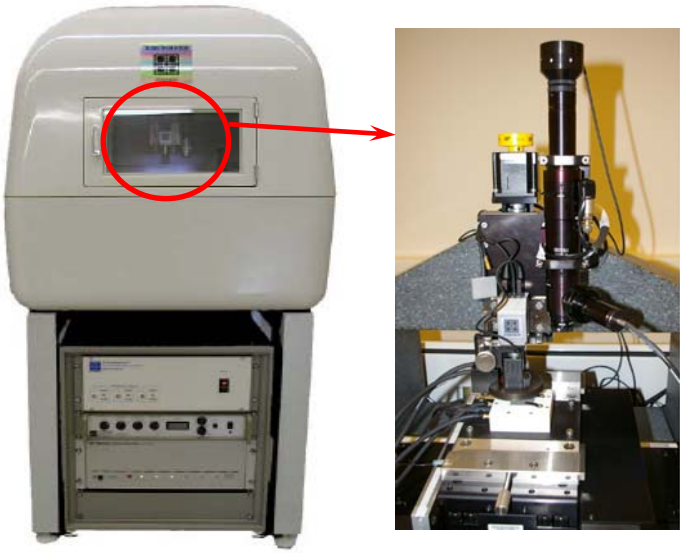

(a)

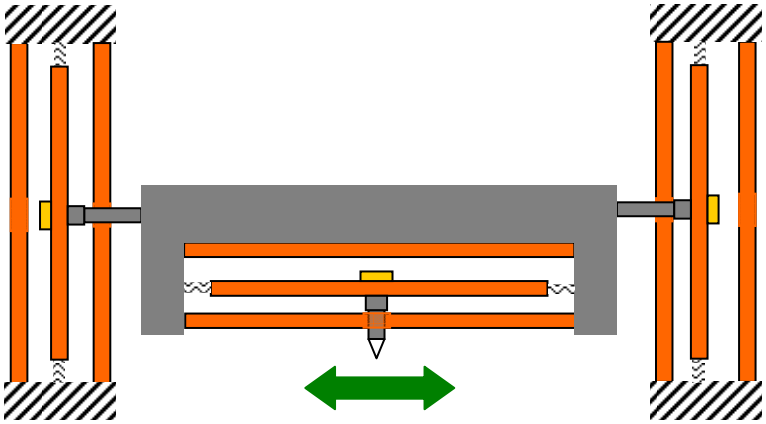

(b)

Figure 2.4 (a) The Hysitron Triboindenter® and (b) the cross-section schematic of three-plate capacitive sensor of transducer.

2.2 Polymer Particle Technology

The polymer particles studied in this thesis are monodisperse spheres [57]-[61] with a narrow size distribution, and with a diameter ranging from 500nm to 30μm. In general, polymer particles and their suspensions (colloids) have been widely used as various industrial materials, for example, paints, adhesives, foods, gels and cosmetics, and also have numerous potential applications in sensors, templates for nanostructure formation, magnetic storage media, and photonic bandgap crystals [62]-[65]. The preparation of polymer particles has been an intensive area of research for a long time. The technologies have been advanced such that a variety of structured particles can be possible including chemical composition, core-shell structure, microdomain and porosity/voids.

There are several methods used to synthesize micron-sized polymer particles. Only four commonly used methods are summarized as follows. First, the polymer particles can be prepared by suspension polymerization, in which all ingredients are mixed through mechanical agitation to form homogeneous solutions before polymerization. By such a method the particle size distribution is largely determined by stirring intensity, resulting in the limitation of a broad size distribution and a particle size larger than 100μm which is unfavorable in a number of applications, for instance within electronic packaging application [67]. Secondly, by means of dispersion polymerization, in which the reaction takes place on the surface of the monomer droplets, monodisperse micron-sized particles may be obtained but the crosslink density is required to be less than 1%. Otherwise, it will result in particles with irregular shape [68]. The third, the emulsion polymerization is often used in batch, semi-batch and continuous processes, which is usually starts with an emulsion incorporating water, monomer and surfactant. The most common type of emulsion polymerization is an oil-in-water emulsion, in which the monomer droplets (oil) are emulsified (with surfactants) in a continuous phase of water [69][70]. The drawback of emulsion polymerization is that the technology for the required emulsion breaking is difficult to control. The above mentioned methods for producing micron-sized polymer particles are the single-step processes. In addition, seeded polymerization has been an effective method to produce micron-sized polymer particles with a narrow size distribution, controllable particle size and high crosslink density [71][72]. Seeded polymerizations are performed for three purposes: (1) enlargement of particle size; (2) formation of skin layer to introduce new functions; and (3) formation of non-spherical or uneven particles caused by phase separation during the polymerization. Enlargement of particles by seeded polymerization had been a very troublesome work before the activated swelling method was developed by Ugelstad [73]. The reformed seeded polymerization which is named as Ugelstad method has been introduced to prepare extremely monodisperse polymer particles which are well controlled with a wide range of particle size and crosslink density [74]-[76]. In this study, all polymer particles are synthesized by using Ugelstad method. For this reason only the Ugelstad method is detailed in the next section.

2.2.1 Ugelstad Method

Ugelstad method, which is based on seeded polymerization and emulsion polymerization, involves a two-step activated swelling process, as shown in Figure 2.5. This method provides large possibility to control the size and the size distribution of micron-sized polymer particles [6]. The main feature of this method is that the activated seed polymer in aqueous dispersion is capable of absorbing monomers far exceeding the case of pure polymer particles. The activation of the seed particles results from the presence of the Y-compound which is highly water-insoluble and has relatively low molecular weight. The Y-compound can be transported through the aqueous phase to be absorbed inside the seed. Therefore, the Y-compound acts as not only an initiator for the polymerization but also an

activator for monomer absorption in the first-step swelling. The second-step swelling is facilitated by attendance of the Z-compound in the form of an emulsion where Z-compound is slightly water soluble and low molecular weight [77]-[80]. As long as the two swelling processes are properly performed, the preparation of polymer particles starts with monosized seeds and experiences an equal swelling of each particle to maintain the monodispersity during the process. When the polymerization is started, all necessary ingredients are present and mixed in the highly swollen seed particles. This implies that the activated swelling method is especially suitable for the synthesis of cross-linked polymer particles. The monomers which have been applied to prepare monosized polymer particles by Ugelstad method are styrene and styrene derivatives, divinylbenzene (DVB), alkyl-acrylate and so on.

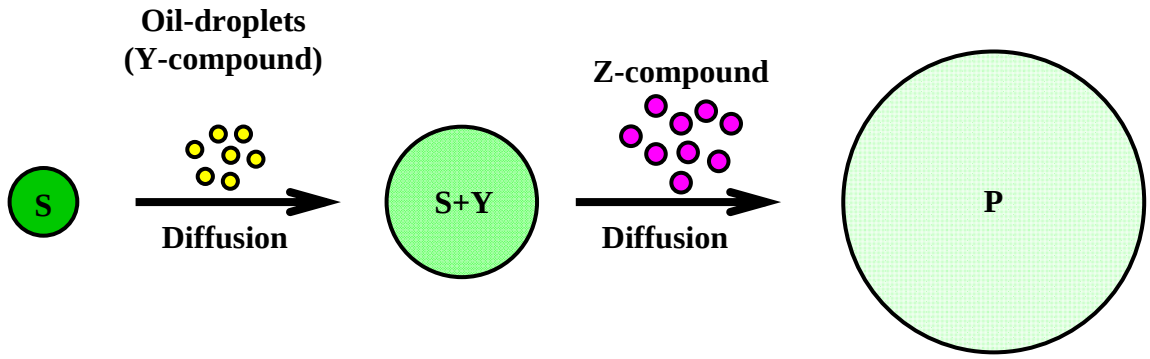

Figure 2.5 Preparation of highly monodisperse polymer particles by using Ugelstad method. S: seed; P: particle.

It has been shown that using Ugelstad method, the micron-sized polymer particles with the size of 100-1000 times of nano-scale seed particles can be obtained with a standard deviation of particle diameter of less than 2% [74]. This method is also suitable for the synthesis of porous macroreticular particles [81] in which the second-step swelling has to be carried out by applying inert diluents in addition to monomers. Besides, polymer particles with special functionalities have been developed through post treatments, such as surface modification and in-site deposition of magnetic iron oxides. A wide range of applications of monosized polymer particles in various sizes and materials have been exploited.

2.2.2 Particle Applications

The Ugelstad method allows manufacturing of polymer particles with a very narrow size distribution with sizes ranging from sub-micron up to several hundred microns. During the last 30 years many applications of monosized polymer particles in various sizes and materials have been developed, which are listed in Figure 2.6. The particles have been proven highly successful in biotechnologies, pharmaceutical and chemical industries.

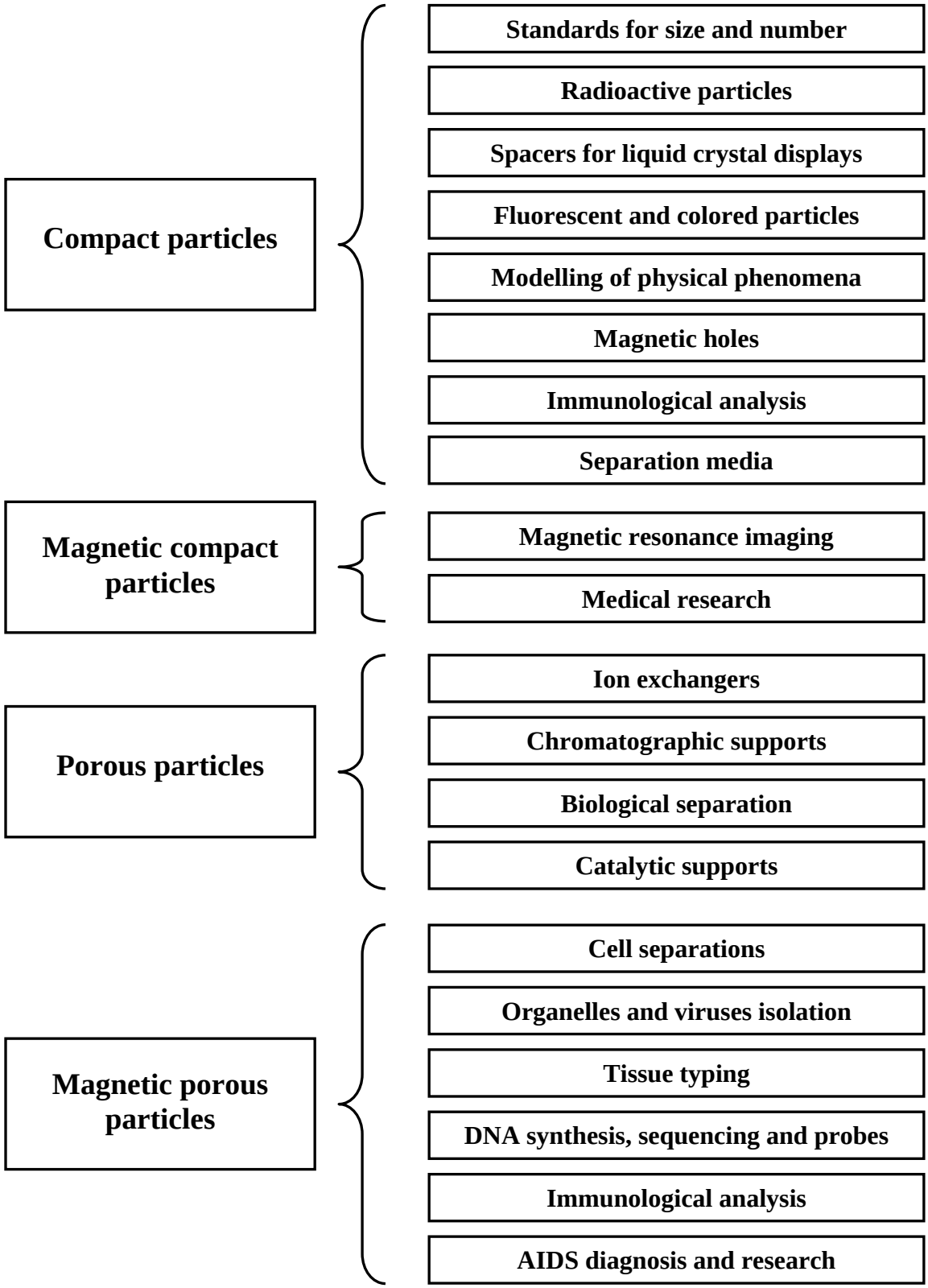

Figure 2.6 Schematic illustration of various applications of compact and porous monosized polymer particles [11].

One common application of monosized polymer particles is as chromatographic support in chemical analysis [82]-[84]. The demands on the packing materials for high performance liquid chromatography are rigidity, chemical stability towards solvents and pH-changes, high load capacities and low non-specific interactions. Highly crosslinked particles prepared from synthetic polymers like polystyrene-co-divinylbenzene (PS-DVB) and acrylate or methacrylate copolymers, which are mechanically and chemically stable and are able to withstand high pressures and high flow rates, have been developed to meet the demands in chromatographic applications. At the same time, the highly crosslinked styrene-divinylbenzene copolymers are very rigid and may be operated over a wide pH range, 1-14.

In addition, monosized crosslinked polymer particles have been also extensively used as model systems to study fundamental aspects of many-body phenomena like packing, aggregation, crystallization, melting and fracture [85]-[88]. Up to now experiments on real systems allowing direct observations have been very few compared to the number of model simulations on computers. However, even the most advanced computers have to operate with very simplified models, and it has been questioned how realistically the computer models reflect nature and how quantitative these results are. In order to carry out analog experiments with particles, it is in many cases required to have a large number of uniformly sized and shaped particles. In this respect highly monodisperse particles including crosslinked particles in different sizes has been used to construct experimental models for a variety of equilibrium and non-equilibrium processes.

2.3 Anisotropic Conductive Adhesive

2.3.1 Reliability of ACA

For the applications discussed, the particle development has mainly focused on the syntheses and functional modification rather than on mechanical performance and characterization. However, as these particles are now introduced in microelectronic and microtechnology applications, mechanical properties becomes very important. For instance the factors that determine the performance and reliability of a typical Anisotropic Conductive Adhesive (ACA) interconnect (as shown in Figure 1.1) can be divided into two categories: one is the properties of components, such as bump size and height, the substrate type and the properties of the metal plated conductive particles; the other is the parameters during bonding process, for instance, temperature, pressure and curing conditions [89]-[95]. In this application the metallized polymer particles are electrical conductors providing current paths between the chip bumps and the corresponding substrate pads through the mechanical contacts obtained during the deformation of the compressed particles. Enlarging the contact area between the bump (substrate) and particles is able to significantly improve the electrical contact of ACA assemblies. Therefore, the mechanical properties of conductive particles under large deformation are of crucial importance for the performance of ACA assembly.

While the literature on the mechanical characterization of particles is relatively sparse, most studies have focused on the performance of the whole ACA assemblies and the effect of conductive particles on the reliability of the ACA assembly. Yim and his colleagues have studied the design, manufacturing, reliability and degradation mechanism of ACA assemblies. Their results showed that there is, as expected, a relationship between particle content and the connection resistance. Increasing the initial particle content in the adhesive will increase the number of particles on the terminal, and the connection resistance decreases [96]-[98]. In 1999, Sarkar et al. published a paper focused on the application of ACA used for Chip-On-Flex technology. They found that increasing the fraction of the conductive particles can seriously affect the manufacturing yield by causing short circuits in the assembly [99]. Later, Chin et al. reported electrical contact properties of ACA assembly including metal coated polymer particles. The effect of elastic recovery of the whole ACA assembly on the electrical contact resistance was investigated and modeled [100][101]. Galloway's group has studied the mechanical, thermal, and electrical behaviors of a compliant interconnect. In their work the particle has a quite large size up to hundreds micrometer, and is mainly used for ball grid array (BGA) package [102]. Dou et al. have reported a mathematical function describing the electrical resistance of an ACA particle. The function includes the effect of particle transformation degree, polymer core diameter, nickel layer thickness, and gold layer thickness, based on a physical model of an ACA particle [103][104].

2.3.2 Mechanical Characterization of Particles

Due to small volume, spherical geometry and composite structure involved in the particles, the mechanical characterization of those particles possesses great challenges. Due to the small size of the particles it is very difficult to obtain accurate data for the mechanical properties using conventional mechanical testing methods. Deformation of a sphere is complex, since the strain of the particles is highly nonuniform. The strain is localized in small area when the compression starts, and the contact is close to a point contact. Besides, if the particle is coated by metal layer, the multilayer structure brings more complexity to the mechanical characterization due to the constitutive difference of polymer and metal materials.

So far, there are only limited investigations focused on the mechanical characterization of micron-sized particles. In the early work, the mechanical behavior of metal coated polymer particles was measured through dispersing a number of particles (typically several hundreds) as a single layer between two silicon chips [105][106]. Additionally, the resolution of load and displacement measurement in this setup is too rough to accurately characterize the particles. So this method is far from sufficient for mechanical testing of single particles use in ACA assembly. Later, the development of nanoindentation techniques has made new methodology available to study the conductive particles.

Nanoindentation with a sharp tip was first used to study the mechanical properties of a cross section of polymer particles within the bulk ACA interconnection at various deformation degrees [107][108]. The aim was to investigate the effect of bonding pressures on the particle properties. It was found that the microhardness at the central area was higher than that at the outside because of the lower constraints at the surface. This work was one of the first to address the properties of single particles, however, only properties in local areas of particles were investigated and the microtomy used to cut the ACA interconnection might alter the surface properties of the particle's cross section. Subsequently, a simple instrument with a flat hammer was constructed to compress single particles and analyzed the effect of particle deformation levels on the ACA performance [109]-[111]. The effects of the swelling ratio, and hence the chemical composition and the backbone chain structure were investigated with respect to macroscopic compression behavior and surface morphologies of particles. A numerical model based on finite element analyses was proposed to determine the elastic properties of micron-sized polymer particles under compression [23][112]. Recently a study on the deformation properties of individual metal-coated polymer particles was reported, and the results showed that the particle deformation process was nonlinear due to both the geometry nonlinearity and material nonlinearity [113]. However, a systematic study on mechanical properties of individual micron-sized polymer particles and metal coated polymer particles has been missing. This thesis will focus on the nanomechanics of those particles and establish the characterization methodology of micron-sized polymer particles.

2.4 Challenges and Tasks

The introduction of micron-sized polymer particles in applications, such as electronic packaging technologies and solar cell assemblies has made it necessary to investigate the mechanical properties of such particles. There are still big challenges to overcome in the mechanical characterization of such particles.

Due to a large surface area resulting from a small volume of particles, dry particles usually occur in a state of clusters. How to disperse particle clusters and get individual particles is an important precondition for mechanical characterization of such particles. Different types of organic solvent, for example acetone, or methanol, may disperse particle clusters but will at the same time modify the particle behavior. In addition, a proper sample substrate is necessary for minimizing the substrate effect on the particle behavior during measurement. This includes low surface roughness, a suitable surface tension to accommodate the dispersion of the particle suspension, as well as high mechanical rigidity.

When considering the deformation of the particles, the properties of particles in two scales should be identified: micro properties and macro properties, and the two are related to each other. Micro properties relate to the hardness of the materials constituting the particles and reflect the local response of materials, while the macro properties relate to

deformation properties of the whole particle. A previous study has been focused on the micro-properties using a nano-indenter on cross sections of ACA samples assembled at different pressures [108]. The macro-properties of the ACA particles are critical to the ACA material performance because they determine how the particle deforms and the resulting contact forces associated with the deformation. Therefore an effective technique is highly required to simulate the working conditions of particles within ACA assemblies and measure the macro-properties of single particles. The method should be capable of accurately measuring the mechanical response of single micron-sized particles under compression. Based on nanoindentation, extreme accuracy of measurement can be obtained for small volume of particles. But the characterization of single particles is challenging to the existing methodology. A well designed method and reproducible experimental setup are necessary to get the repeatable and reliable results.

Chapter 3

POLYMER PARTICLES

This chapter describes the general knowledge of polymer particles and metal-coated polymer particles used in this research. The particle dispersion process and the sample preparation procedure for obtaining single particles are also discussed.

3.1 Particles

The focus of this thesis is on the nanomechanics of single micron-sized particles. The mechanical properties of Ugelstad polymer particles and metal coated Ugelstad polymer particles have been systematically investigated. The structures of two kinds of particles are schematically shown in Figure 3.1.

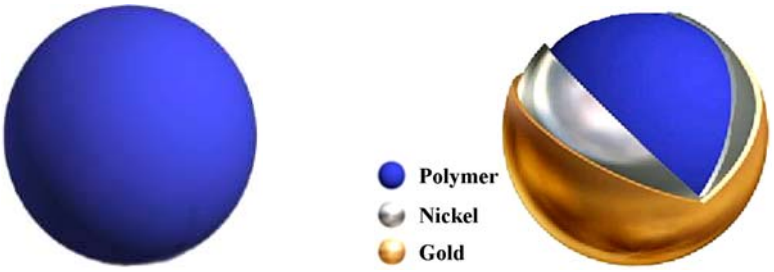

(a) (b)

Figure 3.1 Configurations of (a) a polymer particle (AC or PS-DVB) and (b) a typical metal coated polymer particle (AC core).

3.1.1 Solid Polymer Particles

The polymer particles characterized in this study are manufactured using the Ugelstad method and the particle sizes have ranged from 2.6μm to 78.9μm. The compact polymer particles tested have been made of two distinctly different polymer chemistries. These are

acrylic-diacrylic particles (AC) made by Conpart AS, NO, under the trade name Concore™, and polystyrene-divinylbenzene particles (PS-DVB) made by Invitrogen Dynal AS, NO, under the trade name Dynospheres®. Both particles are amorphous at room temperature and have a crosslinked structure. The AC particle has a constant crosslink density of 60%, but different sizes. The coefficient of variance (CV) of particle size distribution is less than 3%, where CV is defined as the ratio of the standard deviation of the particle size to the mean diameter. The PS-DVB particle is polystyrene based and crosslinked by divinylbenzene and has a wide range of particle size and crosslink density, which are used to check the effect of the size and the crosslink density on the mechanical properties of particles. The CV of size distribution for PS-DVB particle is less than 2%.

The representative SEM photographs of AC and PS-DVB particles are shown in Figure 3.2. From each of the images, it can be observed that the particles have identical size and morphology for each manufacturing batch. There is, however, a significant difference between the morphologies of two particles, showing that the AC particles have a rough surface while the PS-DVB particles display a smooth surface.

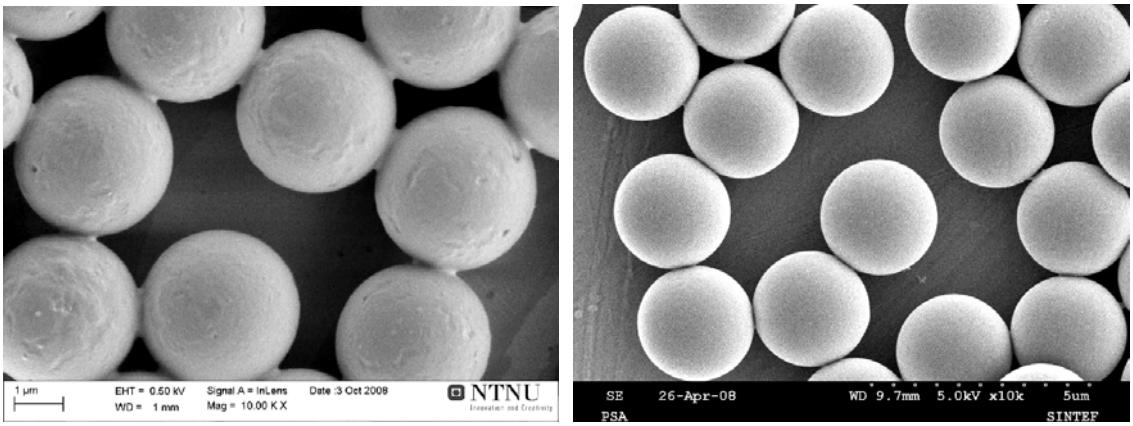

(a) (b)

Figure 3.2 SEM photographs of (a) AC particle with diameter of 3.0µm and (b) PS-DVB particle with diameter of 2.6µm.

3.1.2 Metal Coated Polymer Particles

Metal coated polymer particles are prepared by depositing the metal layer(s) on the AC particles through an electroless plating process [114]. Two metal layers have been deposited on the AC core. First there is typically a 35-50 nanometer Ni inner layer for obtaining electrical conductivity and increasing adhesion to the polymer core. This layer is covered by a 15-25 nanometer Au layer, to improve contact reliability and electrical conduction, partly by protecting the inner layer from oxidation. The morphology of metal coated polymer particles is shown in Figure 3.3. From the image, it can be seen that the

metal coating is formed by a process where nanometer sized metal particles are formed in the solution, and then subsequently adhered to the surface. This results in a metal coating layer which is not very homogeneous. In addition, larger silica particles used as dispersing agent in some of the processes adheres to the polymer particle.

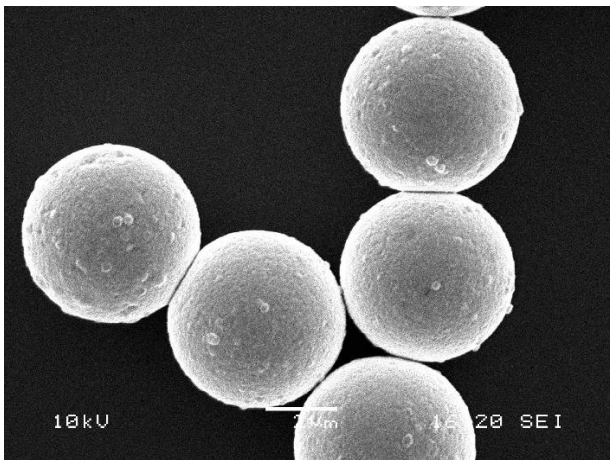

Figure 3.3 SEM photograph of Ni/Au coated AC particle with 4.8μm diameter.

3.2 Particle Dispersion

To investigate properties of single micron-sized particles, the spreading of particles is obviously an important precondition. In order to evenly disperse particles, different types of solvents have been tested: water, acetone and 96% ethanol. The particles spread in water took long time to be dried completely. And also the particles showed a relatively large deformation after drying, which was probably caused by the capillary force as the water evaporated. This pre-deformation varied from particle to particle and was in addition difficult to quantify. Hence the effect of the pre-deformation could not be easily compensated in the results. It was therefore concluded that water is not a proper medium for particle dispersion. When trying to use acetone as the dispersing medium, the particles dried rapidly but large shrinking occurred after drying. This was most likely because the acetone dissolved the non-crosslinked parts of the particle which came from the seed particle used in the Ugelstad process. Much better results were obtained when using 96% industrial ethanol as the dispersant. Due to the low surface tension of ethanol, a very small pre-deformation of the particle was observed. The ethanol did not dissolve the seed of the particle, keeping particle size constant. Ethanol also gave a stable wetting of the substrate as well as a suitable evaporation rate, with very little residues. A lot of experience also showed that the particles were well cleaned in the industrial ethanol. Using industrial ethanol effectively resolved the problem with pre-deformation and shrinking of particles, and also provides good adhesion between the particle and substrate. We therefore finally ended up with 96% industrial ethanol as dispersing medium.

As for the sample substrate, both pieces of microscope glass plate and silicon chip were tested using the different solvents mentioned above. The glass plate displayed a large compliance on the measurement results due to lack of planarity. The silicon chip is sized of $10\times10\times0.5mm^3$ and has good planarity. Furthermore the silicon has much stiffer mechanical properties comparing to the tested particles, i.e. Young's modulus, which will decrease the effect of the substrate on the measuring results according to the Hertz theory [115][116]. On the stage of the Triboindenter there are 9 sample positions and the center of each sample position has a magnet mounted inside the stage, hence the samples are held down magnetically. For this reason a steel disc (Φ15mm×0.25mm) is chosen to provide the magnetic force and thus fix the sample on the stage. The silicon chip was glued onto the steel disc using instant glue Cyanoacrylate [117].

Hereby, a particle dispersion process has been established using 96% ethanol as the solvent and silicon chip as the substrate. The sample preparation procedure has been developed. During the sample preparation, a tiny amount of the polymer particles were immersed in 96% industrial ethanol and exposed to a high frequency ultrasonic vibration to de-agglomerate the particle clusters. A small droplet of the ethanol – particle suspension was placed on the bare silicon chip glued onto the steel disc. The specimens were then left to dry in a clean environment for a specific period of time to remove any ethanol left in particles, usually 12 hours. It was easy to distinguish single particles from a cluster of 2 or more particles using the attached optical microscope in the Triboindenter. One example of AC particles with 3.0μm in diameter is shown in Figure 3.4.

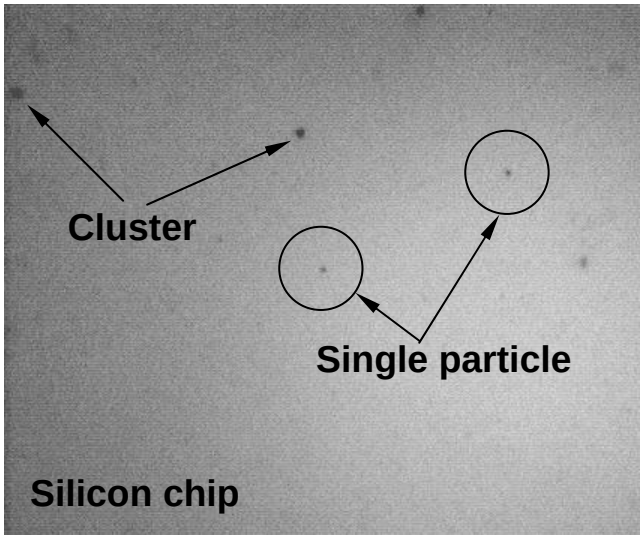

Figure 3.4 The image of AC particles with diameter of 3.0μm under the integrated optical microscope in the Triboindenter.

Chapter 4

METHODOLOGY

This chapter presents the flat punch methodology developed in this PhD study, followed by a discussion on the measurement of mechanical properties of single particles.

4.1 Flat Punch

4.1.1 The Diamond Punch

The conventional nanoindentation is usually used to penetrate the initially flat material surface with a sharp tip for studying the local response of material. However, in this work the macroscopic properties of single particles are the focus, so a modification of the indenter is necessary. Inspired by the large amount of work done on the contact between a rigid plate and a soft sphere, we have successfully developed a nanoindentation-based flat punch method to investigate individual micron-sized particles. Instead of the commonly used sharp tip, a specially designed punch with a flat-end, as shown in Figure 4.1, was manufactured. The punch is made of diamond and the flat end has a diameter of around 100μm. The reason for choosing diamond to make the flat punch is that this material is rigid enough to minimize the influence on the measurement.

4.1.2 Co-planarity

The experimental setup is shown in the image in Figure 4.2. The particles are placed on the silicon chip and compressed between the flat punch and the silicon substrate. Obviously, the coplanarity of the flat punch and the parallelism between the punch surface and the silicon substrate are of crucial importance to the precision of the measurement. If the coplanarity and parallelism of the flat punch is not well calibrated for the small particles, the edge of the punch might reach the substrate before the compression of the particle is finished. There are two factors influencing the coplanarity and parallelism of the flat punch: one is the planarity of the flat punch, and the other is the mechanical mounting of the tip and the TriboScanner. Besides carefully mounting the tip to the transducer and the

TriboScanner to the Triboindenter carriage, the precise calibration of the flat punch is required before the testing.

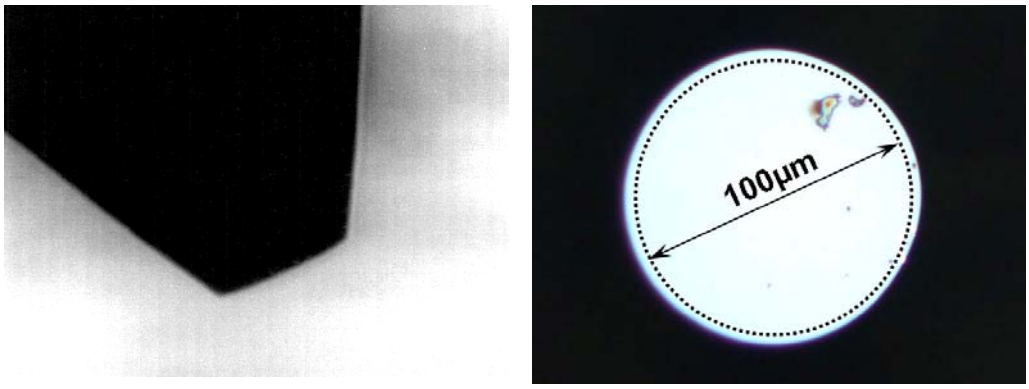

(a) (b)

Figure 4.1 The flat punch tip used: (a) side view and (b) top view.

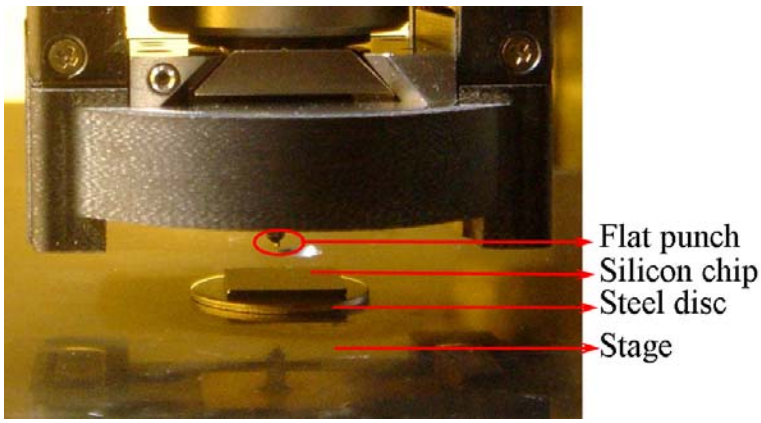

Figure 4.2 Experimental setup of the flat punch test.

The size of the flat punch is about 100μm in diameter and the maximum load of Triboindenter is 10000μN, so the contact stress of the flat punch to an initially flat material surface is about 1.27MPa. This value is quite small for most materials and it is therefore difficult to get a residual indent on them. For instance, single crystal aluminum which is used as a standard sample for the calibration of the sharp tips is too hard to leave any residual imprint. Based on this consideration, an indium which is soft and ductile was selected to calibrate the flat punch.

Before use, the flat punch was first cleaned using acetone to remove any residues such as dust or external impurities. The co-planarity of the flat punch was checked by indents penetrated into the polished indium surface. After indentation, a uniform and circular indent onto the indium surface was regarded to be acceptable. The relative positions of the

integrated optical microscope and the indenter were also calibrated through the indent on the indium. This guarantees the indenter tip is indenting on the same position where has been chosen with the optical microscope.

4.2 Flat Punch Methodology

4.2.1 Procedure

In the current lab environment, the effective accuracies of force and displacement are 100nN and 1nm respectively. These values are obtained by doing indentation in the air. The compression of single micron-sized particles is schematically shown in Figure 4.3. The standard load-control or displacement-control modes have been used in which the applied load or displacement follows a predefined load (displacement) as a function of time. A three-step load (displacement) function which consists of linearly loading to the peak load (displacement), holding at the peak load (displacement) and linearly unloading is usually applied during the test, as shown in Figure 4.4. During the compression, the contact load and displacement are monitored in real time and then the load-displacement relationship is obtained.

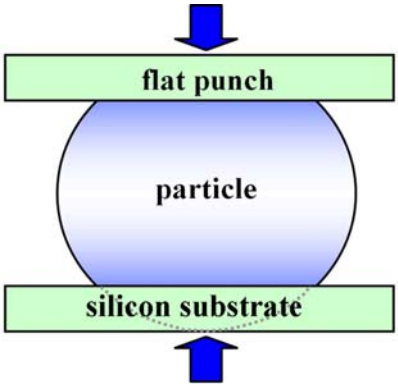

Figure 4.3 The schematic compression of the flat punch on a single particle.

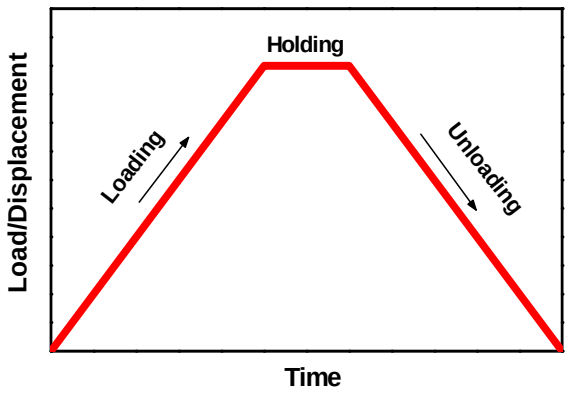

Figure 4.4 The predefined load/displacement function.

Several steps in the experiment can be identified: the sample preparation (See section 3.2), the flat punch calibration (See section 4.1.2), the compliance checking and the particle compression.

Before the compression on the particles, a standard indent (10000μN peak load, 2000μN/s linearly loading/unloading rate and 2s holding at the peak load) has to be performed on the silicon chip to check the compliance between the steel disc and the silicon substrate. The typical load-displacement curves on the silicon chip with and without sample compliance are shown in Figure 4.5. Silicon is a brittle material with very little or without plastic deformation when exposed to a stress smaller than fracture strength. Therefore the load-displacement behavior of silicon is similar to that of a fully elastic material below the fracture strength, as the curve plotted by the solid square points in Figure 4.5. However, when a hysteresis effect is observed, or the deformation is larger than normal, as observed on the curve with unfilled round points, this is caused by an unwanted compliance between the silicon substrate and the steel disc. If there is a large compliance, the sample has to be prepared over again.

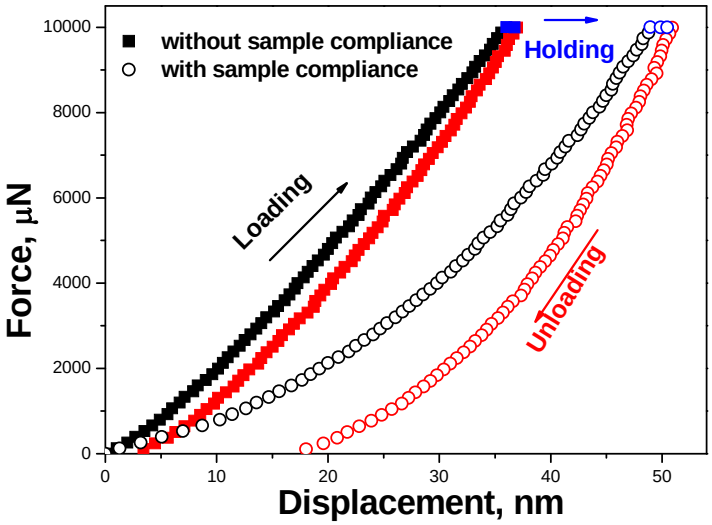

Figure 4.5 Representative load-displacement curves on the silicon chip.

Once all the preparation is finished, the compression on the particles can be carried out, through the following procedure:

1. Identify a single particle on the silicon chip using the integrated optical microscope of Triboindenter and record coordinates and image of the target particle;
2. Perform the mechanical testing following the predefined load (or displacement) function;
3. Record image of the compressed particle;

4. Repeat the procedures on an “untouched” single particle to check the repeatability of the results.

In general, at least four individual particles should be tested to examine the mechanical properties. A lot of experience shows that the particles from same manufacturing batch have a very consistent mechanical behavior. This indicates a very homogeneous material with narrow size distribution and uniform microstructure, as well as highly reproducible experiment setup.

4.2.2 SEM Observation

After the nanomechanical testing, the sample is moved to a field emission scanning electron microscope (SEM) (Ultra 55LE FESEM, Zeiss, DE) to investigate the particle morphology. According to the reference coordinate recorded in the mechanical testing procedure, it is easy to find the tested particle in SEM. To minimize the effect of the electron beam, such as heating due to the insulating properties of the polymer particles, a very low accelerating voltage and beam current is used. Otherwise, the particle will “melt” under the influence of the electron beam. This means that a small working distance has to be used, and the resolution is somewhat limited.

4.3 Deformation of a Single Particle

The nanoindentation-based flat punch method has been used to measure the single micron-sized particles. The contact load-displacement curves of particles under compression which are obtained, reflects the macroscopic response of particles. The load-displacement curves for the two groups of polymer particles acrylic and polystyrene-divinylbenzene, contains a large amount of particle information. The corresponding stress-strain relationship is calculated to reveal the intrinsic properties of particles.

The typical load-displacement relationship and the contact loading/displacement versus testing time for a polymer particle are shown in Figure 4.6. This specific graph shows an AC particle with the diameter 3.0μm during compression using the standard load function. The deformation degree is defined as the ratio of the deformed particle height to the undeformed diameter. The particle stiffness is determined by the slope of the load versus displacement curve. According to the particle behavior, the loading behavior of particle is divided into three stages. In stage I, the displacement is approximately proportional to the applied load. The particle deforms very fast at the beginning of compression which can been observed from the large change in deformation from measurement point to measurement point even with a sampling frequency of 1kHz as shown in the curve in Figure 4.6 (a). The curve in Figure 4.6 (b) further confirms that the particle deforms about 40% at the first second of the compression. Thereafter the particle deforms with a relatively large rate in stage II until the displacement burst occurs, caused by a sudden fragmentation of the particle. The stiffness increases significantly during this stage. In the stage III while

the load is fixed, the particle deformation increased within few milliseconds from about 63% to around 80%. This is more easily observed on the load/displacement versus time curve. As the instrument is operating in the load-control mode, the sudden fracture of the particle means that there will be an abrupt displacement of the indenter, until the polymer fragments is able to support the imposed load. After the fracture of the particle, we find that there is very little further deformation and there is hardly any recovery after unloading. This indicates that the fracture produces a number of smaller fragments which can also be observed in the SEM after the compression. This seems to be the typical fracture pattern for the highly crosslinked acrylic particles studied in this thesis.

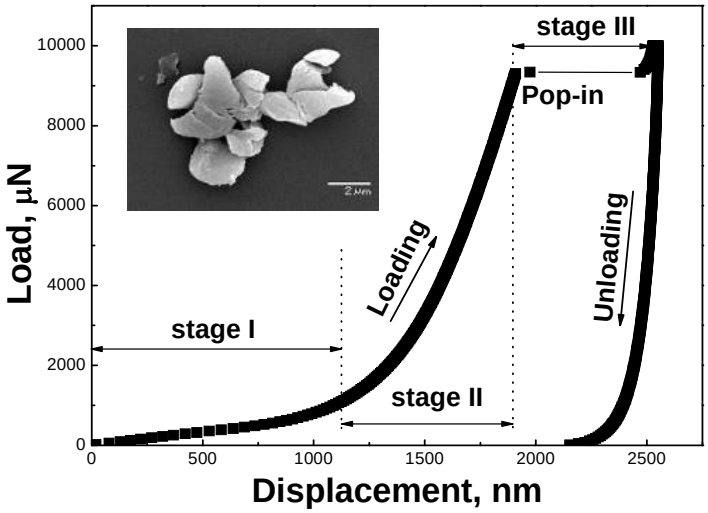

(a)

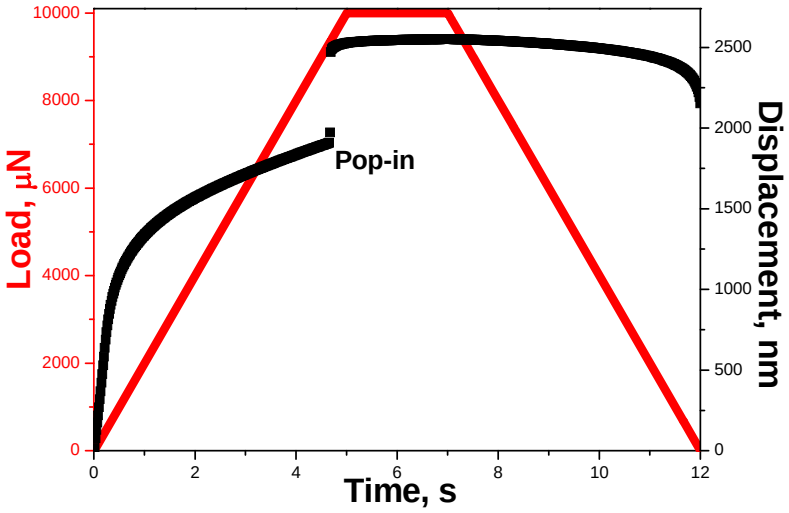

(b)

Figure 4.6 Mechanical testing results of (a) load-displacement relationship and (b) the contact load and displacement versus time.

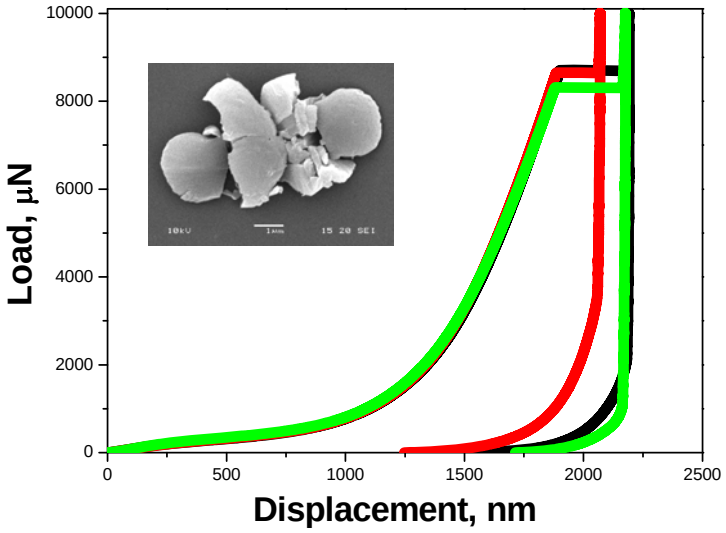

(a)

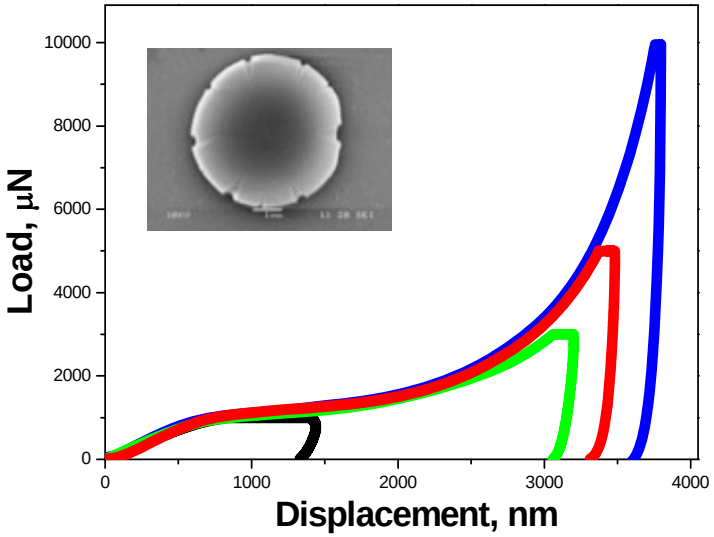

(b)

Figure 4.7 Representative load-displacement curves of (a) AC particle with a size of 3.0μm and (b) PS-DVB particle with a size of 5.1μm.

The representative load-displacement curves for two groups of polymer particles, highly crosslinked acrylic and polystyrene with a very low crosslink density, are shown in Figure 4.7 (a) and (b), respectively. In Figure 4.7 (a), three single fresh AC particles are compressed under the same conditions as the particles in Figure 4.6. The AC particle is compressed to the same peak load and with same linearly loading/unloading rate 2000μN/s. The contact load-displacement curves show that the loading segments are remarkably consistent, even including the point of fraction, which occurs at around 63% deformation.

The fracture pattern is similar as the one in Figure 4.6 (a). In Figure 4.7 (b), the loading curves of the PS-DVB particle are also repeatable, but no pop-in is observed. That is to say, there is no direct evidence on the load-displacement curve that the particle is crushed during compression. This specific particle size reaches a maximum deformation at approximately 76.5% at the peak load of 10000μN. Despite the lack of fragmentation, also these particles do barely recover during unloading. However, the SEM photograph of the compressed particle displays that a couple of surface cracks appears on the particle, which are initiated at the equator plan and propagated in meridian direction if considering that the compression is loaded at two poles. Those cracks continuously grow with the deformation, thus there is no displacement burst occurred on the load-displacement behavior.

Chapter 5

SUMMARY OF PUBLISHED RESEARCH RESULTS

The five published journal articles prepared in this study are shortly summarized and the papers presented in the international conferences are listed in this chapter. The relevant journal articles are attached in the thesis.

5.1 Summary of Journal Articles

Mechanical properties of nanostructured polymer particles for Anisotropic Conductive Adhesives

He J Y, Zhang Z L, Kristiansen H.

International Journal of Materials Research 2007; **98**(5): 389- 392.

This paper reported the preliminary results of a study on two kinds of micron-sized AC particles. For the first time, the nanoindentation-based flat punch method with the sample dispersion procedure has been demonstrated to characterize the mechanical behaviors of single particles under large deformation up to about 60%. The results showed that the particles behavior, including even the point of fracture, were really consistent. The nominal stress-strain behaviors of particles were determined and the compression modulus of particles was calculated. The effect of the loading rate and the nominal strain rate on the particle behavior was investigated. The recommendation for the further investigation was proposed.

Size effect on mechanical properties of micron-sized PS-DVB polymer particles

He J Y, Zhang Z L, Midttun M, Fonnum G, Modahl G I, Kristiansen H, Redford K.

Polymer 2008; **49**(18): 3993-3999.

Five groups of PS-DVB particles with identical chemical compositions but different diameters were tested using the nanoindentation-based flat punch method. All particles were made of 98% polystyrene crosslinked by 2% divinylbenzene. The diameter of the PS-DVB particles varied from 2.6μm to 25.1μm. Constant deformation rate was applied to the particles with two maximum strain levels of 5% and 10%. Results showed that the particle compressive stress-strain behavior was strongly size-dependent which stated that the smaller the particle size was, the stiffer the particle behaved. Analyses indicated that the pre-load and the adhesion during compression played a minor role on the size effect. The presence of a core-shell structure could possibly be a main contribution to the size effect. Finite element analyses were carried out to demonstrate this surface shell effect.

Fracture of micrometre-sized Ni/Au coated polymer particles

He J Y, Helland T, Zhang Z L, Kristiansen H.

Journal of Physics D: Applied Physics 2009; **42**(8): 085405 (5pp).

Deformation and fracture of individual micron-sized Ni/Au coated polymer particles were studied using the nanoindentation-based flat punch method. A wide range of test conditions was applied to characterize both coated and uncoated particles. After indentation, the compression induced cracking of the Ni/Au coating and delamination of the metal coating from the polymer core were investigated by SEM. A three-stage deformation process of the metal coated polymer particle was identified comparing the deformation behaviour of it with that of uncoated particle. The effect of nanoscale metal coating on the deformation capacity and fracture property of the particles was clarified. It revealed that the metal coating played a significant strengthening role within the initial deformation.

Nanomechanical characterization of single micron-sized polymer particles

He J Y, Zhang Z L, Kristiansen H.

Journal of Applied Polymer Science 2009; **113**(3): 1398-1405.

Uncoated AC and PS-DVB particles were compressed using the nanoindentation-based flat punch method. The load-displacement behavior, the stress-strain relationship, and the compression modulus of two groups of particles were compared. It was demonstrated that the compression results could be used to distinguish the mechanical properties of different polymer particles. The evident fracture of polymer particles can be observed directly in the force – displacement curves. The results showed that the highly crosslinked AC particles had brittle fracture behavior while the very low crosslinked polystyrene particles showed a very strong yielding behavior. This was also observed as a number of growing surface cracks on the particles. The smaller particles of both types of polymers displayed more distinct viscosity than the larger particles.

Compression properties of individual micron-sized acrylic particles

He J Y, Zhang Z L, Kristiansen H.

Materials Letters 2009; **63**(20): 1696-1698.

The effect of loading rate on the compression behaviors of single acrylic particles was investigated using a nanoindentation-based flat punch method. The sensitivity of mechanical properties, such as compression modulus, *K*-value, breaking force and breaking displacement, to the loading rate was examined. The results showed that the loading rate had a significant effect on *K*-value and breaking force whereas breaking displacement was independent of loading rate. The results indicated that the particle fracture is controlled by the deformation level.

5.2 List of Conference Papers

Nanoindentation-based flat punch characterization of single monodisperse acrylic particles

He J Y, Zhang Z L, Kristiansen H.

Proceedings of 17th International Conference on Composites/Nano Engineering, CD copy, Kunming, China, 2007

Nanomechanics of micron sized polymer particles

He J Y, Zhang Z L, Kristiansen H.

Proceedings of 21st Nordic Seminar on Computational Mechanics, p253-256, Trondheim, Norway, 2008

Physical properties of metal coated polymer particles for Anisotropic Conductive Adhesive

He J Y, Zhang Z L, Helland T, Kristiansen H.

Proceedings of NSTI Nanotech 2009, p262-265, Houston, Texas, USA, 2009

Chapter 6

CONCLUSIONS AND RECOMMENDATIONS

The research presented in this thesis has advanced the fundamental understanding of the mechanical properties of micron-sized polymer particles. The conclusions from the work and a number of avenues for future work are summarized in this chapter.

6.1 Conclusions

Studies on the micron-sized polymer particles or metal coated polymer particles usually focus on the syntheses process. The aim of this thesis is to investigate the mechanical properties of monodisperse micron-sized particles and provide the essential knowledge for the industrial use of polymer particles where the mechanical properties are critical for the application. The conclusions from the work presented in this thesis are grouped into three parts: the general remarks of the flat punch methodology, the mechanical properties of single micron-sized polymer particles and those of single metal coated polymer particles.

6.1.1 Flat Punch Methodology

A particle dispersion process has been developed to spread particle clusters. The 96% industrial ethanol and the silicon chip have been used as the dispersion medium and the sample substrate, which minimize the effect of the liquid surface tension and provides a mechanically stable substrate for the measurements. A sample preparation procedure has been determined to obtain single particles on the silicon substrate.

A novel methodology for the mechanical testing of single micron-sized particles, so-called nanoindentation-based flat punch method, has been developed in this work. Instead of a commonly used sharp tip for nanohardness measurement, a diamond punch with a flat-end has been prepared to compress individual particles. The contact between the diamond punch and the micron-sized particles can be considered as the inverse indentation. Results have shown that the particles from the same manufacturing batch behave remarkably consistent mechanical properties (as shown in Figure 4.7). This demonstrates a very

homogeneous material including narrow size distribution, uniform microstructure and identical chemistry of those particles, as well as a highly reproducible experiment setup including sample preparation and flat punch compression. The method could be used to test different kinds of micron-sized particles.

A systematic study of mechanical properties of both micron-sized polymer particles and metal coated polymer particles has been made. A number of significant findings have been discovered from the experiment. The relevant knowledge has been transferred to our industrial partners to modify and improve the design and manufacturing of the particles.

6.1.2 Mechanical Properties of Single Polymer Particles

Deformation behaviors

By using the developed nanoindentation-based flat punch method in this work, the mechanical properties of highly crosslinked AC particles and slightly crosslinked PS-DVB particles have been investigated.

- The typical load-displacement behaviors of single AC particles and single PS-DVB particles undergoing deformation have been established. The contact stress-strain relationship of particles (as shown in Figure 6.1) has been determined from the load-displacement results.

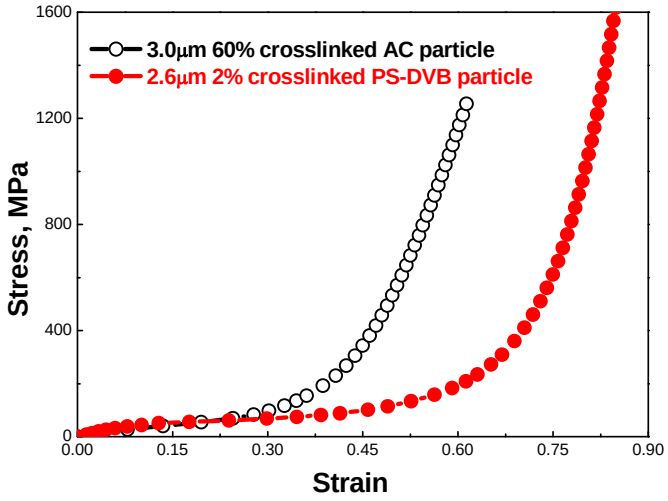

Figure 6.1 Stress-strain behaviors of highly crosslinked AC particles and slightly crosslinked PS-DVB particles.

- For the slightly crosslinked PS particles, a particle deformation up to 80% has been observed, without disintegration of the particle. The failure of the strongly cross-linked AC particles can be directly observed in load-displacement curve, shown as a displacement burst at a certain load level.

- The deformation behavior of two types of polymer particles has been classified that the AC particles with high crosslink density show brittle fracture behavior while the slightly crosslinked PS-DVB particles comply with yield behavior of amorphous particles.

Loading rate effect

- The mechanical properties of single AC particles have been found to be dependent on the loading rate. The larger loading rate induces the stronger particle behavior, as shown in Figure 6.2.
- The compression modulus *K*-value and the breaking force of AC particles are very sensitive to the variation in loading rate. Both are increased with loading rate due to less time for stress relaxation.
- The displacement at fracture for the AC particles appears to be independent of loading rate in the tested range, which indicates that the fracture of AC particles is a deformation controlled event. The exact reason for this behavior is unclear.

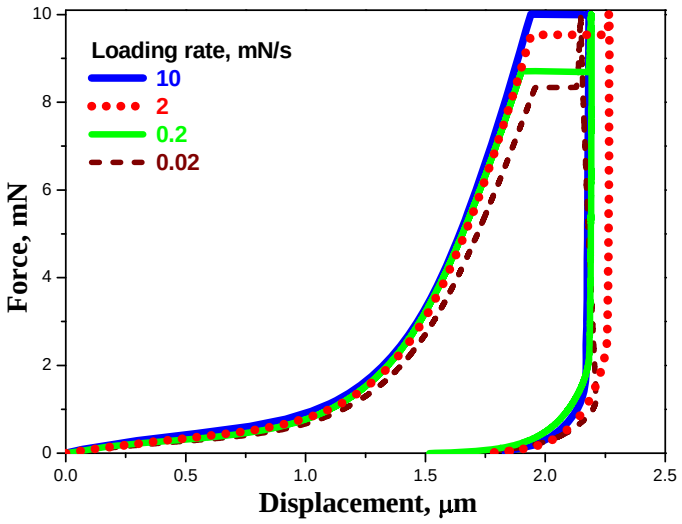

Figure 6.2 The load-displacement behaviors of 3.0μm AC particles under different loading rate.

Particle size effect

- Five groups of PS-DVB particles with same chemical compositions (98% styrene crosslinked with 2% divinylbenzene) have been studied. The particle diameters were 2.6, 5.1, 15.3, and 20 to 25.1μm respectively. For these particles, a strong particle size effect on the stress-strain behavior has been discovered: the smaller the size is, the harder the particle behaves, as shown in Figure 6.3.

- The potential influencing factors on the mechanisms of the particle size effect are analyzed. The accumulative pre-strain induced by the presence of pre-load and the adhesion between the soft particles and the silicon substrate or the rigid flat punch seems to be of secondary nature.
- The surface shell, in which there is a different crosslink distribution resulting in distinct material properties from the particle core, can possibly be used to explain the size effect. FEM solution has verified the influence of "core-shell" structure. Further experimental work and investigation by molecular dynamics simulation is necessary to verify the mechanisms of the particle size effect.

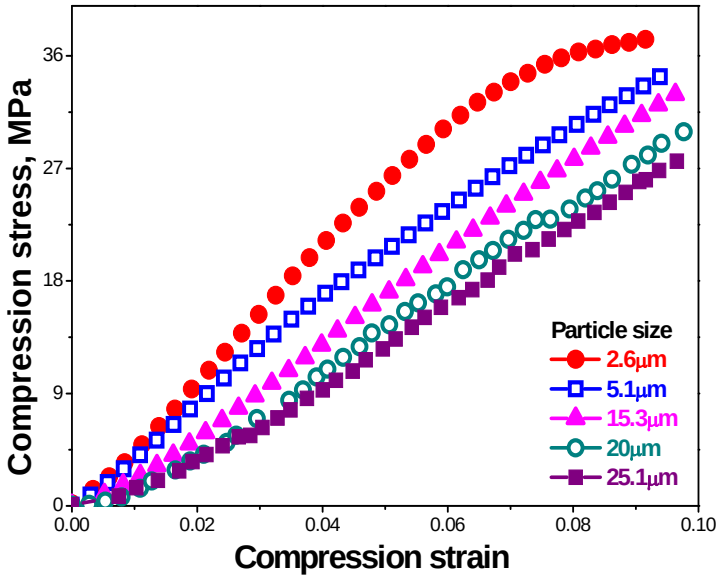

Figure 6.3 The compression stress-strain behaviors of PS particles with same chemistry but different particle size.

Crosslink density effect

- Another series of PS-DVB particles with same size 15μm but different crosslink density varied from 2% to 55% has been characterized using the nanoindentation-based flat punch method. The obtained stress-strain behaviors of particles are shown in Figure 6.4. The crosslink effect on the mechanical properties of particles has been revealed. Increasing the crosslink density induces a shift in the particle deformation behavior from yield behavior to brittle fracture.
- Increasing crosslink density, the compression modulus of the particle increases. The dominating mechanism is that the crosslinking restrict the possibility of the polymer chain to rearrange and hence redistribute the internal stress.

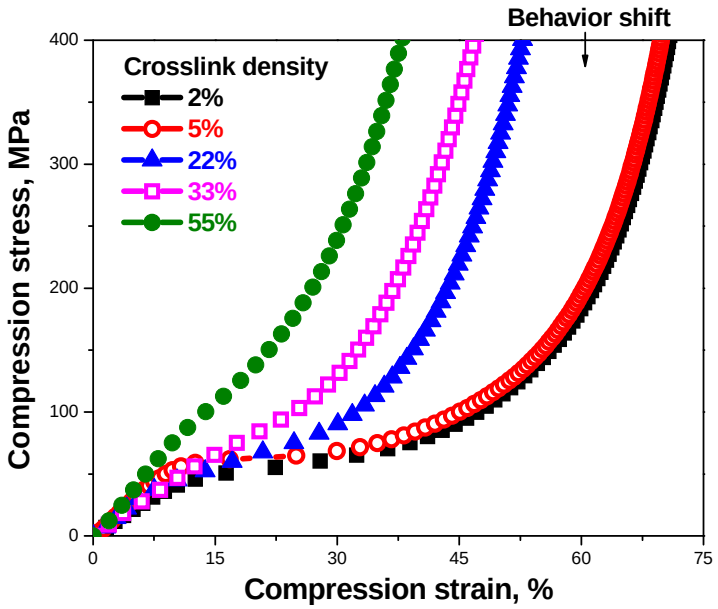

Figure 6.4 The compression stress-strain behaviors of PS particles with same size 15.0μm in diameter but different crosslink density.

6.1.3 Mechanical Properties of Metal Coated Polymer Particles

Nanoscale metal coating effect

- As shown in Figure 6.5, through comparing the mechanical responses of Ni/Au coated acrylic particle with identical but uncoated particles, it has been found that the nanoscale metal coating plays an interesting strengthening effect on the particle behavior.
- Both cracking of the metal coating and the delamination of the coating from the polymer core have been observed during mechanical testing and subsequent investigation by SEM. By increasing the mechanical loads, the cracking and delamination are aggravated.
- The fracture of the polymer core partly happens due to the failure of the metal coating. Two possible explanations for that have been discussed. One is that the Ni/Au coating fragments might induce defects to the polymer core during the cracking of the coating. The other is that the polymer core could be affected by the strong acids used to activate the polymer surface to introduce nucleation sites during the plating process. Further investigation is required to clarify this mechanism.

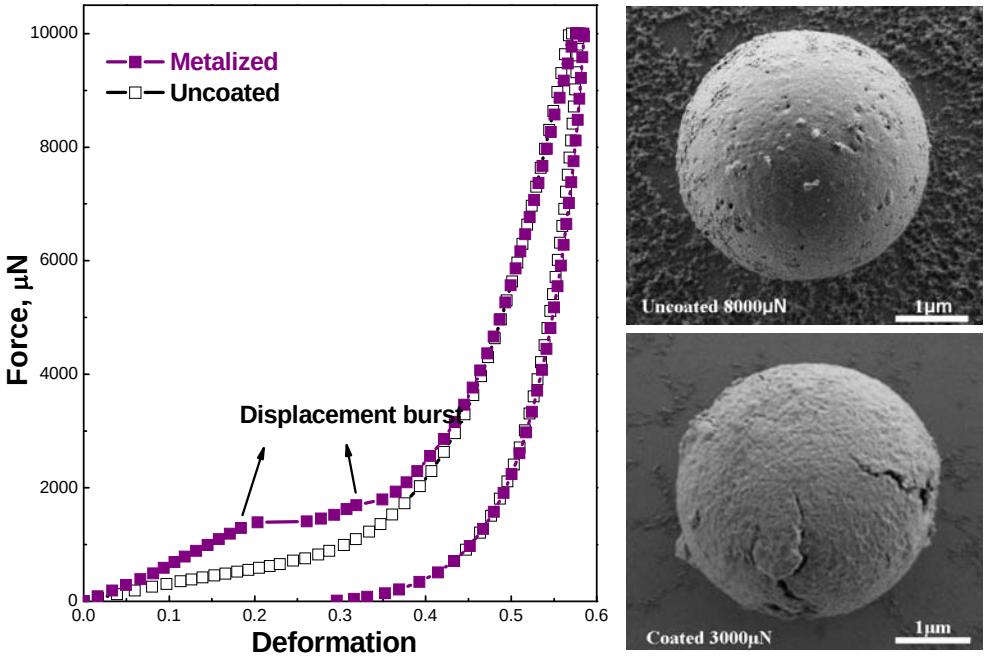

Figure 6.5 The comparison of mechanical behaviors of metal coated and uncoated polymer particles and the corresponding SEM images.

Deformation process

Based on the results of mechanical testing and SEM observation on coated and uncoated particles, a three-stage deformation process of Ni/Au coated acrylic particle has been identified.

- Initially the Ni/Au coating strongly strengthens the particles. The metal coated particle is much stronger than the uncoated one.
- Secondly, the effect of Ni/Au coating is significantly reduced when the cracking of the Ni/Au coating and the delamination between the Ni/Au coating and the polymer core occur. During this stage, the strengthening effect of the metal layer is reduced as the cracking and delamination of the metal continues.
- In the third and last phase with a relatively large deformation, the effect of Ni/Au coating vanishes completely and the coated particle shows nearly identical behavior with the uncoated ones.

Loading rate effect

- By compressing the Ni/Au coated acrylic particle using different loading rate, it has been found that the compression stress-strain relationship is strongly rate-dependent. As shown in Figure 6.6, increasing the deformation rate increases the apparent compression stress of the particle.

- Also the failure mode of the metal coating seems to change with changing deformation rate. A consistent behavior was observed after SEM investigation of the particles. The cracking of the metal coating propagates in the circumferential direction at small loading rate but in the meridian direction under higher loading rates.
- The corresponding mechanisms have been discussed and are possibly contributed by the intrinsic difference between the deformation resistance of metal and polymer under compression.

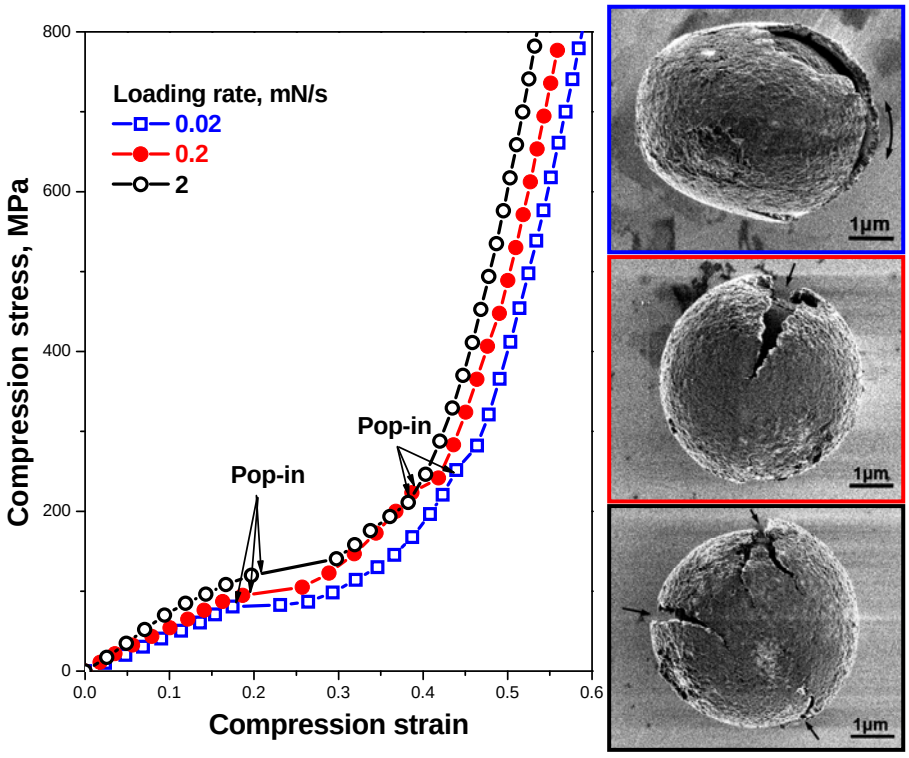

Figure 6.6 The compression stress-strain curves of Ni/Au coated AC particles at three loading rates and the corresponding SEM images of particles.

6.2 Recommendations for Further Work

The research carried out in this thesis has given rise to a number of key topics for future work on the mechanics of micron-sized polymer particles.

- A better understanding of the chemistry and the material structure of the polymer is important to further the understanding of the mechanical behavior of the particles. This includes properties like the effective microscopic crosslink distribution inside particles, the Poisson's ratio as a function of strain and strain rate, and so on. This could be achieved by using advanced characterization methods.

- The temperature effect on the mechanical properties of tested particles is of large interest since the polymer behavior is temperature dependent. The manufacturing of the ACA assembly is actually a combined thermal and mechanical process. Therefore the particle properties under high temperature (up to 180°C) conditions are important to characterize. The Hysitron instrument has an optional heated substrate holder that has been used, however, the indenter will still be at or close to the room temperature which means that there is a large and unknown temperature gradient across the particle, and hence the results are difficult to utilize. To be able to perform high temperature characterization we will need a system for active or passive heating of the indenter, without affecting the transducer.
- It would also be of significant interest to measure the electrical resistance across the metallized particle during mechanical compression. Due to the low expected contact resistance, the test setup will require 4 wire measurement techniques (Kelvin type) and both punch and substrate made of high conductivity materials.
- The interfacial properties between the metal coating and the polymer core are another critical parameter. Due to the complexity and difficulty of investigation on the spherical geometry, the metal thin film – polymer flat substrate system could be considered as reference and tested using for instance scratch testing. Alternatively, a cross section of the particle including the polymer – metal interface can be made using a cryogenic microtome technique.
- Testing of metal coated polymer particles with different polymer chemistry and varied coating thickness could be undertaken to find the conductive particles with optimized properties for ACA application. Analytical and computational modeling could be carried out to investigate the physical basis for this work.
- Analysis using molecular dynamic simulation is highly valuable to undertake, which represents an interface between experiments and theories. The deformation mechanism, the viscoelasticity of the polymer particle, the interfacial properties between the metal coating and the polymer core, etc., could be identified in molecular level. This will link the mechanical properties to the molecular structure of particles. It could assist the understanding of the particle behavior from molecular structure and thus facilitate the design and manufacturing of particles.

REFERENCES

[1] http://www.forskningsradet.no/servlet/Satellite?c=Page&cid=1226993562769&p=1226993562769&pagename=nanomat%2FHovedsidemal.

[2] http://www.forskningsradet.no/.

[3] http://www.conpart.no/.

[4] http://www.invitrogen.com/site/us/en/home/brands/Dynal.html.

[5] Ugelstad J, Mfutakamba H R, Mørk P C, Ellingsen T, Berge A, Schmid R, et al., *Preparation and application of monodisperse polymer particles*. Journal of Polymer Science: Polymer Symposia, 1985; **72**: 225-240.

[6] Ugelstad J, Berge A, Ellingsen T, Schmid R, Nilsen T N, Mor P C, et al., *Preparation and application of new monosized polymer particles*. Progress in Polymer Science, 1992; **17**: 87-161.

[7] http://www.ntnu.no/kjempros/ugelstad_laboratory.

[8] http://no.wikipedia.org/wiki/John_Ugelstad.

[9] Lindmo T, Børmer O, Ugelstad J, Nustad K, *Immunometric assay by flow cytometry using mixtures of two particles of different affinity*. Journal of Immunological Methods, 1990; **126**: 183-189.

[10] Treleaven J G, Gibson F M, Ugelstad J, Rembaum A, Philip T, Caine G D, et al., *The removal of Neuroblastoma cells from bone marrow using monoclonal antibodies conjugated to magnetic microspheres*. Lancet, 1984; **14**: 70-73.

[11] Ellingsen T, Aune O, Ugelstad J, Hagen S, *Monosized stationary phases for chromatography*. Journal of Chromatography, 1990; **535**: 147-161.

[12] Ellingsen T, Aune O, Berge A, Kilaas L, Schmid R, Stenstad P, et al., *Monosized polymer particles in biochemical and biomedical separations*. Makromolekulare Chemie, Macromolecular Symposia, 1993; **70/71**: 315 – 326.

[13] Fommum G, Johansson C, Molteberg A, Morup S, Aksnes E, *Characterisation of Dynabeads® by magnetization measurements and Mossbauer spectroscopy*. Journal of Magnetism and Magnetic Materials, 2005; **193**: 41-47.

[14] http://www.sony.com.

[15] http://www.hitachi-chem.co.jp/english/.

[16] Forrest S R, *The path to ubiquitous and low-cost organic electronic appliances on plastic*. Nature, 2004; **428**: 911-918.

REFERENCES

[17] Lin Y C, Zhong J, *A review of the influencing factors on anisotropic conductive adhesives joining technology in electrical applications*. Journal of Materials Science, 2008; **43**: 3072-3093.

[18] Kwon W S, Paik K W, *Experimental analysis of mechanical and electrical characteristics of metal-coated conductive spheres for anisotropic conductive adhesives (ACAs) interconnection*. IEEE Transactions on Components and Packaging Technologies, 2006; **29**: 528-534.

[19] Kim D O, Jin J H, *Mechanical property investigation of single polymer particles with the variation of molecular structure of crosslinking monomer*. Journal of Applied Polymer Science, 2007; **105**: 783-789.

[20] Dou G, *Mechanical and electrical characterisation of anisotropic conductive adhesive particles*. PhD Thesis, Loughborough University, 2007.

[21] Kristiansen H, Liu J, *Overview of conductive adhesive interconnection technologies for LCDs*. The Proceedings of the First IEEE International Symposium on Polymeric Electronics Packaging, 1997; p223-232.

[22] Kristiansen H, Liu J, *Overview of conductive adhesive interconnection technologies for LCDs*. IEEE Transactions on Components, Packaging, and Manufacturing Technology, 1998; **21**: 208-214.

[23] Kristiansen H, Zhang Z L, Liu J, *Characterization of mechanical properties of metal-coated polymer spheres for anisotropic conductive adhesive*. Proceedings of 10th International Symposium on Advanced Packaging Materials, Processes, Properties and Interfaces, Irvine 2005, p209-213.

[24] Johnson K L, Greenwood J A, *An adhesion map for the contact of elastic spheres*. Journal of Colloid and Interface Science, 1997; **192**: 326-333.

[25] Kogut L, Etsion I, *Elastic-plastic contact analysis of a sphere and a rigid flat*. Journal of Applied Mechanics, 2002; **59**: 657-662.

[26] Kogut L, Etsion I, *Adhesion in elastic-plastic spherical microcontact*. Journal of Colloid and Interface Science, 2003; **261**: 372-378.

[27] He J Y, Zhang Z L, Kristiansen H, *Mechanical properties of nanostructured polymer particles for anisotropic conductive adhesives*. International Journal of Materials Research, 2007; **98**: 389-392.

[28] He J Y, Zhang Z L, Midttun M, Fonnum G, Modahl G I, Kristiansen H, Redford K, *Size effect on mechanical properties of micron-sized PS-DVB polymer particles*. Polymer, 2008; **49**: 3993-3999.

[29] He J Y, Zhang Z L, Kristiansen H, *Nanomechanical characterization of Single Micron-Sized Polymer Particles*. Journal of Applied Polymer Science, 2009; **113**: 1398-1405.

[30] He J Y, Helland T, Zhang Z L, Kristiansen H, *Fracture of micrometre-sized Ni/Au coated polymer particles*. Journal of Physics D: Applied Physics, 2009; **42**: 085405.

[31] He J Y, Zhang Z L, Kristiansen H, *Compression Properties of Individual Micron-sized Acrylic Particles*. Materials Letters, 2009; **63**: 1696-1698.

[32] He J Y, Zhang Z L, Kristiansen H, *Nanoindentation-based flat punch characterization of single monodisperse acrylic particles*. Proceedings of 16th International Conference on Composites/Nano Engineering, 2007; CD copy.

[33] He J Y, Zhang Z L, Kristiansen H, *Nanomechanics of micron sized polymer particles*. Proceedings of 21st Nordic Seminar on Computational Mechanics, 2008; p253-256.

[34] He J Y, Zhang Z L, Helland T, Kristiansen H, *Physical properties of metal coated polymer particles for Anisotropic Conductive Adhesive*. Proceedings of NSTI Nanotech 2009, 2009; p262-265.

[35] He J Y, Zhang Z L, Kristiansen H, *Failure of nanostructured composite particles: the loading rate effect*. Submitted.

[36] Fischer-Cripps A C, *Nanoindentation*. Springer, New York, 2004.

[37] Li X, Bhushan B, *A review of nanoindentation continuous stiffness measurement technique and its applications*. Materials Characterization, 2002; **48**: 11-36.

[38] Vanlandingham M R, *Review of Instrumented Indentation. Journal of Research of the National Institute of Standards and Technology*, 2003; **108**: 249-265.

[39] Oliver W C, Pharr G M, *An improved technique for determining hardness and elastic-modulus using load and displacement sensing indentation experiments*. Journal of Materials Research, 1992; **7**: 1564-1583.

[40] Pharr G M, *Measurement of mechanical properties by ultra-low load indentation*. Materials Science and Engineering A, 1998; **253**: 151-159.

[41] Vlassak J J, Nix W D, *Measuring the elastic properties of anisotropic materials by means of indentation experiments*. Journal of the Mechanics and Physics of Solids, 1994; **42**: 1223-1245.

[42] Vlassak J J, Ciavarella M, Barber J R, Wang X, *The indentation modulus of elastically anisotropic materials for indenters of arbitrary shape*. Journal of the Mechanics and Physics of Solids, 2003; **51**: 1701-1721.

REFERENCES

[43] Mukhopadhyay N K, Paufler P, *Micro- and nanoindentation techniques for mechanical characterisation of materials*. International Materials Reviews, 2006; **51**: 209-245.

[44] Zhu Y, Ke C, Espinosa H D, *Experimental techniques for the mechanical characterization of one-dimensional nanostructures*. Experimental Mechanics, 2007; **47**: 7-24.

[45] Gouldstone A, Chollacoop N, Dao M, Li J, Minor A M, Shen Y L, *Indentation across size scales and disciplines: recent developments in experimentation and modeling*. Acta Materialia, 2007; **55**: 4015-4039.

[46] Lewis G, Nyman J, *The use of nanoindentation for characterizing the properties of mineralized hard tissues: State-of-the art review*. Journal of Biomedical Materials Research - Part B Applied Biomaterials, 2008; **87**: 286-301.

[47] Grabco D, Shikimaka O, Harea E, *Translation-rotation plasticity as basic mechanism of plastic deformation in macro-, micro- and nanoindentation processes*. Journal of Physics D: Applied Physics, 2008; **41**: 074016.

[48] Vlassak J J, Nix W D, *New bulge test technique for the determination of Young's modulus and Poisson's ratio of thin films*. Journal of Materials Research, 1992; **7**: 3242-3249.

[49] De Boer M P, Gerberich W W, *Microwedge indentation of the thin film fine line - II. Experiment*. Acta Materialia, 1996; **44**: 3177-3187.

[50] Clifford C A, Sear M P, *Modelling of nanomechanical nanoindentation measurements using an AFM or nanoindenter for compliant layers on stiffer substrates*. Nanotechnology, 2006; **17**: 5283-5292.

[51] Le Bourhis E, *Indentation mechanics and its application to thin film characterization*. Vacuum, 2008; **82**: 1353-1359.

[52] Cross G L W, O'Connell B S, Pethica J B, Rowland H, King W P, *Variable temperature thin film indentation with a flat punch*. Review of Scientific Instruments, 2008; **79**: 013904 (13pp).

[53] Choi Y, Lee H S, Kwon D, *Analysis of sharp-tip-indentation load-depth curve for contact area determination taking into account pile-up and sink-in effects*. Journal of Materials Research, 2004; **19**: 3307-3315.

[54] Han S M, Saha R, Nix W D, *Determining hardness of thin films in elastically mismatched film-on-substrate systems using nanoindentation*. Acta Materialia, 2006; **54**: 1571-1581.

[55] Zhang H, Li D Y, *The mechanisms of interfacial failure for lateral force-sensing microindentation test: finite element analysis*. Acta Materialia, 2008; **56**: 6197-6204.

[56] Hysitron, *TriboIndenter® User Manual*, NRL-M-023 V.6.0, 2005.

[57] Sjoblom J, Lindman B, Stenius P, *Advances in Colloid Structure. Springer-Verlag*, New York, 1992.

[58] Kawaguchi H, *Functional polymer microspheres*. Progress in Polymer Science, 2000; **20**: 1171-1210.

[59] Zhang G, Niu A, Peng S, Jiang M, Tu Y, Li M, Wu C, *Formation of Novel Polymeric Nanoparticles*. Accounts of Chemical Research, 2001; **34**: 249-256.

[60] Roucoux A, Schulz J, Patin H, *Reduced transition metal colloids: A novel family of reusable catalysts?*. Chemical Reviews, 2002; **102**: 3757-3778.

[61] Van Blaaderen A, *Colloidal molecules and beyond*. Science, 2003; **301**: 470-471.

[62] Vlasov Y A, Bo X Z, Sturm J C, Norris D J, *On-chip natural assembly of silicon photonic bandgap crystals*. Nature, 2001; **414**: 289-293.

[63] Haynes C L, McFarland A D, Smith M T, Hulteen J C, Van Duyne R P, *Angle-resolved nanosphere lithography: manipulation of nanoparticle size, shape, and interparticle spacing*. Journal of Physical Chemistry B, 2002; **106**: 1898-1902.

[64] Patolsky F, Weizmann Y, Katz E, Willner I, *Magnetically amplified DNA assays (MADA): Sensing of viral DNA and single-base mis-matches by using nucleic acid modified magnetic particles*. Angewandte Chemie – International Edition, 2003; **42**: 2372-2376.

[65] Yellen B, Friedman G, Feinerman A, *Printing superparamagnetic colloidal particle arrays on patterned magnetic film*. Journal of Applied Physics, 2003; **93**: 7331-7333.

[66] Odian G, *Principles of polymerization*. 4th ed. Wiley Press, 2004.

[67] Ahmed S M, *Effects of agitation and the nature of protective colloid on particle size during suspension polymerization*. Journal of Dispersion Science and Technology, 1984; **5**: 421-432.

[68] Thomson B, Rudin A, Lajoie G, *Dispersion copolymerization of styrene and divinylbenzene. II. Effect of crosslinker on particle morphology*. Journal of Applied Polymer Science, 1996; **59**: 2009-2028.

[69] Ishizu K, Tahara N, *Microsphere synthesis by emulsion copolymerization of methyl methacrylate with binary macromonomer blends*. Polymer, 1996; **37**: 1729-1734.

[70] Inukai S, Tanma T, Orihara S, Konno M, *A simple method for producing micron-sized highly monodisperse polystyrene particles in aqueous media: effects of impeller speed on particle size distribution*. Trans IChemE Part A, 2001; **79**: 901-905.

[71] K Kobayashi, M Senna, *Independent control of mechanical and chemical properties of monodispersed polystyrene-divinyl benzene microspheres by two-step polymerization*. Journal of Applied Polymer Science, 1992; **46**: 27-40.

[72] Okubo M, Shiozaki M, Tsujihiro M, Tsukuda Y, *Preparation of micron-size monodisperse polymer particles by seeded polymerization utilizing the dynamic monomer swelling method*. Colloid and Polymer Science, 1991; **269**: 222-226.

[73] Ugelstad J, Kaggerud K H, Hansen F K, Berge A, *Absorption of low molecular weight compounds in aqueous dispersions of polymer-oligomer particles*. Makromolekulare Chemie, 1979; **180**: 737-744.

[74] Ugelstad J, Mork P C, Kaggerud K H, Ellingsen T, Berge A, *Swelling of oligomer-polymer particles. New methods of preparation of emulsion and polymer dispersions*. Advances in Colloid and Interface Science, 1980; **13**: 101-140.

[75] Ugelstad J, Mørk P C, Nordhuus J, Mfutakamba H, Soleimany E, Berge A, et al., *Thermodynamics of swelling. Preparation and application of some composite, monosized polymer particles*. Makromolekulare Chemie Supply, 1985; **10/11**: 215-234.

[76] Skjeltorp A T, Ugelstad J, Ellingsen T, *Preparation of nonspherical, monodisperse polymer particles and their self organization*. Journal of Colloid and Interface Science. 1986; **113**: 557-582.

[77] Hansen F K, Ugelstad J, *Particle nucleation in emulsion polymerization. I. A theory for homogeneous nucleation*. Journal of Polymer Science: Polymer Chemistry Edition. 1978; **16**: 1953-1979.

[78] Hansen F K, Ugelstad J, *Particle nucleation in emulsion polymerization. II. Nucleation in emulsifier-free systems investigated by seed polymerization*. Journal of Polymer Science: Polymer Chemistry Edition. 1979; **17**: 3033-3045.

[79] Hansen F K, Ugelstad J, *Particle nucleation in emulsion polymerization. III. Nucleation in systems with anionic emulsifier investigated by seeded and unseeded polymerization*. Journal of Polymer Science: Polymer Chemistry Edition. 1979; **17**: 3047-3067.

[80] Hansen F K, Ugelstad J, *Particle nucleation in emulsion polymerization. IV. Nucleation in monomer droplets*. Journal of Polymer Science: Polymer Chemistry Edition. 1979; **17**: 3069-3082.

[81] Christensen B E, Myhr M H, Aune O, Hagen S, Berge A, Ugelstad J, *Macroporous, monodisperse particles and their application in aqueous size exclusion chromatography of high molecular weight polysaccharides*. Carbohydrate Polymers, 1996; **29**: 217-223.

[82] Ugelstad J, Soderberg L, Berge A, Bergstrom J, *Monodisperse polymer particles — a step forward for chromatography*. Nature, 1983; **303**: 95-96.

[83] Kulin L I, Flodin P, Ellingsen T, Ugelstad J, *Monosized polymer particles in size-exclusion chromatography: I. Toluene as solvent*. Journal of Chromatography, 1990; **514**: 1-9.

[84] Berge A, ellingsen T, Skjeltorp A T, Ugelstad J, *Scientific Methods for the Study of Polymer Colloids and their Application*. (Candau F and Ottewill R H Eds.), Kluwer Academic Publisher, 1990.

[85] Skjeltorp A T, *One- and two-dimensional crystallization of magnetic holes*. Physical Review Letters, 1983; **51**: 2306-2309.

[86] Skjeltorp A T, *Monodisperse particles and ferrofluids: a fruit-fly model system*. Journal of Magnetism and Magnetic Materials, 1987; **65**: 195-203.

[87] Skjeltorp A T, *Fracture in microsphere monolayers studied by experiment and computer simulation*. Nature, 1988; **335**: 424-426.

[88] Helgesen G, Pieranski P, Skjeltorp T, *Nonlinear phenomena in systems of magnetic holes*. Physical Review Letters, 1990; **64**: 1425-1428.

[89] Watanabe I, Takemura K, Shiozawa N, Watanabe O, Kojima K, Ohta T, *Flip-chip interconnection to various substrates using anisotropic conductive adhesive films*. Journal of Electronics Manufacturing, 1995; **5**: 273-276.

[90] Lai Z, Liu J, *Anisotropically conductive adhesive flip-chip bonding on rigid and flexible printed circuit substrates*. IEEE transactions on components, packaging, and manufacturing technology. Part B, Advanced packaging, 1996; **19**: 644-660.

[91] Liu J, Tolvgård A, Malmodin J, Lai Z, *Reliable and environmentally friendly packaging technology - flip-chip joining using anisotropically conductive adhesive*. IEEE Transactions on Components and Packaging Technologies, 1999; **22**: 186-190.

[92] Yeung N H, Chan Y C, Tan C W, *Effect of bonding force on the conducting particle with different sizes*. Journal of Electronic Packaging, Transactions of the ASME, 2003; **125**: 624-629.

[93] Tan C W, Chan Y C, Yeung N H, *Behavior of anisotropic conductive joints under mechanical loading*. Microelectronics Reliability, 2003; **43**: 481-486.

[94] Whalley D C, Kristiansen H, Liu J, *Characterisation of anisotropic conductive adhesive compression during: The assembly process*. Advances in Electronic Packaging, 2003; **1**: 183-189.

[95] Yue J, Camelio J A, Chin M, Cai W, *Product-oriented sensitivity analysis for multistation compliant assemblies*. Journal of Mechanical Design, Transactions of the ASME, 2007; **129**: 844-851.

[96] Yim M J, Paik K W, *Design and understanding of anisotropic conductive films (ACF's) for LCD packaging*. IEEE Transactions on Components, Packaging, and Manufacturing Technology Part A, 1998; **21**: 226-234.

[97] Yim M J, Hwang J S, Kim J G, Ahn J Y, Kim H J, Kwon W, Paik K W, *Highly reliable Flip-Chip-on-Flex Package using multilayered anisotropic conductive film*. Journal of Electronic Materials, 2004; **33**: 76-82.

[98] Yim M J, Kim H J, Chung C K, Paik K W, *Degradation mechanism and reliability of flip chip interconnects using anisotropic conductive adhesives for high current density packaging applications*. Proceedings of IEEE the 56th Electronic Components & Technology Conference, San Diego, 2006, p338-343.

[99] Sarkar G, Mridha S, Tan T C, Wu Y T, Sem C K, *Flip chip interconnect using anisotropic conductive adhesive*. Journal of Materials Processing Technology, 1999; **89-90**: 484-490.

[100] Chin M, Iyer K A, Hu S J, *Prediction of electrical contact resistance for anisotropic conductive adhesive assemblies*. IEEE Transactions on Components and Packaging Technologies, 2004; **27**: 317-326.

[101] Chin M, Barber J R, Hu S J, *Effect of elastic recovery on the electrical contact resistance in anisotropic conductive adhesive assemblies*. IEEE Transactions on Components and Packaging Technologies, 2006; **29**: 137-144.

[102] Galloway J, Syed A, Kang W, Kim J Y, Cannis J, Ka Y H, et al., *Mechanical, thermal, and electrical analysis of a compliant interconnect*. IEEE Transactions on Components and Packaging Technologies, 2005; **28**: 297-302.

[103] Dou G B, Chan Y C, Liu J, *Electrical conductive characteristics of anisotropic conductive adhesive particles*. Journal of Electronic Packaging, Transactions of the ASME, 2003; **125**: 609-616.

[104] Dou G, Whalley D, Liu C, *The effect of co-planarity variation on anisotropic conductive adhesive assemblies*. Proceedings – Electronic Components and Technology Conference, 2006; p932-938.

[105] Kristiansen H, Shen Y, Liu J, *Characterisation of mechanical properties of metal-coated polymer spheres for anisotropic conductive adhesive*. First International IEEE Conference on Polymers and Adhesives in Microelectronics and Photonics, 2001; p344-348.

[106] Kristiansen H, Gronlund T O, Liu J, *Characterisation of metal-coated polymer spheres and its use in anisotropic conductive adhesive*. Proceedings of 16th IEEE CPMT Conference on High Density Microsystem Design and Packaging and Component Failure Analysis, 2004; p259-263.

[107] Wang X, Wang Y, Chen G, Liu J, Lai Z, *Quantitative estimate of the characteristics of conductive particles in ACA by using nano indenter*. IEEE transactions on components, packaging, and manufacturing technology. Part A, 1998; **21**: 248-251.

[108] Fu Y, Wang Y, Wang X, Liu J, Lai Z, Chen G, Willander M, *Experimental and theoretical characterization of electrical contact in anisotropically conductive adhesive*. IEEE Transactions on Advanced Packaging, 2000; **23**: 15-21.

[109] Paik K W, Kwon W S, *Conduction mechanism of Anisotropic Conductive Adhesives (ACAs): Conductor ball deformation and build-up of contraction stresses*. Proceedings of 10th International Symposium on Advanced Packaging Materials, Processes, Properties and Interfaces, Irvine 2005, p214-220.

[110] Kim D O, Jin J H, Won II S, Seok H O, *Observation for mechanical property variations of single polymer particles*. Journal of Applied Polymer Science, 2007; **105**: 585-592.

[111] Kim D O, Jin J H, *Investigation for surface morphology and mechanical property variations of single polymer particles*. Journal of Applied Polymer Science, 2007; **104**: 2350-2360.

[112] Zhang Z L, Kristiansen H, Liu J, *A method for determining elastic properties of micron-sized polymer particles by using flat punch test*. Computational Materials Science, 2007; **39**: 305-314.

[113] Dou G, Whalley D C, Liu C, *Mechanical characterization of individual NiAu coated microsize polymer particles*. Applied Physics Letters, 2008; **92**: 104108 (3pp).

[114] Lee J H, Lee Y, Nam J D, *Tunable surface metal morphologies and electrical properties of monodispersed polystyrene beads coated with metal multilayers via electroless deposition*. Intermetallics, 2009; **17**: 365-369.

[115] Johnson K L, *Contact Mechanics*. University Press: Cambridge, 2003.

[116] Liu K K, Williams D R, Briscoe B J, *Large deformation of a single micro-elastomeric sphere*. Journal of Physics D: Applied Physics, 1998; **31**: 294-303.

[117] http://en.wikipedia.org/wiki/Cyanoacrylate.

Paper I

Mechanical properties of nanostructured polymer particles for Anisotropic Conductive Adhesives

He J Y, Zhang Z L, Kristiansen H.

International Journal of Materials Research 2007; **98**(5): 389- 392.

Is not included due to copyright

Paper II

Size effect on mechanical properties of micron-sized PS-DVB polymer particles

He J Y, Zhang Z L, Midttun M, Fonnum G, Modahl G I, Kristiansen H, Redford K.

Polymer 2008; **49**(18): 3993-3999.

Size Effect on Mechanical Properties of Micron-sized PS-DVB Polymer Particles

J. Y. He[a], Z. L. Zhang[a], M. Midttun[a], G. Fonnum[b], G. I. Modahl[b],

H. Kristiansen[c], K. Redford[c]

[a] NTNU Nanomechanical Lab, Department of Structural Engineering, Norwegian University of Science and Technology, 7491, Trondheim, Norway

[b] Invitrogen Dynal AS, PO box 114 Smestad, 0309 Oslo, Norway

[c] Conpart AS, 2013, Kjeller, Norway

ABSTRACT

A nanoindentation-based flat punch method has been developed to determine the stress-strain behaviour of single micron-sized Ugelstad polystyrene-co-divinylbenzene (PS-DVB) particles in compression. Five groups of particles with identical chemical compositions but different diameters have been tested. The diameter of the PS-DVB particles varied from 2.6μm to 25.1μm. Constant relative deformation rate has been applied with two maximum strain levels of 5% and 10%. Results show that the particle compressive stress-strain behaviour is strongly size-dependent. The smaller the particle size is, the stiffer the particle behaves. Analyses indicate that the pre-load and adhesion during the flat punch test play a minor role on the size effect. The presence of a core-shell structure can possibly be a main contribution to the size effect. Finite element analyses have been carried out to demonstrate this surface shell effect.

Keywords: PS-DVB particles; Flat punch indentation; Size effect.

1. Introduction

Nanoindentation is now a well established tool for probing the mechanical properties, for example, Young's modulus and hardness, at the micro- and nano-scales [1]. During the indentation, the indentation load and displacement are simultaneously monitored and load-displacement curves are recorded. The material hardness and reduced modulus can be

calculated from the contact area determined by the contact depth using an area function of the indentation tip and the contact stiffness obtained by fitting the initial portion of the unloading curve.

One interesting phenomenon, namely indentation size effect (ISE) was revealed more than 50 years ago [2] but so far the mechanisms involved are not fully understood. The hardness defined as the ratio of the applied force to the contact area, is commonly assumed to be independent of the measurement scale. But the hardness measured by nanoindentation for certain metals has been shown to increase with decreasing depth of indentation size within a range typically less than 10μm [3]. In fact, every metal has an intrinsic material length scale, and for indentation depth less than this, the ISE occurs.

The strain gradient effect [4-6], surface effect [7], non-uniformly deformed microstructure [3], interaction between the indenter and the sample [8] are the possible mechanisms for the ISE. The various mechanisms imply a complicated nature of the ISE. During the last decade, the theory of strain gradient plasticity (SGP) developed by Nix and Gao [4] has received attention. In a nanoindentation test, plastic deformation is confined within a small volume, which results in a strain gradient. According to Taylor's dislocation hardening theory, the stored dislocations, which are caused by a homogeneous strain, and the so-called geometrically necessary dislocations, which are significantly affected by the strain gradient, both contribute to the hardness [9].

Most of the studies on the ISE focused on single crystals and polycrystals. This study will report a new area of the indentation related size effect, related to mechanical deformation of monodisperse polymer particles with low cross linking density. The particles are synthesized by the Ugelstad method [10], which is a well known and versatile technology for the manufacturing of monosized polymer particles by a multi-step swelling process. A large number of monomers can be used, and in this case a combination of styrene and DVB has been used giving a cross linking density of about 2%. The coefficient of variance (C.V.) of the size distribution is less than 2%, in which C.V. is the scatter of probability distribution and is defined by the ratio of the standard deviation to the mean.

Micron-sized polymer particles, of 0.5-100μm in diameter, are widely used in food, chemical industries and biotechnology. Recently there is a growing interest in extending the polymer particle technology also for microsystem applications by producing nanostructured polymer particles, especially in Anisotropic Conductive Adhesive (ACA) [11-15]. As a substitute for compact metal particles, the polymer core particles increase the compliance of the interconnection and hence improve the reliability. The introduction of ACA technology can also contribute with reduced package size, lower assembly temperature, and possibly lower cost. For lager particles used for Ball Grid Arrays (BGA) and Chip Scale Packaging (CSP) there is also a significant advantage in terms of reduced environmental impact [16-19]. The functional performance in these applications is strongly connected to the contact area, which is coupled to the deformation level. Therefore, the mechanical properties of

polymer particles are of crucial importance. However, mechanical characterization of single micron-sized particles possesses great challenges, due to the inherent complexity of the spherical geometry and the large deformation involved.

Polymer particles have been used to reinforce the bulk properties of composite materials. The effect of particle size on the bulk mechanical properties of concrete [20], high-impact polystyrene [21-23], polymer blends [24, 25] and polymer latex [26] has been studied extensively. Recently, the mechanical properties of bulk polymer materials reinforced with polystyrene and poly (butyl acrylate) core/shell particles with sizes in tens of nanometers have been reported [27]. The mechanical behaviour of the bulk polymer was found to be strongly influenced by the particle size and the distribution of the composing polymers.

In the present study, the effect of the particle size on the mechanical properties of single particles has been studied. Five groups of commercially available polystyrene-co-divinylbenzene (PS-DVB) particles (Dynospheres®, Invitrogen Dynal AS, NO) with identical chemical compositions but different diameters have been tested using a nanoindentation-based flat punch method. The particles have the same synthesis procedures and chemical compositions but different diameters. The diameter varied from 2.6 to 25.1μm. The nominal compressive stress-strain behaviours of particles are obtained from nanoindentation-based flat punch test results. The effect of the particle diameter on the compressive stress-strain behaviour is analyzed experimentally and the nature of the particle size effect is discussed.

2. Experiment

2.1 Materials

The five groups of polymer particles are made of the same chemical compositions: 98% polystyrene crosslinked with 2% divinylbenzene by Ugelstad method. The diameters of the particles are 2.6, 5.1, 15.3, 20 and 25.1μm. The C.V.s of the size distribution are 1.7, 0.8, 1.2, 1.6 and 1.0%, respectively. The SEM photographs of the smallest and largest particles are shown in Fig. 1. The dry particles are dispersed in 95% industrial ethanol. The very diluted dispersion is exposed to a high frequency ultrasonic vibration to redisperse the particle clusters. A drop of the ethanol–particle suspension is placed on a bare silicon chip (10×10×0.5mm). The specimens are then conditioned in a clean environment for a specific period of time to remove any ethanol left in the particle.

2.2 Apparatus

The indentation tests are performed using a nanomechanical testing system (TriboIndenter® Hysitron Inc., MN., USA) which has a standard mode and a multi-range mode. The standard mode can reach a maximum load capacity of 10mN and a maximum indentation depth of 5μm with a load and displacement resolution of 1nN and 0.1nm, respectively. The

multi-range mode has a maximum load of 4N and a maximum indentation depth of 80μm with a load and displacement resolution of 500nN and 2nm. For the polymer particles in this study, a diamond flat punch with 100μm in diameter was used.

The flat punch is cleaned to remove external impurities such as dust before testing. The flat punch in this experiment requires precise calibration, especially flat punch planarity. The planarity calibration is evaluated by the indents produced by penetration into a polished indium surface. A clean, 100μm diameter circle impressions well pressed on the surface of the polished indium are required for a flat punch to be acceptable. The relatively tip-optics position is also accurately calibrated through the indents on the polished indium.

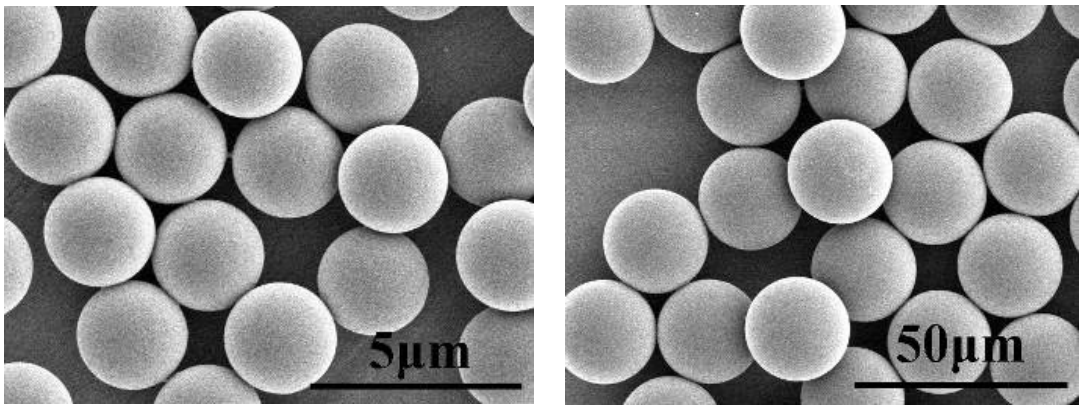

(a) (b)

Fig. 1. SEM photographs of (a) the smallest particle and (b) the largest particle.

2.3 Method

Using the optical microscope, single particles with a sufficient distance (>75μm) to its closest neighbour is located and used for the indentation tests. Fig. 2 illustrates the contact between a rigid flat punch and a single PS-DVB particle. All indentation tests are performed in air and at room temperature (23°C). The room humidity is kept constant about 30% through an air ventilation system. The displacement controlled mode which operates the indentation depth versus time is selected in order to control the nominal strain rate for each group of particles. Two deformation levels, 5% and 10% with corresponding nominal strain rates of 0.01/s and 0.02/s with reference to particle diameter, have been applied to all the particles. A typical test is completed in 12 s where the testing displacement function consists of a linear displacement-increasing segment for 5 s, a 2 s displacement-holding segment, and linear displacement-decreasing segment for 5 s. The heat drift of displacement is monitored for 40 s at pre-load 1μN, and the drift rate calculated by fitting a straight line to the drift displacement versus time graph during the latter 20 s is used to

correct the resulting data. For every group of particles, at least three individual particles are tested in order to check uniformity of particle properties and the repeatability of the results.

Both the standard mode and the multi-range mode are applied. The standard mode is used for testing all the particles up to 5% deformation. For the 10% deformation, multi-range loading mode must be used on the two largest groups of particles. Since two loading modes are involved, it is essential to calibrate the system such that both the standard mode and the multi-range mode yield identical results. The typical indentation force-depth results from the two loading modes with a deformation up to 20% for the 15.3μm diameter particles are shown in Fig. 3. The results are well matched; however, the curve obtained by the multi-range mode is less smooth due to its inferior feedback system compared with the standard mode. Fig. 3 indicates that it is reasonable to believe the both loading modes give the same results.

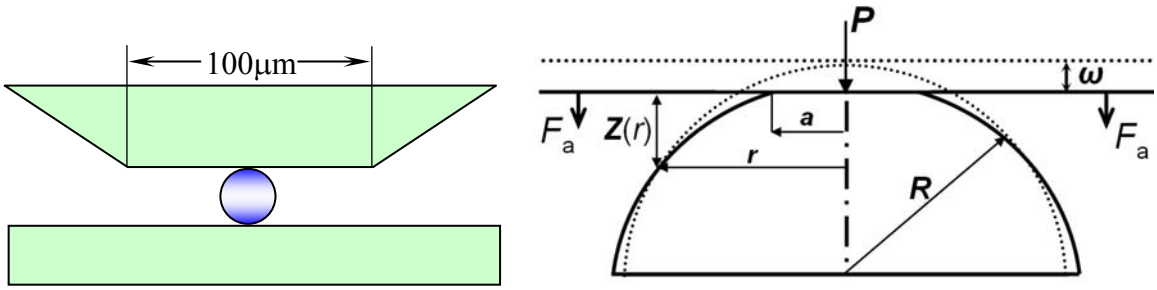

Fig. 2. Schematic plot of the flat punch test (a) and model description (b).

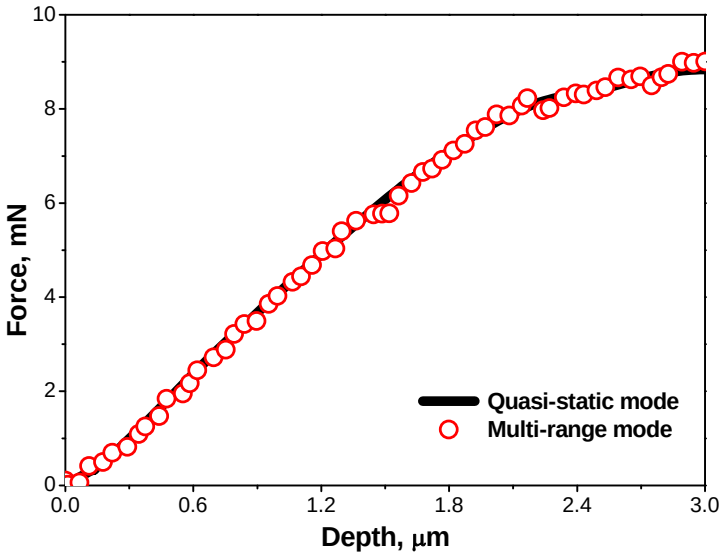

Fig. 3. The loading curves of the 15.3μm diameter particles with different load modes.

3. Results

Load-displacement curves are obtained for all PS-DVB particles at two deformation levels, 5% and 10% deformation shown in Fig. 4(a) and (b), respectively. In Fig. 4(a), every group of particles is compressed to a maximum of 5% deformation and represented by four indentation curves. In Fig. 4(b), each group has three indentation curves and is loaded to a maximum of 10% deformation. The loading segments of each group of particles at the same deformation level are found to be quite repeatable and consistent. This is in contrast to typical bulk polymer materials where mechanical properties show a significant scatter due to variations in microstructure, anisotropy, molecular weight, crosslink density, etc. [28]. Thus, the highly consistent load-displacement curves demonstrated for every group of the PS-DVB particles indicate a very homogeneous material including size distribution, microstructure, chemistry and molecular weight. At the same time it also gives confidence to the experimental setup and reproducibility. To reach 10% deformation the two bigger particles have to be tested using the multi-range mode, and the curves are slightly bumpy, but the trends are very similar to those using the standard mode.

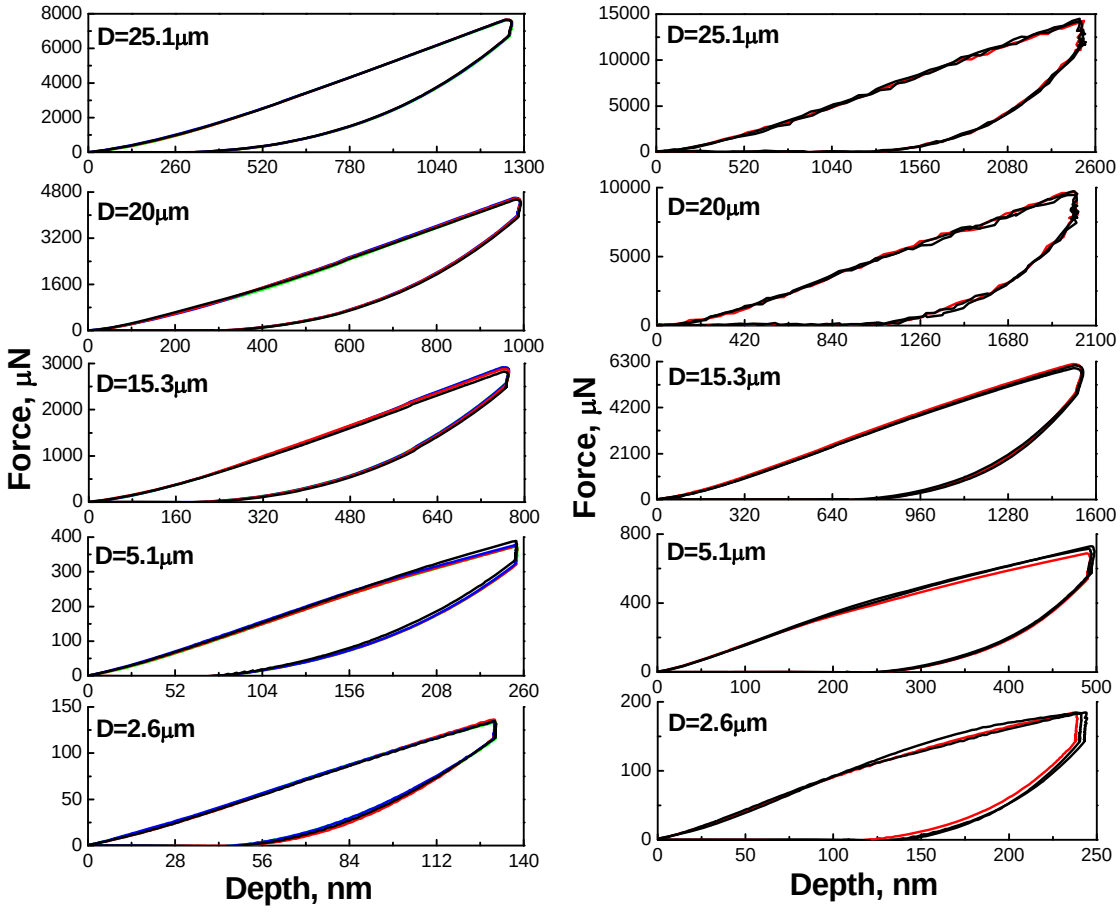

Fig. 4. Indentation load-displacement curves of five group particles (a) at 5% deformation with 0.01/s strain rate and (b) at 10% deformation with 0.02/s strain rate.

During the large deformation compression, the volume and Poisson's ratio of the polymer particles may change continuously with the deformation because of the spherical geometry. It is not possible to obtain the true stress-strain behaviour of particles from those conditions. To compare the mechanical properties of particles with different sizes, the nominal compressive stress-strain behaviours have been used. These are obtained by normalizing the force to the initial cross-section area and the displacement to the initial diameter of particles [29]:

$$\sigma_c = \frac{P}{\pi R^2} \tag{1}$$

$$\varepsilon_c = \frac{2\omega}{D} = \frac{\omega}{R} \tag{2}$$

where σ_c is the nominal compressive stress, ε_c is the nominal compressive strain, P is the contact load, D is particle diameter, R is the initial particle radius, and ω is the half deformation of the sphere (Fig. 2(b)). The nominal compressive stress-strain curves of the five groups of particles at two deformation levels are displayed in Fig. 5(a) and (b), respectively. The focus of this study is the loading part and the unloading stress-strain curves are omitted in Fig. 5.

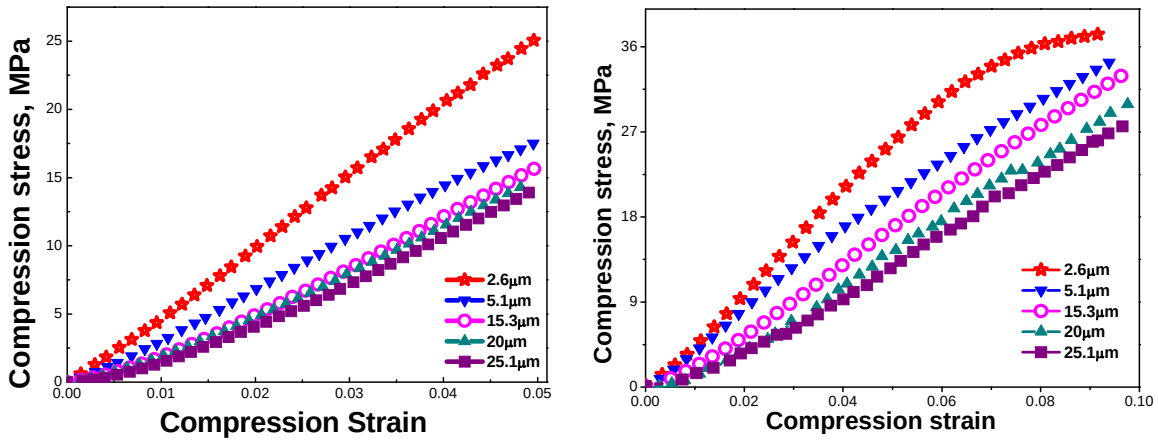

(a) (b)

Fig. 5. Compressive stress-strain curves (a) at 5% deformation with 0.01/s strain rate and (b) at 10% deformation with 0.02/s strain rate.

From the continuum mechanics point of view, stress-strain behaviour is one of the constitutive properties of materials. For particles with different sizes but same chemistry and same strain rate, all the stress-strain curves should collapse into one. But Fig. 5 clearly shows that the compressive stress-strain behaviours of particles are strongly size-dependent, the smaller the particle size, the harder the particles. The smallest particle is the hardest

while the biggest particle is the softest. With the increase of particle size, the size dependence of compressive stress-strain behaviour diminishes gradually.

The nominal compressive stress of all the five groups of particles at 4% deformation level with strain rates 0.01/s and 0.02/s is plotted in Fig. 6, in which the compressive stress is normalized by the corresponding value of the smallest particle. Particles display distinct size effect at both stain rates. The compressive stress of the biggest particle is almost 50% lower than that of the smallest particle at a strain rate of 0.01/s. As the strain rate increases to 0.02/s, the size effect becomes even more pronounced. The size effect also seems to have different trends depending on the strain rate. With the smaller strain rate, the size effect is most evident for the two smaller particle sizes, whereas for the larger strain rate the size effect is more evenly distributed.

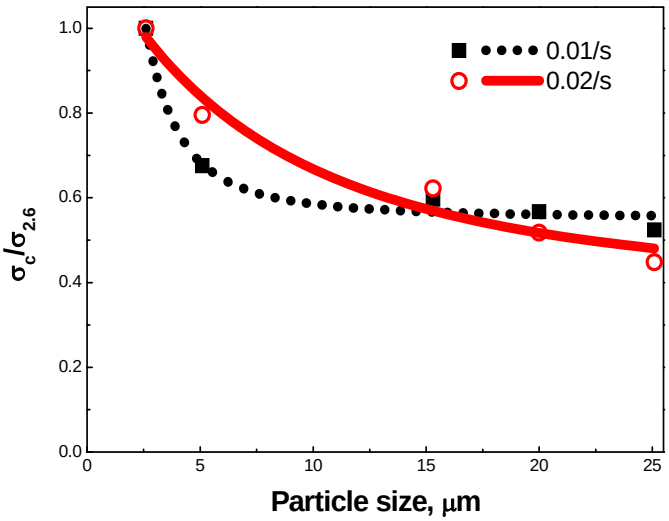

Fig. 6. Particle size dependence of the normalized stress with strain rate 0.01/s and 0.02/s at deformation level 4%.

4. Discussion

The existing theories for indentation size effect are mainly based on dislocation movement and can not predict the behaviour observed for the polymer particles. The deformation mechanisms in polymers are very different from metals due to the absence of dislocations. There are three types of solid polymer behaviours [30]: brittle fracture behaviour, yield behaviour and rubber-like behaviour. Brittle fracture behaviour is characterized by no apparent yield point and obeys Hooke's law at low strain level. Yield behaviour exhibits a maximum point followed by strain softening, usually associated with crazing or shear banding which leads to ductile fracture. Rubber-like behaviour is characterized by a plateau in the stress-strain curve. Polystyrene as linear (non-crosslinked) polymer is known to exhibit brittle fracture causing crazing under tensile stress, however, the same material

shows yield behaviour displaying shear banding in compression. Crazing deformation is a localized yielding behaviour and can be observed as a whitening of the polymer in the region of maximum deformation. The volume of the polymer increases through formation of micro-cracks, which are bridged by polymer fibrils. Shear banding deformation which is highly dependent on temperature and strain rate is characterized by planes of slip at 45° to the direction of stress and involves the local orientation of the polymer. In contrast, PS-DVB has the microstructure of the crosslinked network, which deforms by the slip of flexible chain. The crosslinking is important to avoid the inter-chain slip. The crosslink density should not only be in a certain range to keep away from the inter-chain slip but also have an enough space between two crosslink points to allow a good deformability.

For the PS-DVB particles there are possibly many factors contributing to the size effect. The experimental method itself may bring some uncertainties to the results. For instance, the pre-load used for determining the zero contact surfaces on the nanoindentation sample is applied to the particles before indentation. Given that the particles do not fully recover after this pre-load, the indentation does therefore not begin from a perfect point contact but with a finite contact area, which will have significant influence at small deformations. Similarly, the adhesion between the soft polymer particle and the rigid flat punch or the substrate could pose a similar effect. During synthesis of PS-DVB particles from water suspension there has been observed a "core-shell" structure [31] on the particles by TEM. In the shell, the cross-link density is much higher than that in the inner particle. This surface shell effect might be prominent for smaller particles.

In the following, potential factors both in the particle synthesis and in the experiments are analyzed in order to clarify the mechanisms of the observed size effect.

4.1 The effect of pre-load

One of these factors is caused by the factory settings of the Hysitron TriboIndenter. During the nanoindentation, the flat punch will first contact the particle using a certain pre-load and define the corresponding height as the indentation starting contact point. The instrument keeps a defined pre-load for a certain time, and uses the acquired information to determine the thermal drift of the system. Before starting the indentation, the machine retracts a certain distance. However, the particle might not fully recover after the pre-load cycle, meaning that the indentation starts from an already deformed particle. The induced stress σ_D during the pre-load is given by:

$$\sigma_D = \frac{P_r}{\pi R^2} \tag{3}$$

Using the Hertz equation [32], the corresponding strain ε_D can be calculated as:

$$\varepsilon_D = \left(\frac{\sigma \cdot \pi}{E}\right)^{2/3} = \left(\frac{P_r}{ER^2}\right)^{2/3} \tag{4}$$

where P_r is the pre-load which was set to 1μN for all the particles and for both standard and multi-range modes. R is the initial particle radius as shown in Fig. 2(b). E is the reduced modulus defined as $E = \frac{4}{3}[\frac{1-\nu_1^2}{E_1} + \frac{1-\nu_2^2}{E_2}]^{-1}$, in which, E_1, ν_1 and E_2, ν_2 are the elastic moduli and Poisson's ratios of the two contacted objects, respectively. The diamond is a rigid body therefore the contribution of the diamond flat punch can be regarded as negligible. The silicon substrate used in the experiment has the following characteristics, $E_{Si} = 150GPa$ [33] and $\nu_{Si} = 0.27$ [34]. For the PS-DVB particle, the elastic modulus and Poisson's ratio are both unknown, so the empirical values $E_{PS} = 1.5GPa$ and $\nu_{PS} = 0.33$ [29] are used in the analysis. With an *E*-modulus two order of magnitudes higher than the polymer, also the contribution from the substrate can be regarded as negligible. Obviously the constant pre-load has the largest effect on the 2.6μm diameter particle. Using the values above, the strain, ε_D, imposed onto the smallest particle during the pre-load is found to be 4.14×10^{-3} which is maximum if there is no recovery.

4.2 The adhesion effect

The contact of an elastic sphere with an undeformed flat plane is of interest since the interaction between them is applicable in problems such as post-chemical mechanical polishing cleaning [35] and the thermal and electrical conductivities between contacting rough surfaces [36] and more specifically in applications like ACA where metal-coated polymer particles are compressed between two contact pads. Two basic adhesion models have been suggested in the literature. One model developed by Johnson, Kandall and Roberts, known as JKR model [37] assumes that attractive intermolecular surface forces are confined to the area of the contact, is more suitable for large radius compliant solids. The other model by Derjaguin, Muller and Toporov, known as DMT model [38] is based on calculating the attractive forces outside of the actual contact area, and is suitable for small high modulus spheres. The improved DMT adhesion model [39] shown in Fig. 2(b) is employed to study the adhesion induced pre-strain.

According to the Lennard-Jones interaction potential [40], the attractive pressure outside the contact region $P(Z)$ is equal to:

$$P(Z) = \frac{8}{3}\frac{\Delta\gamma}{\delta}[(\frac{\delta}{Z})^3 - (\frac{\delta}{Z})^9] \tag{5}$$

where δ is the intermolecular distance about 0.3-0.5nm, Z is the local separation and $\Delta\gamma$ is the energy of adhesion given by

$$\Delta\gamma = \gamma_1 + \gamma_2 - \gamma_{12} \tag{6}$$

γ_1 and γ_2 are two unattached surface energies before contact and γ_{12} is the interface energy during contact. The values of surface energy for various metals can be found in

literature [40], but it is difficult to get the exact interface energy for polymer and diamond or silicon.

The adhesion force can be expressed as:

$$F_a \approx 2\pi R\Delta\gamma \tag{7}$$

Therefore the adhesion induced stress and pre-strain is calculated by:

$$\sigma_a = \frac{F_a}{\pi R^2} = \frac{2\Delta\gamma}{R} \tag{8}$$

$$\varepsilon_a = (\frac{\sigma \cdot \pi}{E})^{2/3} = (\frac{2\pi\Delta\gamma}{E \cdot R})^{2/3} \tag{9}$$

From the above equations it can be seen that the adhesion induced stress and strain depend on the particle size. Due to lack of values for the energy of adhesion for the present materials, the solution of the energy of adhesion is taking the empirical energy of adhesion 25mJ/m2 [41] as reference and arbitrary duple and quadruple values are also considered. The pre-strain is estimated using the following values for energy of adhesion: 25, 50 and 100mN/m. For the smallest particle, 2.6μm in diameter, the adhesion induced pre-strain will be 1.98×10^{-3}, 3.14×10^{-3} and 5.00×10^{-3}, respectively.

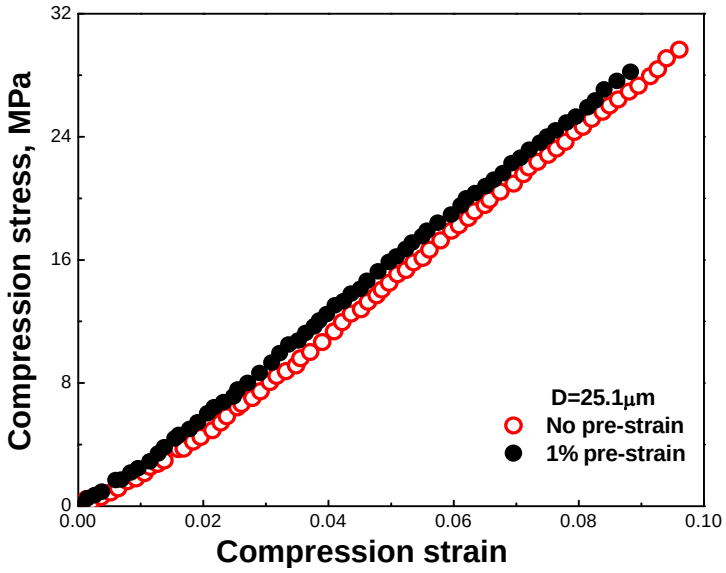

Fig. 7. The effect of estimated accumulative pre-stain 1% on the 25.1μm diameter particles.

Therefore, the maximum accumulative pre-stain from pre-load and adhesion is about 1% for the smallest particles. For the other four groups of particles, the accumulative pre-strain should be much smaller than that of the smallest particle. To examine the pre-strain effect, 1% accumulated pre-stain is addressed on the 25.1μm particle. By neglecting the

pre-strain of the largest particles and taking their stress-strain curves as a reference curve, the effect of pre-strain can be illustrated by translating the reference curve by the amount of pre-strain in Fig. 7. The curve marked “no pre-strain” in the reference curve is from experiment and the curve with 1% pre-strain is obtained by directly translating the “no pre-strain” curve to a new origin which is the corresponding point at 1% strain in the reference curve. It can be observed from Fig. 7 that the compressive stress-strain curve with 1% pre-strain rises only slightly compared with the stress-strain behaviour without pre-strain. It can be concluded that the effect of pre-load and adhesion on the size effect of PS-DVB particle is of secondary nature.

4.3 The surface effect

During particle preparation, polystyrene is crosslinked with divinylbenzene by an activated swelling method [42]. The degree of crosslinking modifies the microstructure of the polymer and influences the polymer properties strongly. Increasing the crosslink density can result in more heterogeneous and porous polymer [43]. The structure of a slightly crosslinked polymer seems much more homogeneous and resists larger deformation than the structure of a strongly crosslinked one. Typical techniques employed to measure crosslink degree are based on the measurement of equilibrium swelling by sedimentation in the analytical ultracentrifuge. The degree of swelling is used directly as a relative measure of the degree of crosslinking, but which do not provide spatially resolved information but rather bulk averages [44].

The average crosslink density of the tested PS-DVB particles is assessed through the measurement of the swelling degree in toluene. All five particles have the same swelling degree. The local crosslink density in PS-DVB particles is a result of the local distribution of divinylbenzene. If the crosslink distribution is not uniform in shell and core, the presence of the surface shell comes to existence. The surface shell mentioned here is different from the metal coating on the particle surface. There will be no sharp interface between the shell and the core. This surface effect might result from different hydrophilicities of the monomers involved, or due to different kinetics of the chemical reaction due to the correlation of the diffusion and crosslink reaction rate, and induce the gradient of crosslink distribution within a particle size-dependent thickness. So this crosslink distribution does influence the mechanical properties to a certain extent but it is difficult to make quantitative assessment.

Hereby the finite element analyses using ABAQUS [45] have been carried out to estimate the influence of the surface shell effect. The linear elastic material is assumed and axisymmetric elements are used to model particles. Axisymmetric analytic rigid surface is used to model the diamond flat punch. Only 5% deformation level is considered. The assigned Young’s modulus E and Poisson’s ratio ν for the particles are 1.5GPa and 0.33, respectively. Different sets of shell thickness and Young’s modulus are applied to get the corresponding compressive stress-strain behaviour.

The finite element solutions of the compressive stress-strain behaviours for five groups of particles at maximum 5% deformation are obtained with three sets of thickness and Young's modulus of the surface shell. The Young's modulus of particle core is kept constant 1.5GPa. The normalized compressive stresses of five groups of particles at 4% deformation are presented in Fig. 8 from both experiment and the finite element results with 0.01/s strain rate. When the surface shell has the same elastic properties as the polymer core, namely both surface shell and polymer core have identical Young's modulus, the size effect disappeared and a horizontal line is obtained as in Fig. 8. This coincides with the viewpoint of continuum mechanics. Once the surface shell is assigned different property to the polymer core, the particles display an explicit size dependence. When the thickness and Young's modulus of the surface shell are assigned to 100nm and 30GPa where this Young's modulus value is totally unrealistic for polymer, the corresponding finite element solution agrees with the experiment results quite well. But this 30GPa Young's modulus of the surface shell is obviously hypothetical. In the case of 300nm thickness and 5.5GPa Young's modulus of the surface shell, the modelling result would do an equally good fit with the experimental results. It should be noted that there are no experimental data available to support or disapprove the shell properties used. Nevertheless, the finite element simulation demonstrates that the hypothesis that a surface shell can play a significant role on the particle size effect is tenable.

Finally it should be mentioned that the liquid surface tension caused by absorption of water on the different surfaces has been neglected in this work. The assumption that particle is a perfect sphere after sample preparation has been made.

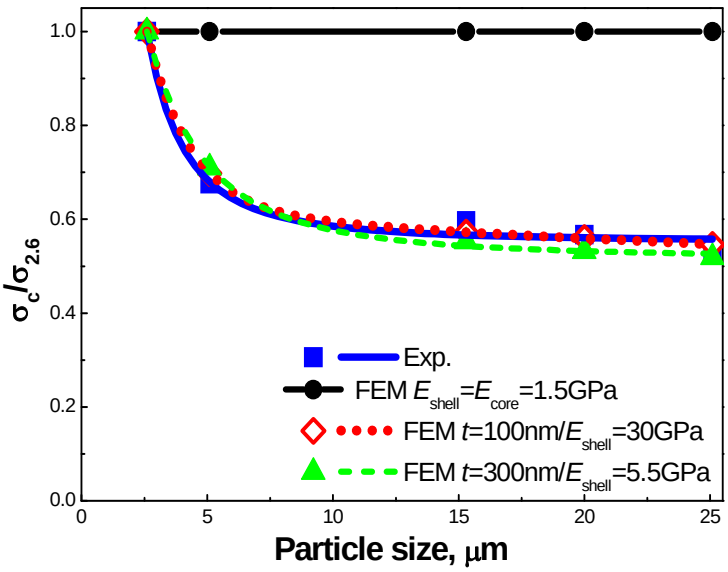

Fig. 8. Finite element solutions of the normalized compressive stress for the cases with three sets of thickness and Young's modulus of the surface shell.

5. Conclusion

By using a nanoindentation-based flat punch test method, the mechanical properties of five groups of PS-DVB particles have been studied. The particles are made of same chemical compositions but different sizes, 2.6, 5.1, 15.3, 20 and 25.1μm in diameter. The nominal compressive stress-strain curves are calculated from the indentation load-displacement results. The particle stress-strain behaviour up to 5% and 10% deformation is considered. The results demonstrate that nominal stress-strain behaviour of the PS-DVB particles have significant size dependence: the smaller the size, the harder the particles.

The potential influencing factors on the mechanisms of the particle size effect are analyzed. The accumulative pre-strain induced by the presence of pre-load and the adhesion between the soft particles and the silicon substrate or the rigid flat punch seems to be of secondary nature in the size effect. The surface shell in which there is a different cross-link distribution resulting in distinct material properties from the particle core can possibly be used to explain the size effect. Further experimental investigation is necessary to verify the mechanisms of the particle size effect.

Acknowledgement

The authors acknowledge a financial support from The Research Council of Norway via a NANOMAT KMB Project.

References

[1] Oliver W C, Pharr G M, *An improved technique for determining hardness and elastic-modulus using load and displacement sensing indentation experiments*. Journal of Materials Research, 1992; **7**: 1564-1583.

[2] Onitsch E M, *Über die Mikrohärte der Metalle*. Microskopie, 1947; **2**: 131-151.

[3] Manika I, Maniks J, *Size effects in micro- and nanoscale indentation*. Acta Materialia, 2006; **54**: 2049-2056.

[4] Nix W D, Gao H, *Indentation size effects in crystalline materials: a law for strain gradient plasticity*. Journal of the Mechanics and Physics of Solids, 1998; **46**: 411-425.

[5] Shu J Y, Fleck N A, *Prediction of a size effect in micro-indentation*. International Journal of Solids and Structures, 1998; **35**: 1363-1383.

[6] Gao H, Huang Y, Nix W D, Hutchinson J W, *Mechanism-based strain gradient plasticity - I. Theory*. Journal of the Mechanics and Physics of Solids, 1999; **47**: 1239-1263.

[7] Gerberich W W, Tymiak N I, Grunlan J C, *Interpretations of indentation size effects*. Journal of Applied Mechanics, 2002; **69**: 433-442.

[8] Li H, Ghosh A, Han Y H, *Frictional component of the indentation size effect in low load microhardness testing*. Journal of Materials Research, 1993; **8**: 1028-1032.

[9] Taylor G I, *Plastic strain in metals*. Institute of Metals – Journal, 1938; **62**: 307-324.

[10] Ugelstad J, *Swelling capacity of aqueous dispersions of oligomer and polymer substances and mixtures thereof*. Makromolekulare Chemie – Macromolecular Chemistry and Physics, 1978; **179**: 815-817.

[11] Lai Z, Liu J, *Anisotropically conductive adhesive flip-chip bonding on rigid and flexible printed circuit substrates*. IEEE transactions on components, packaging, and manufacturing technology. Part B, Advanced packaging, 1996; **19**: 644-660.

[12] Wang X, Wang Y, Chen G, Liu J, Lai Z, *Quantitative estimate of the characteristics of conductive particles in ACA by using nano indenter*. IEEE transactions on components, packaging, and manufacturing technology. Part A, 1998; **21**: 248-251.

[13] Kristiansen H, Liu J, *Overview of conductive adhesive interconnection technologies for LCDs*. IEEE Transactions on Components, Packaging, and Manufacturing Technology, 1998; **21**: 208-214.

[14] Kristiansen H, Gronlund T O, Liu J, *Characterisation of metal-coated polymer spheres and its use in anisotropic conductive adhesive*. Proceedings of 16th IEEE CPMT Conference on High Density Microsystem Design and Packaging and Component Failure Analysis, 2004; p259-263.

[15] Yim M J, Kim H J, Chung C K, Paik K W, *Degradation mechanism and reliability of flip chip interconnects using anisotropic conductive adhesives for high current density packaging applications*. Proceedings of IEEE the 56th Electronic Components & Technology Conference, San Diego, 2006, p338-343.

[16] Liu J, Tolvgård A, Malmodin J, Lai Z, *Reliable and environmentally friendly packaging technology - flip-chip joining using anisotropically conductive adhesive*. IEEE Transactions on Components and Packaging Technologies, 1999; **22**: 186-190.

[17] Galloway J, Syed A, Kang W, Kim J Y, Cannis J, Ka Y H, et al., *Mechanical, thermal, and electrical analysis of a compliant interconnect*. IEEE Transactions on Components and Packaging Technologies, 2005; **28**: 297-302.

[18] Dou G, Whalley D, Liu C, *The effect of co-planarity variation on anisotropic conductive adhesive assemblies*. Proceedings – Electronic Components and Technology Conference, 2006; p932-938.

[19] Kwon W S, Paik K W, *Experimental analysis of mechanical and electrical characteristics of metal-coated conductive spheres for anisotropic conductive*

adhesives (ACAs) interconnection. IEEE Transactions on Components and Packaging Technologies, 2006; **29**: 528-534.

[20] Miled K, Sab K, Roy R L, *Particle size effect on EPS lightweight concrete compressive strength: Experimental investigation and modelling*. Mechanics of Materials, 2007; **39**: 222-240.

[21] Cook G, Rudin A, Plumtree A, *Use of latex rubber-modified polystyrene as a model system for HIPS: Effect of particle size*. Journal of Applied Polymer Science, 1993; **48**: 75-84.

[22] Dagli G, Argon A S, Cohen R E, *Particle-size effect in craze plasticity of high-impact polystyrene*. Polymer, 1995; **36**: 2173-2180.

[23] Alfarraj A, Nauman E B, *Super HIPS: Improved high impact polystyrene with two sources of rubber particles*. Polymer, 2004; **45**: 8435-8442.

[24] Jeon H K, Zhang J, Macosko C W, *Premade vs. reactively formed compatibilizers for PMMA/PS melt blends*. Polymer, 2005; **46**: 12422-12429.

[25] Shibata M, Teramoto N, Inoue Y, *Mechanical properties, morphologies, and crystallization behavior of plasticized poly(l-lactide)/poly(butylene succinate-co-l-lactate) blends*. Polymer, 2007; **48**: 2768-2777.

[26] Mittal V, Matsko N B, Butte A, Morbidelli M, *Functionalized polystyrene latex particles as substrates for ATRP: Surface and colloidal characterization*. Polymer, 2007; **48**: 2806-2817.

[27] Perez-Carrillo L A, Puca M, Rabelero M, Meza K E, et al., *Effect of particle size on the mechanical properties of polystyrene and poly(butyl acrylate) core/shell polymers*. Polymer, 2007; **48**: 1212-1218.

[28] VanLandingham M R, Villarrubia J S, Guthrie W F, Meyers G F, *Nanoindentation of polymers: an overview*. Macromolecular Symposia, 2001; **167**: 15-43.

[29] Zhang Z L, Kristiansen H, Liu J, *A method for determining elastic properties of micron-sized polymer particles by using flat punch test*. Computational Materials Science, 2007; **39**: 305-314.

[30] Chow T S, *Stress-strain behavior of polymers in tension, compression, and shear*. Journal of Rheology, 1992; **36**: 1707-1717.

[31] Yang W, Ming W, Hu J, Lu X, Fu S, *Morphological investigation of crosslinked polystyrene microspheres by seeded polymerization*. Colloid & Polymer Science, 1998; **276**: 655-661.

[32] Johnson K L, *Contact Mechanics*. Cambridge University Press, 9th printing, 2003.

[33] http://en.wikipedia.org/wiki/Silicon.

[34] Franssila S, *Introduction to Microfabrication*. NY: John Wiley and Sons, 2004.

[35] Cooper K, Gupta A, Beaudoin S, *Simulation of the adhesion of particles to surfaces*. Journal of Colloid and Interface Science, 2001; **234**: 284-292.

[36] Liu G, Wang Q J, Liu C, *A survey of current models for simulating the contact between rough surfaces*. Tribology Transactions, 1999; **42**: 581-591.

[37] Johnson K L, Kendall K, Roberts A D, *Surface energy and the contact of elastic solids*. Proceedings Royal Society London Series A, 1971; **324**: 301-313.

[38] Derjaguin B V, Muller V M, Toprov Y P, *Effect of contact deformation on the adhesion of particles*. Journal of Colloid and Interface Science, 1975; **53**: 314-326.

[39] Chang W R, Etsion I, Bogy D B, *Adhesion model for metallic rough surfaces*. Journal of Tribology, 1988; **110**: 50-56.

[40] Muller V M, Derjaguin B V, Toporov Y P, On two methods of calculation of the force of sticking of an elastic sphere to a rigid plane. *Colloids and Surfaces,* 1983;**7**:251-259.

[41] Rabinowicz E, *Friction and Wear of Materials*. 2nd ed, NY: Wiley Interscience; 1995.

[42] Ugelstad J, Berge A, Ellingsen T, Schmid R, Nilsen T N, Mor P C, et al., *Preparation and application of new monosized polymer particles*. Progress in Polymer Science, 1992; **17**: 87-161.

[43] Knaebel A, Rebre S R, Lequeux F, *Determination of the elastic modulus of superabsorbent gel beads*. Polymer gels and networks, 1997; **5**: 107-121.

[44] Sen M, Yakar A, Guven O, *Determination of average molecular weight between cross-links (M(c)) from swelling behaviours of diprotic acid-containing hydrogels*. Polymer, 1999; **40**: 2969-2974.

[45] ABAQUS, Version 6.6, User's Manual.

Paper III

Fracture of micrometre-sized Ni/Au coated polymer particles

He J Y, Helland T, Zhang Z L, Kristiansen H.

Journal of Physics D: Applied Physics 2009; **42**(8): 085405 (5pp).

Fracture of Micrometre-sized Ni/Au Coated Polymer Particles

J. Y. He[a], T. Helland[a], Z. L. Zhang[a], H. Kristiansen[b]

[a] NTNU Nanomechanical Lab, Department of Structural Engineering, Norwegian University of Science and Technology (NTNU), 7491, Trondheim, Norway

[b] Conpart As, 2013, Skjetten, Norway

ABSTRACT

Deformation and fracture of individual micron-sized Ni/Au coated polymer particles have been studied by a nanoindentation-based flat punch method. A wide range of test conditions has been applied to deform the coated particles and uncoated particles. The compression induced cracking of the Ni/Au coating and delamination between the metal coating and the polymer core have been investigated and provide insight into the effect of nanoscale metal coating on the deformation capacity and fracture process of the particles. A three-stage deformation and fracture behaviour of the particles has been identified. The results are essential for the design of metal coated polymer particles for industrial applications.

Keywords: Ni/Au coated polymer particles; Nanoindentation; Flat punch; Deformation; Fracture.

1. Introduction

The Ugelstad method is a well-known and versatile technology for manufacturing highly monodisperse polymer particles [1]. The technology has been proven highly successful within chemical and biological industries [2]. In the past decade this technology has been exploited for the use within electronics and microsystems. By metallizing polymer particles they can be utilized as flexible electrical contacts in numerous potential applications [3]. Until now, the focus has been on the use of metal coated polymer particles for developing new electrical packaging technology, such as Anisotropic Conductive Adhesive (ACA). Usually the metal coated polymer particles used in ACA application have polymer core — double metal layer structure that consists of a polymer core for improving contact compliance, Ni inner layer for electrical conductivity and Au outer layer for protecting

inner layer from the oxidation and increasing the reliability of electrical performance. Therefore the ACA technology is of high interest because it is lead-free, reduces package size and achieves high-density interconnections. During the ACA bonding process, the electrical characteristics are strongly connected to the contact area between the chips and metal coated particles. A large contact area is required to enhance the electrical performance as well as the reliability of the interconnection. Therefore a large deformation is applied to metal coated particles to obtain a reliable and low resistance connection, which may result in the failure of metal coated particles. This can bring a significant impact on the electrical performance of the interconnect. For these reasons the detailed knowledge of mechanical properties of individual particles is essential for the design of electrical assemblies.

However, only limited research has been conducted regarding mechanical properties of the micron-sized polymer particles because of the small volume and spherical geometry involved. The aggregate mechanical properties of a large number of particles (typically several hundreds) have been previously estimated through grouping particles between two polished silicon chips [4]. For individual particles, a nanoindentation-based flat punch method has been recently developed for measuring mechanical response of both metal coated particles and uncoated polymer particles [5-9]. The contact load-displacement relationship, large deformation and size effect of individual particles have been investigated. However, the study of deformation and fracture processes on metal coated polymer particles has not been reported to date. The goal of this work is to characterize the deformation behaviour and fracture track of metal coated polymer particles.

2. Experimental setup

The metal coated polymer particles used in this work were 3.8 μm in diameter consisting of a strongly crosslinked acrylic copolymer core coated with Ni and Au layers, as shown in Fig. 1 (a). The coefficient of variance (C.V.) of the particle size distribution is 1.7%, where C.V. is defined as the ratio of the standard deviation to the mean diameter. The polymer core is amorphous and has been synthesized by using the Ugelstad method with a multi-step swelling process [1]. The Ni/Au coating was plated on the polymer particle surface with Ni inner layer of about 50 nm thickness and Au outer layer of about 25 nm. For comparison, uncoated particles with the same polymer chemistry and same size were also prepared and tested.

The mechanical test was performed using a commercially available nanoindentation device (TriboIndenter® Hysitron Inc., MN., USA). The nanoindentation-based flat punch method was employed to characterize individual particles, schematically shown in Fig. 1 (b). A diamond flat punch of 100 μm in diameter was specially designed to compress the particles instead of a common sharp tip used for nanohardness measurement [10-12]. The

planarity and the parallelism of the flat punch are significant to the test precision and have been carefully calibrated through the impression on the well polished indium surface. The standard load-control mode in which the applied force on specimens follows a predefined load function has been used. A three-step loading protocol has been set, which contains linear loading/unloading segments with 2000 μN/s loading rate.

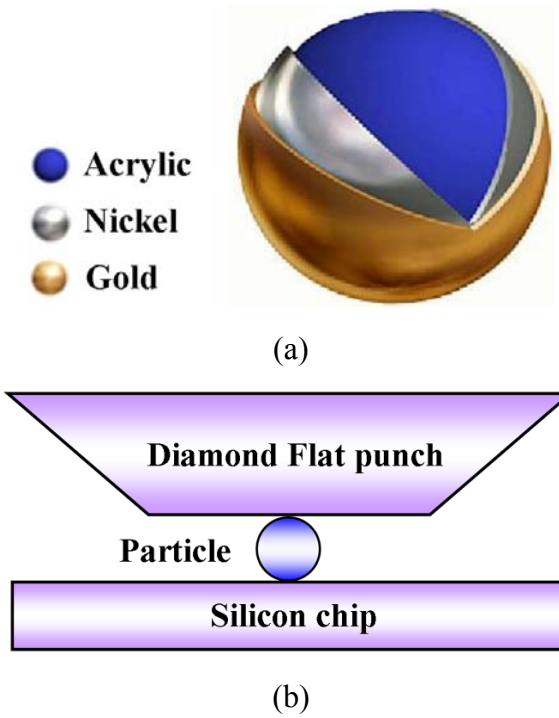

Fig. 1. Schematic plots of (a) the Ni/Au coated polymer particles with 3.8 μm in diameter and (b) the compression test with a diamond flat punch of 100 μm in diameter.

A tiny amount of particles were dispersed onto a polished silicon chip of the size 10×10×0.5 mm. Using the integrated optical microscope, individual particles with more than 75 μm distance to the closest neighbour were identified for the test. The chosen particles were only tested once, which means that each test was performed on a virgin particle. For each set of experiments, at least five individual particles were tested in order to check the repeatability of the results. After the mechanical test, the morphological observation of tested particles was performed using a scanning electron microscope (SEM) Zeiss Ultra 55 LE FESEM.

3. Results and discussion

Typical compression force-deformation curves for a Ni/Au coated polymer particle and an uncoated polymer particle are shown in Fig. 2. Here deformation is defined as the ratio of the deformed particle height to the undeformed diameter. The loading behaviour of the

coated particle can be divided into three stages comparing with the loading behaviour of the uncoated one. In stage I, the stiffness of the coated particle is prominently higher than the uncoated one and increase monotonously until about 18% deformation. In stage II, the deformation increases from 18% to around 43%. A displacement burst at about 18% deformation indicates that a very significant event is taking place in the Ni/Au coating, probably including both cracking and delamination from the polymer core. Within the 20 ms timeframe of the displacement burst, given by the measurement sampling frequency, the deformation rapidly increases from typically 18% to 23%. However, the coated particle behaves still harder than the uncoated one, indicating that there are some mechanical integrity in the metal layer and adhesion to the polymer core left. Once the deformation exceeds around 43%, the loading curves of the coated and uncoated particles seem to overlap each other and the metal coating does not influence the particle behaviour in stage III. The results reveal that the Ni/Au coating initially plays a significant strengthening effect on the mechanical behaviour of the particle. As the deformation is up to approximately 18%, the influence of the coating gradually decreases. Until approximately 43% deformation where the effect of the Ni/Au coating disappears completely, the coated particle behaves the same as the uncoated particle.

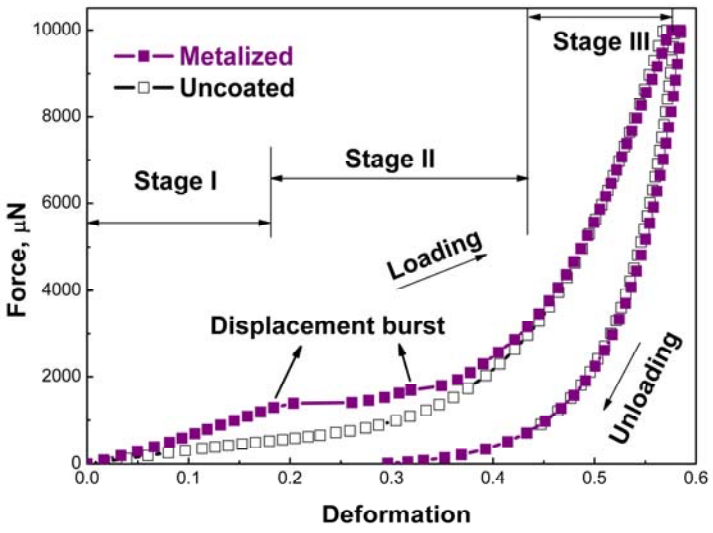

Fig. 2. Representative compression force-deformation curves of a metal coated and an uncoated polymer particle.

Fig. 3 shows the representative force-deformation behaviour of Ni/Au coated particles compressed to five applied peak loads 1000, 1500, 2000, 3000 and 10000 μN with loading/unloading rate 2000 μN/s. The loading segments of the five curves, and even the displacement burst points at approximately 18% deformation, are remarkably coincident. The characteristic SEM images of the corresponding five particles are shown in Fig. 4. All images are taken from top view, in the direction of the compression.

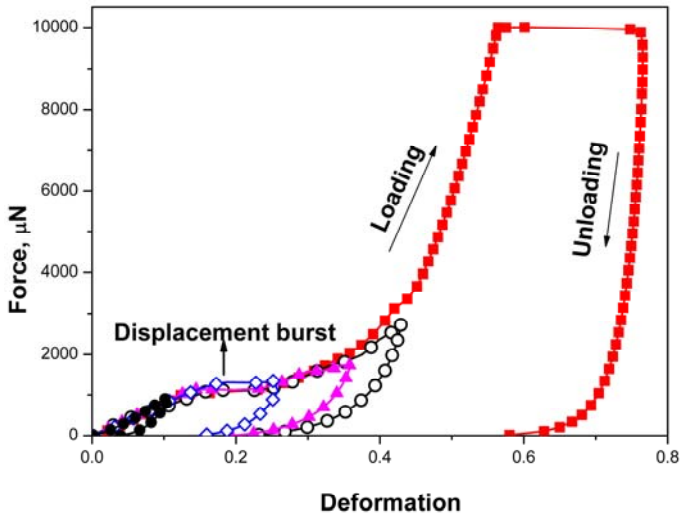

Fig. 3. Representative compression force-deformation curves of the metal coated polymer particles at five peak loads 1000, 1500, 2000, 3000 and 10000 μN.

The loading behaviour of the particle tested at 1000 μN peak load is located in the stage I. The maximum deformation of the particle is about 11% and less than the displacement burst deformation 18%. After unloading the particle recovers completely without any residual deformation. The hysteresis effect observed in the force-deformation curves is mainly caused by the viscoelastic properties of the polymer core [13,14]. The corresponding SEM image of this particle is displayed in Fig. 4 (a). The microcracks can be observed within what has been the contact area between the flat punch and the particle. Because of the complete recovery, these microcracks can be considered as the local response to the initial deformation and have a neglectable influence on the macroscopic behaviour of the particle.

Increasing the peak load to 1500, 2000 and 3000 μN, the loading behaviours of the particles go into the stage II in Fig. 2 and the force-deformation curve passes through the burst point. In these cases, the particles partly recover and have a residual deformation after unloading. The micrographs of three particles are shown in Fig. 4 (b), (c) and (d). A flattened surface area in each image is observed which indicates residual deformation and corresponds with the expected contact area under maximum deformation. All images clearly exhibit cracking of the Ni/Au coating and delamination between the metal coating and the polymer core. The cracking and delamination are obviously aggravated with increasing peak loads. The crack propagation is parallel to the longitudinal direction of the particles, and the delamination usually occurs underneath the cracks or by the warping of the Ni/Au coating. In Fig. 4 (d) two microcracks on the top-left are observed, probably starting from the “bottom” side of the particle. The results demonstrate that the displacement burst in the stage II is caused by the cracking of the Ni/Au coating, or the delamination between the Ni/Au coating and the polymer core or a combination of the two. From thereon the strengthening effect of the metal coating is reduced dramatically.

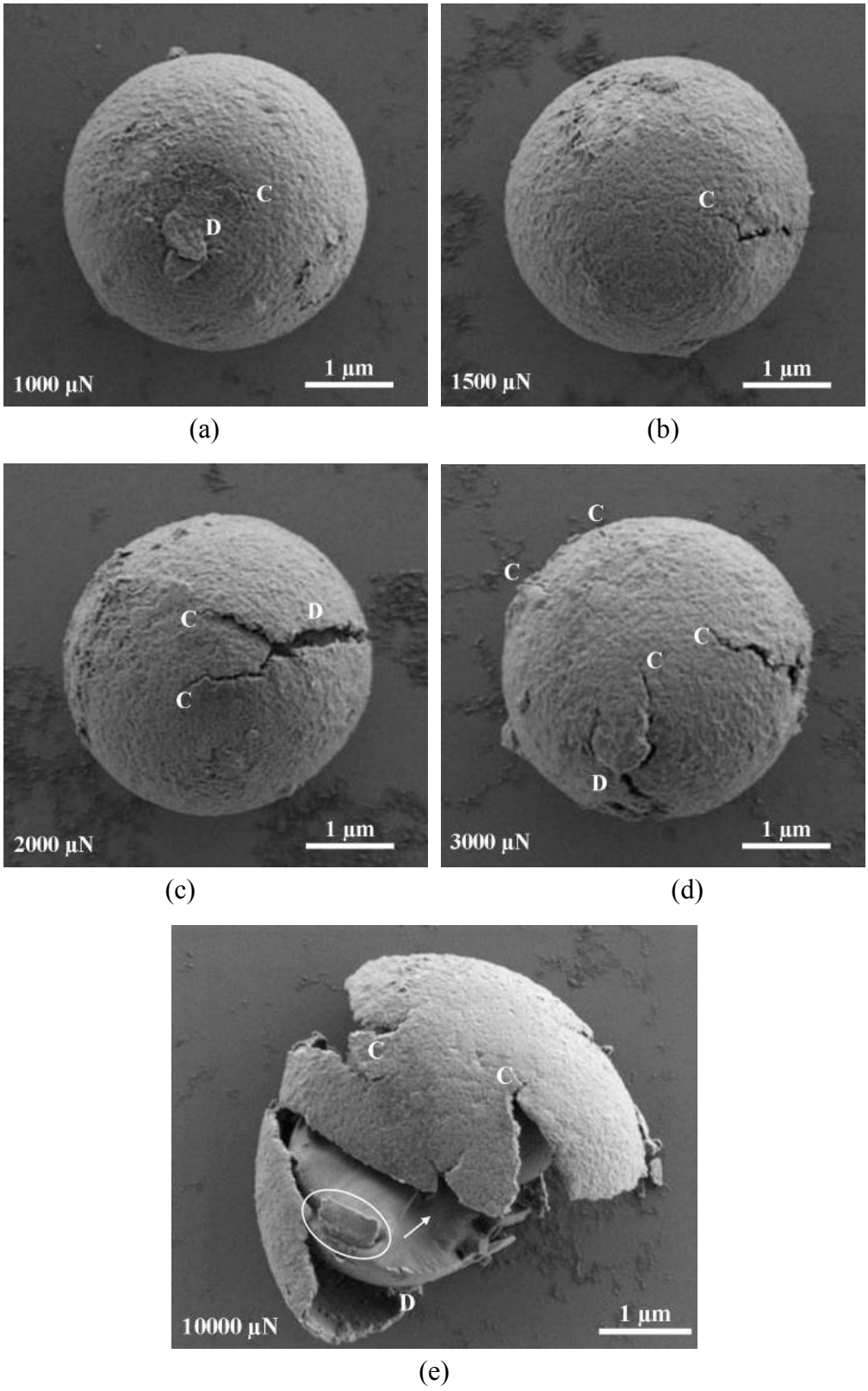

Fig. 4. Characteristic SEM images of Ni/Au coated particles at five peak loads (a) 1000 µN; (b) 1500 µN; (c) 2000 µN; (d) 3000 µN and (e) 10000 µN. C represents the crack behaviour on the Ni/Au coating and D the delamination of the metal coating. Electron high tension (EHT)=1.0 kV; working distance (WD)=4.0 mm. (Photo by Tor A. Nilsen)

The final fracture of the entire particle is observed in Fig. 3, which means the polymer core is also crushed and presented by the second displacement burst at about 58% deformation on the force-deformation curve. The crushed fragment of the particle is shown in Fig. 4 (e). The micrograph explicitly shows the polymer core fracture together with cracking and delamination of the Ni/Au coating. It is difficult to identify the fracture direction of the polymer core because the particle is possibly rotated during the final fracture. Through comparing two force-deformation curves presented by the solid square lines in Fig. 2 and Fig. 3, it is worth noting that not all coated particles show the polymer core fracture. A statistical result that about 50% coated particles showed the final fracture has been obtained by additionally compressing a number of individual particles. However, there was no fracture observed on the uncoated particles at the same 10000 μN peak load. There are three possible explanations for this observation. One is that the Ni/Au coating fragments might induce defects to the polymer core during the cracking of the coating. As shown in Fig. 4 (e), the coating fragment marked in ellipse has entered the polymer core and possibly creates an initiation site for the polymer core fracture. The second explanation is that the total load carried by the Ni/Au coating is transferred to the polymer core instantly when the cracking of the coating happens. This may induce an impact effect to the polymer core. Considering that the coated particle behaves almost identically with the uncoated particles when deformation is up to 43%, that is to say, no significant dynamic effect is observed on the coated particle in this region. Therefore this “impact” mechanism is of secondary nature. The last explanation is that the polymer core could be lightly altered during the plating process. A typical plating process involves a relative strong etching on the polymer surface to introduce nucleation sites.

4. Conclusions

This work investigates the effect of the metal coating, and its cracking and delamination on the deformation behaviour of the Ni/Au coated polymer particles. According to the effect of the metal coating, three stages could be identified in the deformation process. Initially the Ni/Au coating has a striking strengthening effect, where the deformation is mainly contributed by stretching the Ni/Au coating so the coated particle is harder than the uncoated one. Secondly, the effect of Ni/Au coating is significantly reduced when the cracking of the Ni/Au coating and the delamination between the Ni/Au coating and the polymer core occur. The critical deformation for the cracking and delamination of the metal coating is around 18%. In the third and last phase with a deformation above approximately 43%, the coated particle shows nearly identical behaviour as the uncoated one. Fracture of the polymer core does partly occur on metal coated particles while not on uncoated polymer particles. These results are integrated effects of particles geometry and material. The findings have important implications in the design of the metal coated polymer particles for the ACA application.

Acknowledgement

This work is funded by the Research Council of Norway, Conpart AS and Invitrogen AS via a NANOMAT KMB Project (Grant No. NANOMAT-169737/S10).

References

[1] Ugelstad J, Berge A, Ellingsen T, Schmid R, Nilsen T N, Mor P C, et al., *Preparation and application of new monosized polymer particles*. Progress in Polymer Science, 1992; **17**: 87-161.

[2] Toprak M S, Mckenna B J, Mikhaylova M, Waite J H, Stucky G D, *Spontaneous assembly of magnetic microspheres*. Advanced Materials, 2007; **19**: 1362-1368.

[3] Liu J, Tolvgård A, Malmodin J, Lai Z, *Reliable and environmentally friendly packaging technology - flip-chip joining using anisotropically conductive adhesive*. IEEE Transactions on Components and Packaging Technologies, 1999; **22**: 186-190.

[4] Kristiansen H, Liu J, *Overview of conductive adhesive interconnection technologies for LCDs*. IEEE Transactions on Components, Packaging, and Manufacturing Technology, 1998; **21**: 208-214.

[5] Kwon W S, Paik K W, *Experimental analysis of mechanical and electrical characteristics of metal-coated conductive spheres for anisotropic conductive adhesives (ACAs) interconnection*. IEEE Transactions on Components and Packaging Technologies, 2006; **29**: 528-534.

[6] He J Y, Zhang Z L, Kristiansen H, *Mechanical properties of nanostructured polymer particles for anisotropic conductive adhesives*. International Journal of Materials Research, 2007; **98**: 389-392.

[7] Kim D O, Jin J H, *Mechanical property investigation of single polymer particles with the variation of molecular structure of crosslinking monomer*. Journal of Applied Polymer Science, 2007; **105**: 783-789.

[8] Dou G, Whalley D C, Liu C, *Mechanical characterization of individual NiAu coated microsize polymer particles*. Applied Physics Letters, 2008; **92**: 104108 (3pp).

[9] He J Y, Zhang Z L, Midttun M, Fonnum G, Modahl G I, Kristiansen H, Redford K, *Size effect on mechanical properties of micron-sized PS-DVB polymer particles*. Polymer, 2008; **49**: 3993-3999.

[10] Zhou J, Komvopoulos K, Minor A M, *Nanoscale plastic deformation and fracture of polymers studied by in situ nanoindentation in a transmission electron microscope*. Applied Physics Letters, 2006; **88**: 181908 (3pp).

[11] Tranchida D, Piccarolo S, Loos J, Alexeev A, *Accurately evaluating Young's modulus of polymers through nanoindentations: A phenomenological correction factor to the Oliver and Pharr procedure*. Applied Physics Letters, 2006; **89**: 171905 (3pp).

[12] Yang B, Wadsworth J, Nieh T G, *Thermal activation in Au-based bulk metallic glass characterized by high-temperature nanoindentation*. Applied Physics Letters, 2007; **90**: 061911 (3pp).

[13] Chakravartula A, Komvopoulous K, *Viscoelastic properties of polymer surfaces investigated by nanoscale dynamic mechanical analysis*. Applied Physics Letters, 2006; **88**: 131901 (3pp).

[14] Zhou J, Komvopoulos K, *Interfacial viscoelasticity of thin polymer films studied by nanoscale dynamic mechanical analysis*. Applied Physics Letters, 2007; **90**: 021910 (3pp).

Paper IV

Nanomechanical characterization of single micron-sized polymer particles

He J Y, Zhang Z L, Kristiansen H.

Journal of Applied Polymer Science 2009; **113**(3): 1398-1405.

Nanomechanical Characterization of Single Micron-sized Polymer Particles

J. Y. He[a], Z. L. Zhang[a], H. Kristiansen[b]

[a] NTNU Nanomechanical Lab, Department of Structural Engineering, Norwegian University of Science and Technology(NTNU), 7491, Trondheim, Norway

[b] Conpart AS, 2013, Skjetten, Norway

ABSTRACT

The mechanical characterization of single micron sized polymer particles is very important for understanding the Anisotropic Conductive Adhesives (ACA) interconnection. In this paper, a nanoindentation-based flat punch method has been employed to investigate the mechanical properties of single polymer particles. A diamond flat tip, instead of a commonly used sharp tip for indentation, has been specially designed to deform single polymer particles. The maximum applied load is 10mN and the linear loading/unloading rate is 2mN/s. Two types of amorphous polymer particles have been examined. The polymer particles display significantly different stress-strain behaviours. The material responses at different strain levels have been analyzed and compared. A particle size effect, the smaller the diameter is, the harder the particle is, on the compression stress-strain behaviour has been observed.

Keywords: Amorphous; Crosslinking; Mechanical properties; Stress; Strain.

1. Introduction

Polymer particles have received much attention in materials science, pharmaceutical and chemical industries because of their novel characteristics, such as the strong adsorption capability, the surface reactive ability and the large specific surface area. Examples include carriers for biomolecules in the biomedical field [1], the reinforced composite in light concrete [2], and the toughening phase in the high-impact polymer materials [3-6], etc. Recently there is a renewed interest in exploiting polymer particles towards the use in the manufacturing of electronics and microsystems. One example is the use of metal-coated

polymer particles in the Anisotropic Conductive Adhesives (ACA), in which typical size of particles are from 3 to 10 microns. The metal-coated polymer particles have potential advantages in terms of reduced package size, being lead-free and by reducing manufacturing cost. The substitute of compact metal particles with metal-coated polymer particles improves the compliance of the interconnection and hence enhances the reliability of the assembly [7-12]. The electrical characteristics as well as the reliability of the interconnection are partly determined by mechanical performance of polymer particles. There is also a significant interest for lager metal-coated polymer particles with the diameter of 50 to several hundred microns for use in Ball Grid Arrays (BGA) and Chip Scale Packaging (CSP). In these applications, the added compliance is expected to improve the reliability of the interconnect. There is a also crucial advantage in terms of reduced environmental impact, by reducing the amount of heavy metals [13-15]. Therefore the knowledge of mechanical properties of single polymer and metal-coated polymer particles is of great interest for many potential applications.

Most of studies on polymer particles have been focused on synthetic methods and processes. The literature concerning mechanical properties of single particles is relatively sparse. However, mechanical characterization of single particles possesses challenges due to the inherent complexity of the spherical geometry as well as the large deformation involved.

In the past, the mechanical behaviour and electrical resistance of ACA assemblies were typically measured through grouping a number of particles (typically several hundreds) between two polished silicon chips [8,16]. Mostly, ACA assemblies were designed to determine the mechanical and electrical contact properties of the interconnect component including metal-coated polymer particles. The effect of elastic recovery on the electrical contact resistance, the degradation mechanism and the reliability of ACA interconnections were investigated [17,18]. Nanoindentation with a sharp tip has been used to study mechanical behaviours on the cross section of polymer particles within the bulk ACA interconnection at various deformation degrees. The aim was to investigate the effect of bonding pressures on the particle properties. It was found that the microhardness at the central area was higher than that at the outside because of the lower constraints at the outside [19,20]. Subsequently, nanoindentation-based flat punch method was tentatively developed to compress single polymer particles and analyzed ACA performance under different deformation levels [11,21]. A study on mechanical properties of single polymer particles by nanoindentation-based flat punch test has been performed. The effects of the swelling ratio and the backbone chain structure on mechanical properties and surface morphologies were investigated [22,23]. Recently the study on the deformation of single Ni/Au coated polymer particles was reported [24]. The results showed that the particle deformation process was nonlinear and the force/deformation at which particle crushing occurs was affected by the loading rate.

The present work reports the results of an experimental study on single polymer particles under compression. A nanoindentation-based flat punch method has been employed to test the particles with two different types of polymer compositions and different sizes in micron scale. The compression force – displacement behaviours have been established and the stress-strain relationships have been analyzed to examine the material response of polymer particles at different strain levels.

2. Experimental setup

2.1 Apparatus

The mechanical testing of single polymer particles has been performed using a nanomechanical testing system (TriboIndenter® Hysitron Inc., MN., USA) which is capable of operating in load or displacement controlled modes with load and displacement noise floor of 100nN and 1nm, respectively. During indentation, the force – displacement curves of tested materials are recorded. Nanoindentation-based flat punch method has been developed to characterize an individual particle and a schematic figure is shown in Fig. 1 (a). A square diamond flat punch with 100μm sides has been specially designed to compress polymer particles. The flat punch requires precise calibration, especially with respect to coplanarity. The flat punch was first cleaned to remove defects such as dust or external impurities. The coplanarity of the flat punch was calibrated by indents into a polished indium surface. A clear impression on the indium surface was required for the flat punch to be acceptable. Also the relative position between the integrated optical microscope and the flat punch is evaluated in the same way to calibrate the in-situ test setting. Using the optical microscope, single particles with more than 75μm distance to the closest neighbour was selected for the test. The single particle was then compressed between the diamond flat punch and the silicon substrate.

2.2 Materials

The commercially available acrylic copolymer (AC) particles (Concore™, Conpart AS, NO) and polystyrene (PS) particles (Dynospheres®, Invitrogen Dynal AS, NO) have been tested. Both particles have been synthesized by an activated swelling method developed by Ugelstad, which produce highly mono-sized particles [25]. The coefficient of variance (CV) of the particle size distribution is less than 2%, where CV is defined as the ratio of the standard deviation to the mean diameter. The AC particles are strongly crosslinked, whereas the PS particles are slightly crosslinked with divinylbenzene (DVB). The particles have an amorphous structure at room temperature. The glass transition temperatures have been estimated based on the chemical compositions of the particles. The particles and their physical properties are given in Table 1. AC1, AC2 and AC3 have identical chemical compositions but different sizes, and the same is true for particle PS1 and PS2.

Table 1 The physical properties of the tested particles.

Particle	Diameter $2R$, μm	estimated T_g,°C	Composition, wt%			
			diacrylic	acrylic	styrene	DVB
AC1	3.0	42	60	40	——	——
AC2	3.8	42	60	40	——	——
AC3	4.8	42	60	40	——	——
PS1	2.6	100	——	——	98	2
PS2	5.1	100	——	——	98	2

During the sample preparation, a very small amount of the polymer particles were immersed in 95% industrial ethanol and exposed to a high frequency ultrasonic vibration to redisperse the particle clusters and to minimize the liquid surface tension effect. A droplet of the ethanol – particle suspension was placed onto a bare silicon chip (10mm×10mm×0.5mm). The specimen was then left to dry in a clean environment for a specific period of time to remove any ethanol left in particles. It was easy to distinguish single particles from a cluster of two or more particles using the attached optical microscope in the Triboindenter.

2.3 Method

Fig. 1 shows the contact between a diamond flat punch and a single polymer particle. All tests were been performed in air and at room temperature (23°C). The room humidity was kept constant about 30% through an air ventilation system. The standard load-controlled mode has been selected for all particles in which the applied load is following a predefined load function. The load function with a peak load of 10mN and linear loading/unloading rate of 2mN/s has been used. A typical indentation has been completed in 12 seconds which consists of a linear loading/unloading segment for 5 seconds and a 2 seconds load holding segment at peak load. Before indentation started, the drift rate of the instrument was monitored for 40 seconds at a pre-load of 1μN, and an average drift rate calculated by fitting a straight line to the drift displacement versus time during the last 20 seconds was used to correct the resulting data. Typically small drift rates of the order of 0.1 nm/s was observed. For each group of particles, at least four single particles have been tested in order to check the repeatability of the results.

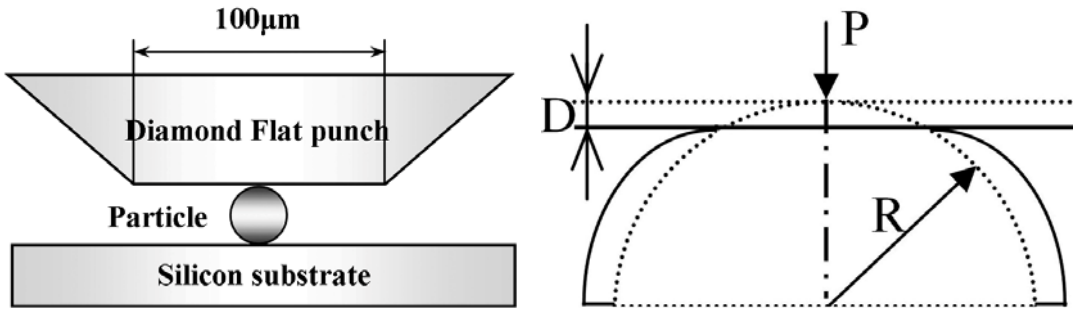

Fig. 1. Schematic plots of the flat punch test (a) and model description (b).

3. Results and discussion

3.1 Experimental results

The loading and unloading behaviours of different indentations for each group of particles are found to be very consistent. Even the fracture of the smallest AC particles occurs at the almost same load level each time. The indentation curves for single AC particles with identical chemical compositions, 60% diacrylate and 40% acrylate, AC1, AC2 and AC3 are shown in Fig. 2. The particle AC1 shows destructive failure at a displacement of 1.84±0.02μm, which is corresponding to 61.3±0.7% deformation level. At this point, the particle immediately breaks down with a close to 20% increase in deformation. No failure points are observed for AC2 and AC3 under the 10mN peak load where maximum deformation for AC2 is 56.7±0.3% and for AC3 51.5±0.9%, respectively. After unloading the displacement recoveries for AC2 and AC3 are around 47.3% and 54.7%, which is defined as the ratio of the recovered displacement to the maximum displacement and represents the particle recoverability after being deformed by compression.

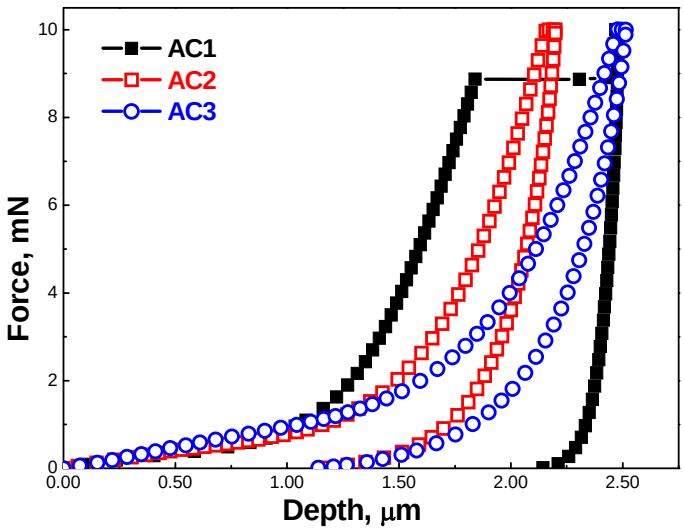

Fig. 2. Representative flat punch test load-displacement curves of particle AC1, AC2 and AC3.

Another widely used polymer material, polystyrene particles PS1 and PS2 are also tested. Two PS particles are made of same chemistry: 98% polystyrene slightly crosslinked with 2% divinylbenzene. The compression force – displacement curves for two single PS particles are plotted in Fig. 3. Unlike the AC particles, the smaller PS particles do not show the explicit fracture behaviour. However, there is hardly any displacement recovery for either PS1 or PS2 after unloading. The maximum deformation at the 10mN peak load for PS1 and PS2 are 87±0.6% and 74.8±0.5%, respectively.

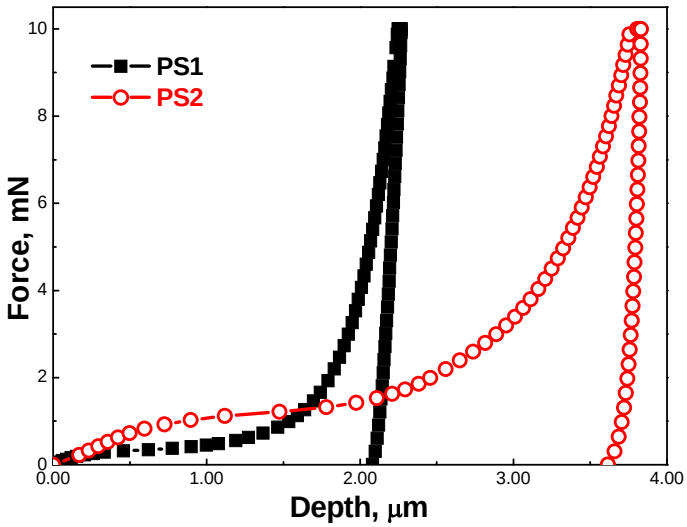

Fig. 3. Representative flat punch test load-displacement curves of particle PS1 and PS2.

3.2 Stress-strain behaviours

There are several analytical models describing the contact between a deformable sphere and a rigid flat [26]. The well-known Hertz theory can be applied for small deformation contact of linear elastic materials and states that the contact force is proportional to the power 1.5 of the displacement [27,28]. Hertz model is based on the following assumptions: the contact area between two elastic spheres is much smaller than the sphere size; the normal contact between two spheres is frictionless; and the stress distribution within the contact area is obtained by considering concentrated force applied to an elastic half space and the effect of the sphere boundary on the contact deformation is neglected. For a somewhat larger deformation scale, Tatara theory could be used to predict the non-linear elastic response of elastomeric spheres, which predicts the contact force – displacement relationship with the power of 3 [29,30]. Tatara theory can be considered as an extension of Hertz model, which is the result of removing two of the main requirements for using Hertz theory, namely the small deformations and linear elasticity. However, Hertz and Tatara theories are still valid in small strain scale. Zhang's model, which is based on finite element analysis, introduces explicit solutions for the compression stress-strain relationship of linear elastic materials for large deformation [31]. Zhang's model claims that the contact force is approximately

proportional to the power 1.52 of the displacement. However, in this study a deformation above 50% has been reached and none of the existing theories are therefore applicable.

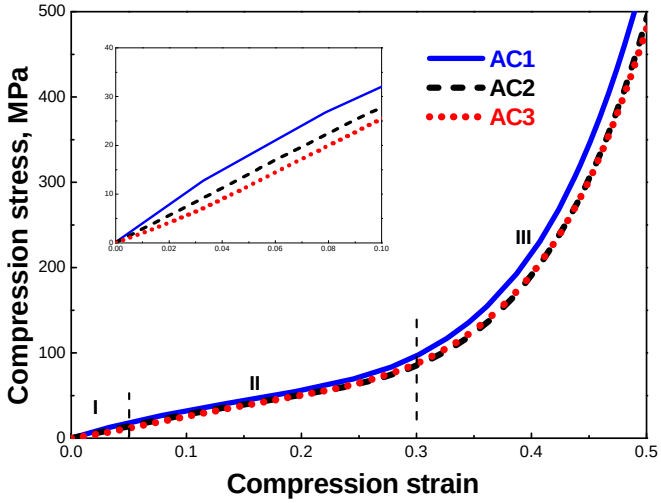

(a)

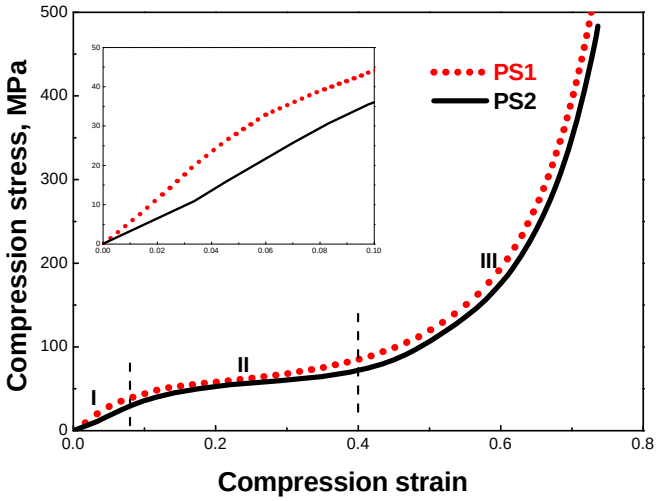

(b)

Fig. 4. Compression stress-strain behaviours of polymer particle (a) AC1, AC2 and AC3 and (b) PS1 and PS2.

During indentation, both microstructure and geometry of particles influence the compression behaviour. Therefore normalization of the experimental results should be used to remove the effect of particle dimensions. The volume and Poisson's ratio of polymer particles might change continuously with the large deformation because of the polymer nature and the sphere geometry [32,33]. It is impossible to obtain the true stress-strain behaviours of particles from the actual experiment. The nominal compression stress-strain

relationships of the particles are therefore calculated based on the diameter and the cross sectional area of the undeformed particle:

$$\sigma_N = \frac{P}{\pi R^2} \text{ and } \varepsilon_N = \frac{D}{R} \tag{1}$$

where P is the applied force, D is the half displacement and R is the initial particle radius, shown in Fig. 1 (b). The resulting stress-strain curves are plotted in Fig. 4. The focus of this study is the loading part and the unloading stress-strain curves are omitted.

A comparison of the AC particle and PS particle is shown in Fig. 5 where the smaller particles AC1 and PS1 are plotted. The stress-strain curve of the AC particle appears to rise monotonically. The PS particle displays a longer plateau than the AC particle, which means that the PS particle has better deformation resistance at lower stress level. The AC particle behaves softer than the PS particle when the strain is less than 22%. The AC particle therefore shows more brittle behaviour than the PS particle.

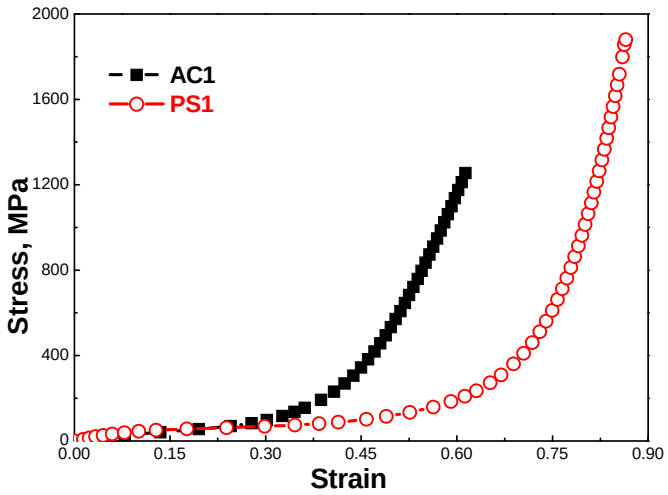

Fig. 5. Comparison of AC and PS particles.

According to Zhang's model [31], the compression stress-strain behaviour for any given Poisson's ratio can be described as:

$$\sigma_C = \left(\frac{\sigma_C}{K}\right)_{\nu=0.3} K_\nu \tag{2}$$

where $\left(\frac{\sigma_C}{K}\right)_{\nu=0.3}$ is the finite element solution with Poisson's ratio of 0.3 and K_ν is the reference compression modulus. It has been shown that for the cases with larger Poisson's ratio ($\nu > 0.3$) involved, the reference modulus is a good representation of the actual compression modulus.

The finite element solution for the case with Poisson's ratio of 0.3 has been fitted by a cubic polynomial:

$$(\frac{\sigma_C}{K})_{\nu=0.3} = 0.033\varepsilon_C + 0.99{\varepsilon_C}^2 - 1.122{\varepsilon_C}^3, \text{ for } 1\% \le \varepsilon_C \le 10\% \quad (3)$$

$$(\frac{\sigma_C}{K})_{\nu=0.3} = 0.0667\varepsilon_C + 0.5105{\varepsilon_C}^2 + 0.5724{\varepsilon_C}^3, \text{ for } 10\% < \varepsilon_C \le 20\% \quad (4)$$

When the deformation rises over 20%, there is no unique solution for particle compression and the finite element results for each group of particles have to be considered separately. The reference compression modulus K_ν with $\nu = 0.3$ for the particles is shown in Fig. 6 for a range up to 40 % strain. The compression modulus of the PS particles is more evenly distributed than the AC particles. The compression modulus of the PS particles is steadily decreasing in the strain interval from 1% to 40%. This can possibly be explained by local plastic flow as well as observed surface cracking in the material.

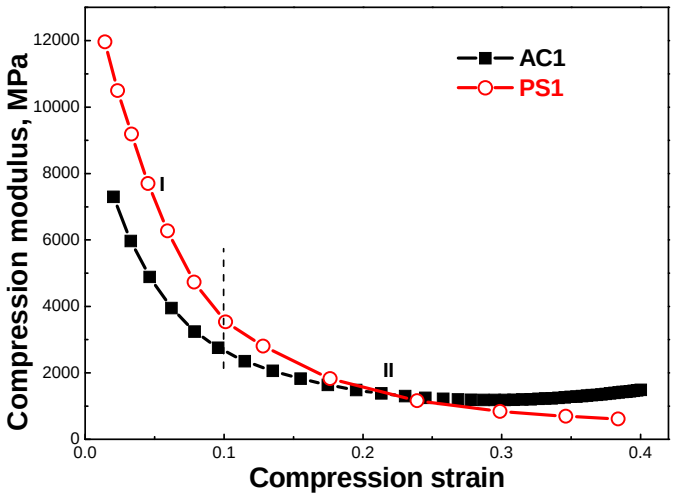

Fig. 6. Estimated reference compression modulus.

To investigate the stress-strain behaviours of amorphous polymers, the most reliable method is uniaxial compression or shear measurement, in order to avoid the craze formation that can occur in tensile tests. Depending on materials and deformation conditions such as strain rate and temperature, the amorphous polymer usually contains three types of nonuniform deformation processes which are yield behaviour, rubber-like behaviour and brittle fracture [34-36]. Yield behaviour exhibits an initially linear portion corresponding to purely elastic behaviour. With increasing stress, a non-linear elastic behaviour occurs where the strain goes back to zero after unloading, but along a curve slightly lower than the linear elastic one. A yielding and strain softening portion is observed,

representing the presence of a permanent deformation. At a large strain level, polymer begins to show strain hardening which is evident by a dramatic upturn in the stress-strain curve. For rubber-like behaviour the plastic flow occurs at the same stress level as that required for the yielding so the strain softening does not exist. The polymer is experienced a long plastic flow process due to the stretch of long chains. In the case of brittle fracture behaviour, the strain hardening happens very close to yield point or even no clear yield point exists resulting from the suppressed strain softening and plastic flow.

In the compression stress-strain curves for the three AC particles in Fig. 4 (a), it is important to note that there is no clear yielding evidence and no presence of plastic flow. The AC particles behave more or less brittle fracture. The AC particles first possess a stiff response shown as zone I in Fig. 4 (a). And at zone II, the particles exhibit a non-linear deformation in which particles reach yielding and have a continuous process of local configurational rearrangements of molecular segments [32,37]. At higher strain level around 30%, an abrupt increase of stress occurs which represents the strain hardening in zone III. Finally, the smallest particle AC1 collapses at around 61% strain whereas the larger particles AC2 and AC3 deform up to 56% and 51% strain. Unlike the AC particles, the PS particles agree with the rubber-like behaviour pattern, seen in Fig. 4 (b). In the stress-strain curves the PS particles have an initially stiff response as zone I, the definite yielding point, long plateau implying the plastic flow behaviour within zone II and the final strain hardening in zone III. The larger particle PS1 displays a plateau from 20% to 40% strain and the smaller particle PS2 exhibits even longer plateau of plastic flow from 15% to 38% strain. The PS2 deforms up to 80% without showing any critical fracture point. In Fig. 5 the stress-strain behaviours of two types of particles are plotted and the difference between them is very clear. The PS particles experience a high degree of deformation with a long plateau while the AC particles rise continuously.

In Fig. 6 the compression modulus is considered as occurring in two zones according to the proceeding analysis. In zone I the compression modulus of particles decreases very fast within 10% compression strain. When the compression strain is above 10%, as shown in zone II, the decrease of the compression modulus becomes slower and trends to be constant. At the small strain level, the strain rate is much higher than the large strain level. In this case the deformation of particles is dominated by viscosity through resisting shear flow. As the strain increases the strain rate is decreasing gradually and the effect of viscosity becomes weaker and weaker.

3.3 Size effect

The stress-strain relationship is one of the constitutive properties of materials. From the continuum mechanics point of view, for a specific material with different specimen dimensions but same chemistry, all stress-strain curves should collapse into one. But in Fig. 4 (a) and (b), a particle size effect can be clearly observed for both AC and PS particles in the embedded diagrams. For the AC particles in Fig. 4 (a), the compressive stress-strain

behaviours are particle size dependent, the smaller the diameter is, the harder the particles behave. The smallest particle AC1 is the hardest while the biggest AC3 is the softest. In Fig. 4 (b), for the PS particles, the size dependence of the stress-strain behaviours becomes even more pronounced.

The nominal compression stress of the AC and PS particles at 4% and 8% deformation levels are plotted in Fig. 7, in which the compression stress is normalized by the corresponding value of the smallest particle AC1 for AC particles and the smaller particle PS1 for PS particles. At 4% strain level, the compression stress of the particle AC3 is almost 40% lower than that of the particle AC1; and PS2 is even 50% lower than PS1. Increasing strain to 8%, the particle size-dependence becomes weaker which shows that the difference between AC1 and AC3 decreases to 26% and it is 30% between PS1 and PS2. The trend of particle size-dependent stress is consistent to the previous findings, where constant displacement rates and constant deformation levels were used [38].

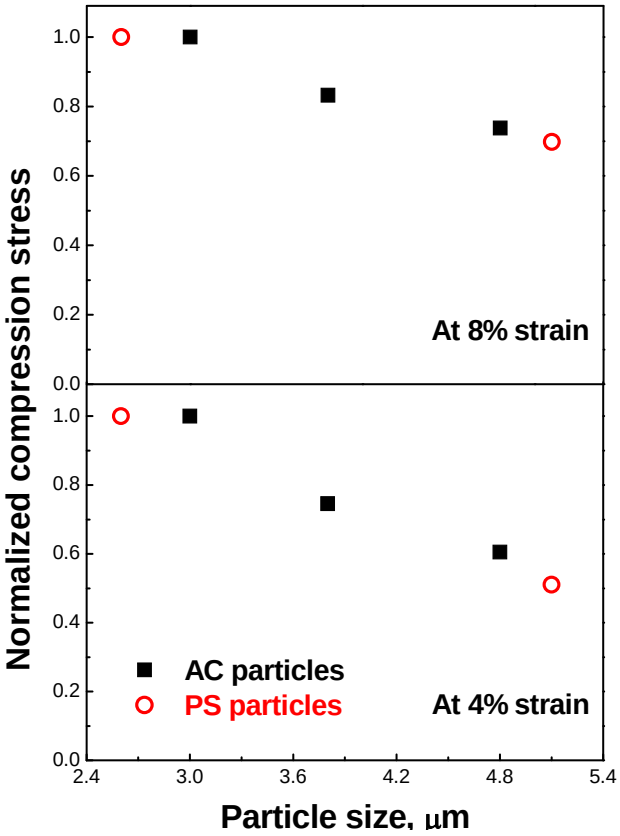

Fig. 7. Particle size dependence of the normalized stress.

In the present study the instrument is operating with a constant loading rate and peak load, which means that the strain rate is significantly reduced as the displacement increases. This can possibly be interpreted by a viscous material model where the viscous effects are

significant at low contact strain. The nonuniform strain rate can possibly cause the different viscous response resulting in the dependence of the stress-strain behaviours on the particle size. During the synthesis of the polymer particles, the crosslinking monomer diffuses through the water phase and into the polymer seeds causing it to expand [25]. After polymerization, the distribution of the crosslinking monomer inside the polymer particles is determined by diffusion conditions such as monomer concentration in solvent, temperature, monomer hydrophilicity and reaction time. A conceivable inhomogeneity of crosslink distribution can induce uneven microstructure, which might influence mechanical behaviours of the polymer particles. The particle size effect can also be induced by a pre-strain due to the liquid surface tension and the adhesion between particles and the silicon chip or the diamond flat punch. The pre-strain has a relatively significant effect on the smaller particles than the larger particles. Also the energy imposed onto the particles during indentation can cause temperature effects that can alter the mechanical properties of the polymer particles. There is a significant hysteresis in the loading – unloading curve, which suggests that mechanical energy is transformed into heat and therefore leads to a temperature rise of the particles. Within the time scale of the experiment some of this thermal energy is dissipated to the silicon chip and the diamond flat punch. The thermal effect is varied with the different particle sizes. The strong temperature dependence of mechanical properties then leads to the variation of the stress-strain behaviours.

4. Conclusion

An experimental investigation of the mechanical behaviours of micron-sized polymer particles is performed using the nanoindentation-base flat punch method. The following conclusions can be drawn from the presented results and interpretations.

The compression force – displacement behaviours of two polymer particles (acrylic and polystyrene) have been established using nanoindentation-based flat punch technique. It has been demonstrated that it is possible to distinguish the mechanical properties of different polymer particles from indentation results. The evident fracture of polymer particles can be observed directly in the force – displacement curves.

Comparing the stress-strain relationships of AC and PS particles, the AC particles show brittle fracture behaviour while the polystyrene particles comply with yield behaviour. The smaller particles of both types of polymers display more distinct viscosity than the larger particles.

A particle size effect on the stress-strain behaviours is observed on both polymer particles: the smaller the diameter is, the harder the particles are. The size-dependence of the compression stress is reduced when the strain increases. Further understanding of the particle size-dependent mechanisms is required.

The results can be used to design particle properties for ACA assemblies.

Acknowledgement

The authors acknowledge a financial support from The Research Council of Norway, Conpart AS and Invitrogen AS via a NANOMAT KMB Project (Grant No. NANOMAT-169737/S10).

Reference

[1] Ahmad H, Tauer K, *Production of micron-sized polystyrene particles containing PEG near the particle surface*. Colloid & Polymer Science, 2003; **281**: 476-484.

[2] Miled K, Sab K, Roy R L, *Particle size effect on EPS lightweight concrete compressive strength: Experimental investigation and modelling*. Mechanics of Materials, 2007; **39**: 222-240.

[3] Cook G, Rudin A, Plumtree A, *Use of latex rubber-modified polystyrene as a model system for HIPS: Effect of particle size*. Journal of Applied Polymer Science, 1993; **48**: 75-84.

[4] Dagli G, Argon A S, Cohen R E, *Particle-size effect in craze plasticity of high-impact polystyrene*. Polymer, 1995; **36**: 2173-2180.

[5] Alfarraj A, Nauman E B, *Super HIPS: Improved high impact polystyrene with two sources of rubber particles*. Polymer, 2004; **45**: 8435-8442.

[6] Kuboki T, Jar P Y B, Takahashi K, Shinmura T, *Mechanical deformation of high-impact polystyrene under uniaxial tension at various strain rates*. Macromolecules, 2002; **35**: 3584-3591.

[7] Lai Z, Liu J, *Anisotropically conductive adhesive flip-chip bonding on rigid and flexible printed circuit substrates*. IEEE transactions on components, packaging, and manufacturing technology. Part B, Advanced packaging, 1996; **19**: 644-660.

[8] Kristiansen H, Liu J, *Overview of conductive adhesive interconnection technologies for LCDs*. IEEE Transactions on Components, Packaging, and Manufacturing Technology, 1998; **21**: 208-214.

[9] Liu J, Tolvgård A, Malmodin J, Lai Z, *Reliable and environmentally friendly packaging technology - flip-chip joining using anisotropically conductive adhesive*. IEEE Transactions on Components and Packaging Technologies, 1999; **22**: 186-190.

[10] Kristiansen H, Gronlund T O, Liu J, *Characterisation of metal-coated polymer spheres and its use in anisotropic conductive adhesive*. Proceedings of 16th IEEE CPMT Conference on High Density Microsystem Design and Packaging and Component Failure Analysis, 2004; p259-263.

[11] Paik K W, Kwon W S, *Conduction mechanism of Anisotropic Conductive Adhesives (ACAs): Conductor ball deformation and build-up of contraction stresses*. Proceedings of 10th International Symposium on Advanced Packaging Materials, Processes, Properties and Interfaces, Irvine 2005, p214-220.

[12] Kim D O, Jin J H, Won II S, Seok H O, *Observation for mechanical property variations of single polymer particles*. Journal of Applied Polymer Science, 2007; **105**: 585-592.

[13] Galloway J, Syed A, Kang W, Kim J Y, Cannis J, Ka Y H, et al., *Mechanical, thermal, and electrical analysis of a compliant interconnect*. IEEE Transactions on Components and Packaging Technologies, 2005; **28**: 297-302.

[14] Dou G, Whalley D, Liu C, *The effect of co-planarity variation on anisotropic conductive adhesive assemblies*. Proceedings – Electronic Components and Technology Conference, 2006; p932-938.

[15] Kwon W S, Paik K W, *Experimental analysis of mechanical and electrical characteristics of metal-coated conductive spheres for anisotropic conductive adhesives (ACAs) interconnection*. IEEE Transactions on Components and Packaging Technologies, 2006; **29**: 528-534.

[16] Kristiansen H, Zhang Z L, Liu J, *Characterization of mechanical properties of metal-coated polymer spheres for anisotropic conductive adhesive*. Proceedings of 10th International Symposium on Advanced Packaging Materials, Processes, Properties and Interfaces, Irvine 2005, p209-213.

[17] Chin M, Iyer K A, Hu S J, *Prediction of electrical contact resistance for anisotropic conductive adhesive assemblies*. IEEE Transactions on Components and Packaging Technologies, 2004; **27**: 317-326.

[18] Yim M J, Kim H J, Chung C K, Paik K W, *Degradation mechanism and reliability of flip chip interconnects using anisotropic conductive adhesives for high current density packaging applications*. Proceedings of IEEE the 56th Electronic Components & Technology Conference, San Diego, 2006, p338-343.

[19] Wang X, Wang Y, Chen G, Liu J, Lai Z, *Quantitative estimate of the characteristics of conductive particles in ACA by using nano indenter*. IEEE transactions on components, packaging, and manufacturing technology. Part A, 1998; **21**: 248-251.

[20] Fu Y, Wang Y, Wang X, Liu J, Lai Z, Chen G, Willander M, *Experimental and theoretical characterization of electrical contact in anisotropically conductive adhesive*. IEEE Transactions on Advanced Packaging, 2000; **23**: 15-21.

[21] He J Y, Zhang Z L, Kristiansen H, *Mechanical properties of nanostructured polymer particles for anisotropic conductive adhesives*. International Journal of Materials Research, 2007; **98**: 389-392.

[22] Kim D O, Jin J H, *Mechanical property investigation of single polymer particles with the variation of molecular structure of crosslinking monomer*. Journal of Applied Polymer Science, 2007; **105**: 783-789.

[23] Kim D O, Jin J H, *Investigation for surface morphology and mechanical property variations of single polymer particles*. Journal of Applied Polymer Science, 2007; **104**: 2350-2360.

[24] Dou G, Whalley D C, Liu C, *Mechanical characterization of individual NiAu coated microsize polymer particles*. Applied Physics Letters, 2008; **92**: 104108.

[25] Ugelstad J, Berge A, Ellingsen T, Schmid R, Nilsen T N, Mor P C, et al., *Preparation and application of new monosized polymer particles*. Progress in Polymer Science, 1992; **17**: 87-161.

[26] Liu K K, *Deformation behaviour of soft particles: a review*. Journal of Physics D: Applied Physics, 2006; **39**: R189-R199.

[27] Johnson K L, *Contact Mechanics*. Cambridge University Press, 9th printing, 2003.

[28] Liu K K, Williams D R, Briscoe B J, *Large deformation of a single micro-elastomeric sphere*. Journal of Physics D: Applied Physics, 1998; **31**: 294-303.

[29] Tatara Y, *Extensive theory of force-approach relations of elastic spheres in compression and in impact*. Journal of Engineering Materials and Technology, 1989; **111**: 163-168.

[30] Tatara Y, *On compression of rubber elastic sphere over a large range of displacements – Part I Theoretical study*. Journal of Engineering Materials and Technology, 1991; **113**: 285-291.

[31] Zhang Z L, Kristiansen H, Liu J, *A method for determining elastic properties of micron-sized polymer particles by using flat punch test*. Computational Materials Science, 2007; **39**: 305-314.

[32] Chow T S, *Fractal dynamic theory of glasses and physical aging. Linear and cross-linked polymers*. Macromolecules, 1992; **25**: 440-444.

[33] Li Y, Hu Z, Li C, *New method for measuring Poisson's ratio in polymer gels*. Journal of Applied Polymer Science, 1993; **50**: 1107-1111.

[34] Chow T S, *Stress-strain behavior of polymers in tension, compression, and shear*. Journal of Rheology, 1992; **36**: 1707-1717.

[35] Monnerie L, Halary J L, Kausch H H, *Deformation, yield and fracture of amorphous polymers: relation to the secondary transitions*. Advances in Polymer Science, 2005; **187**: 215-372.

[36] Strobl G, *The Physics of Polymers*. Springer Berlin Heidelberg, 3rd Edition, 2007.

[37] Klapperich C, Komvopoulos K, Pruitt L, *Nanomechanical properties of polymers determined from nanoindentation experiments*. Journal of Tribology, 2001; **123**: 624-631.

[38] He J Y, Zhang Z L, Midttun M, Fonnum G, Modahl G I, Kristiansen H, Redford K, *Size effect on mechanical properties of micron-sized PS-DVB polymer particles*. Polymer, 2008; **49**: 3993-3999.

Paper V

Compression properties of individual micron-sized acrylic particles

He J Y, Zhang Z L, Kristiansen H.

Materials Letters 2009; **63**(20): 1696-1698.

Compression Properties of Individual Micron-sized Acrylic Particles

J. Y. He[a], Z. L. Zhang[a], H. Kristiansen[b]

[a] NTNU Nanomechanical Lab, Department of Structural Engineering, Norwegian University of Science and Technology(NTNU), 7491, Trondheim, Norway

[b] Conpart AS, 2013, Skjetten, Norway

ABSTRACT

Compression behaviours of individual micron-sized acrylic particles have been studied by using a nanoindentation-based method with a flat-end tip, instead of a commonly used sharp tip. The effect of loading rate on the mechanical properties of the high monodisperse acrylic particles, such as *K*-value, breaking force and breaking displacement, has been investigated. A wide range of loading rate conditions has been applied to examine the sensitivity of selected mechanical properties. It has been observed that the loading rate has a significant effect on *K*-value and breaking force whereas breaking displacement is independent of loading rate. These results facilitate the industrial applications of acrylic particles.

Keywords: Acrylic particle; Nanoindentation; Flat punch; Compression; Mechanical properties; Fracture.

1. Introduction

Monodisperse polymer particles in micron size have gained a lot of interest due to wide and potential applications. Recently, the focus has been on the development of new electronic packaging technologies by metallizing polymer particles, such as the application in Anisotropic Conductive Adhesives (ACAs) [1,2]. The use of metal coated polymer particles in ACAs is an effective method for making products smaller/lighter and developing the environmentally friendly processes by replacing conventional solders. However, mechanical properties of these polymer particles are important to achieve a reliable and low

resistance connection. Because of the small volume and the spherical geometry involved, mechanical characterization of polymer particles possesses great challenges, especially individual particles. Only limited studies have been conducted on the mechanical characterization of such particles so far. Nanoindentation-based flat punch technique has been recently developed to test individual particles and analyze the deformation effect on the electrical performance of ACA assemblies [3-9].

The present work reports the mechanical response of individual acrylic copolymer particles under compression. The effect of loading rate on compression modulus *K*-value, breaking force and breaking displacement of particles, have been investigated by using a nanoindentation-based flat punch method.

2. Experiment

The commercially available acrylic copolymer particles (Concore^{TM}, Conpart AS, NO) with a size of 3.0μm in diameter have been studied. The particles are synthesized using a multi-step swelling method developed by Ugelstad, which produces highly monosized particles [10]. The coefficient of variance (CV) of particle size distribution is 1.7% in which CV is defined as the ratio of the standard deviation to the mean diameter. From the SEM micrograph in Fig.1 it can be seen that the tested particles have remarkably uniform size. The particles are strongly crosslinked by 40wt% acrylic with 60wt% diacrylic, and show an amorphous structure at room temperature. The dry particles have been dispersed into ethanol and then the diluted suspension has been dropped onto a silicon chip. After this process, a number of individual particles are easily identified on the silicon chip using an optical microscope.

A nanoindentation device (Triboindenter® Hysitron Inc., MN, USA) has been employed to test individual acrylic particles. The effective accuracies are 100nN and 1nm in current lab circumstances which are obtained through the indentation in air. Instead of an ordinary spherical or pyramidal tip for nanohardness measurement, a diamond flat punch with 100μm in diameter has been specially designed to compress individual particles. The planarity of the flat punch and the parallelism of the tip surface and the sample substrate have been carefully calibrated using a polished indium sample. The conditions of four loading/unloading rates 0.02, 0.2, 2 and 10mN/s and peak load 10mN have been applied to compress particles. For each set of loading conditions, at least three individual particles have been tested in order to check the uniformity of results. A lot of experience with testing Ugelstad particles has proven that particles from the same manufacturing batch show remarkably consistent behaviour [4]. This indicates a very homogeneous material including narrow size distribution, uniform microstructure and identical chemistry as well as highly reproducible test setup.

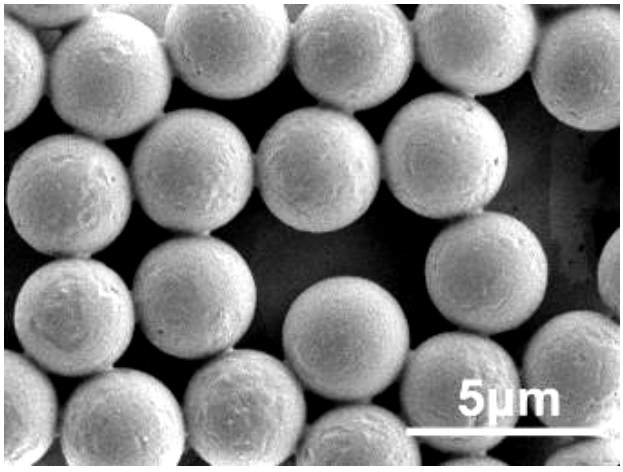

Fig. 1. The SEM photograph of acrylic particles with the size of 3.0μm in diameter.

3. Results and discussion

The representative force-displacement curves of particles at four applied loading rates are shown in Fig.2a. In the initial period of compression, the particles deform very fast and the particle stiffness increases with the deformation, where the stiffness and the deformation are defined as the ratio of the force to the contact displacement and the ratio of the displacement to the undeformed particle diameter, respectively. The rate of stiffness increase drops when the deformation reaches a relatively high level. Over 50% deformation, particles show a displacement burst, which means the fracture of particles. The characteristic SEM images of particles before and after compression are shown in Fig.2b and Fig.2c, respectively. The particle is completely fragmented under the compression with the 2mN/s loading rate and the 10mN peak load.

The *K*-value represents the compression modulus of particles and is examined at points of 10% and 20% deformation. According to Zhang's finite element analysis (FEA) based contact model [11], K-value can be calculated from:

$$\sigma_C = (\frac{\sigma_C}{K})_{\nu=0.3} K_\nu \tag{1}$$

where σ_C is the nominal compression stress and defined as $\sigma_C = \frac{P}{\pi R^2}$, and the corresponding nominal compression strain is defined as $\varepsilon_C = \frac{D}{R}$. Here P is the applied force, R is undeformed particle radius and D is compression displacement of the half sphere, respectively. The term $(\frac{\sigma_C}{K})_{\nu=0.3}$ is the FEA solution with Poisson's ratio of 0.3 and K_ν is the reference compression modulus. It has been shown that the reference modulus is a good representation of the actual compression modulus for the cases of larger Poisson's ratio

($\nu > 0.3$) involved [11]. The FEA solution for the case with Poisson's ratio of 0.3 has been fitted by two cubic polynomials for different deformation levels:

$$(\frac{\sigma_C}{K})_{\nu=0.3} = 0.033\varepsilon_C + 0.99\varepsilon_C^{\,2} - 1.122\varepsilon_C^{\,3}, \text{ for } 1\% \le \varepsilon_C \le 10\% \quad (2)$$

$$(\frac{\sigma_C}{K})_{\nu=0.3} = 0.0667\varepsilon_C + 0.5105\varepsilon_C^{\,2} + 0.5724\varepsilon_C^{\,3}, \text{ for } 10\% < \varepsilon_C \le 20\% \quad (3)$$

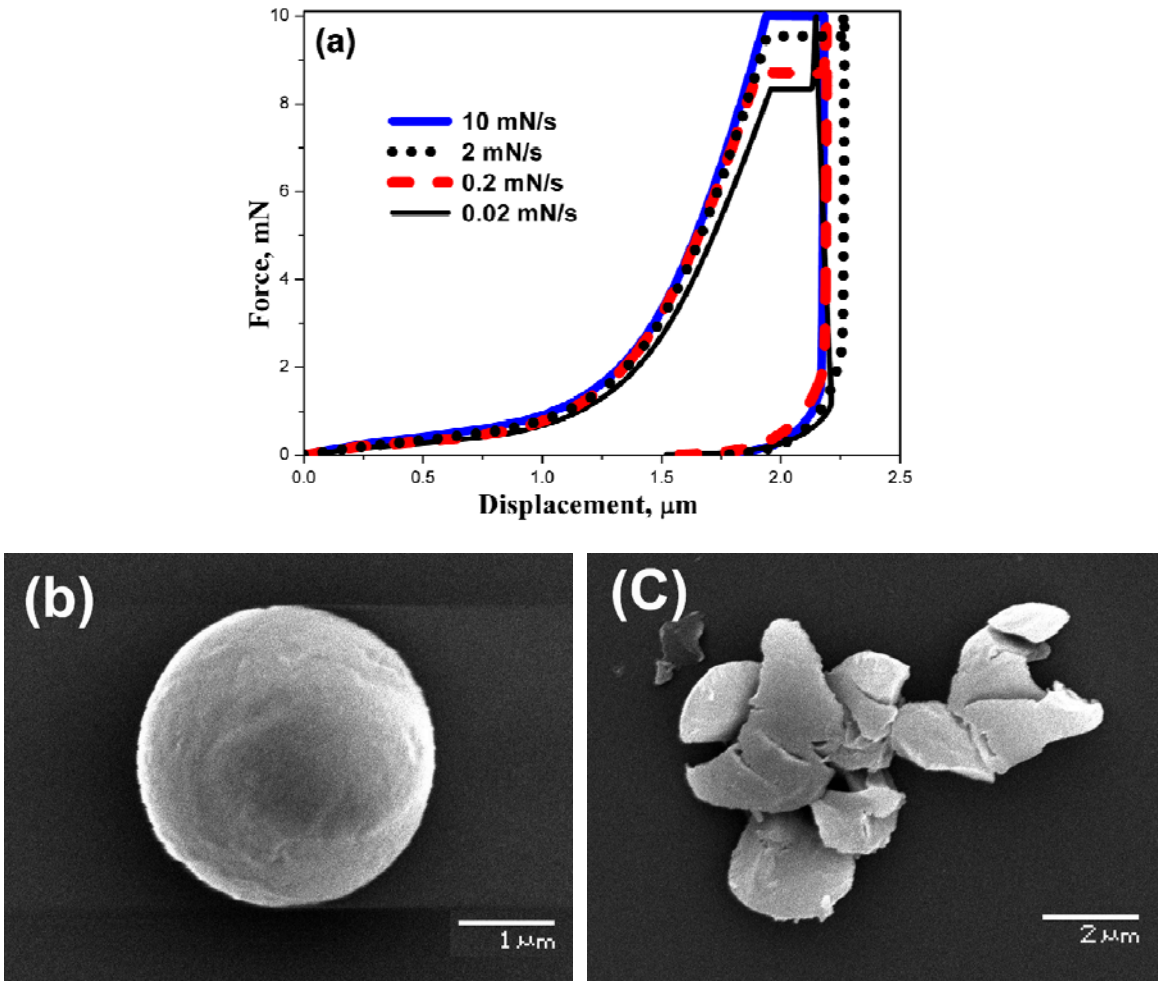

Fig. 2. Representative compression force-displacement curves of acrylic particles at different loading rate (a), and characteristic SEM images of (b) a fresh particle and (c) a compressed particle at the peak load of 10mN with the loading rate of 2mN/s.

The relationship of the K-value to the loading rate is displayed in Fig.3. K_{10} which represents the *K*-value at 10% deformation is obtained using Equation (2). Similarly K_{20} is calculated by Equation (3) at 20% deformation. Both *K*-values are increasing with increased loading rate. The value of K_{20} at the loading rate 10mN/s is 54.7% higher than

that at the loading rate 0.02mN/s. The increase of K_{10} with loading rates is more pronounced than K_{20}. The increment of K_{10} is 62.1% when the loading rate is varied from 0.02 to 10mN/s. It is worth noting that K_{10} is much larger than the corresponding K_{20} at the same loading rate. From the continuum mechanics viewpoint, Young's modulus is one of the material constitutive properties and a material constant. The possible explanation for the observation in this study is that the Young's modulus of polymer particles can be strain dependent under compression. Since the density of polymer particles is varied with deformation due to the polymer nature and the sphere geometry, the volume and Poisson's ratio are also changed [12]. This will result in a variation on Young's modulus of the polymer particles. However, deformation of the polymer particle is complex, since the high strain is located in very small areas when the compression starts from the point contact. Those behaviours are a combination of geometrical effect and material nonlinearity.

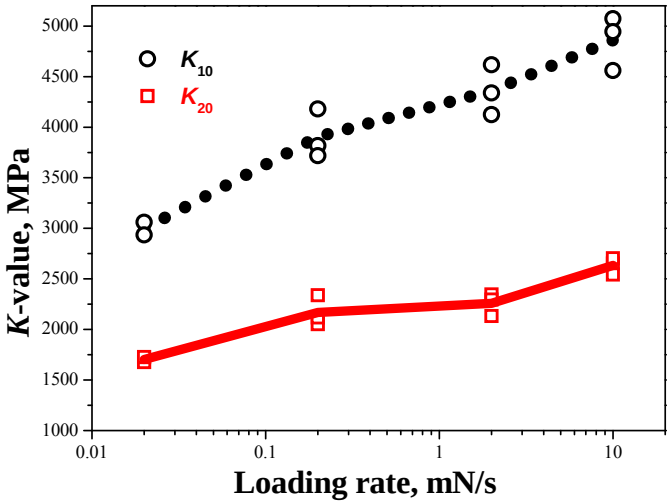

Fig. 3. Plots of particle K-value at 10% and 20% deformation points versus loading rate.

In Fig.2a the particles show the clear evidence of final fracture represented by a displacement burst in loading curves and it has been further proven by the SEM micrograph in Fig.2c. The fracture properties of polymer particles are also influenced by the loading conditions. The effect of varying loading rates on the breaking force and the breaking displacement which are the corresponding values at the rupture point is shown in Fig.4. The results show that the force at the crush point is at its highest, about 9.7mN when the loading rate is 10mN/s. Subsequently the breaking force decreases to 8.5mN at the smallest loading rate 0.02mN/s. Unlike the breaking force which increases with loading rates, the values of breaking displacement at different loading rates are scattered within a very small range. At the 10mN/s loading rate, particles deform 1.94μm before crushing, which is around 64.3% of the original particle size. When the loading rate is 2mN/s, breaking displacement drops to about 1.91μm or 63.7% deformation. The smallest breaking displacement which is about

1.88μm, around 62.7% deformation, occurs at the loading rate of 0.2mN/s. As the loading rate is down to 0.02mN/s, breaking displacement shows an almost identical value as that at 10mN/s. However, such small variations on the breaking displacement can be caused by experimental errors rather than material responses. It indicates that the polymer particles contain a very homogenous microstructure without noticeable material flaws or inclusions. It appears that breaking displacement is independent of the compression loading rate, whereas breaking force is influenced by the loading rate in accordance with the increased compression modulus.

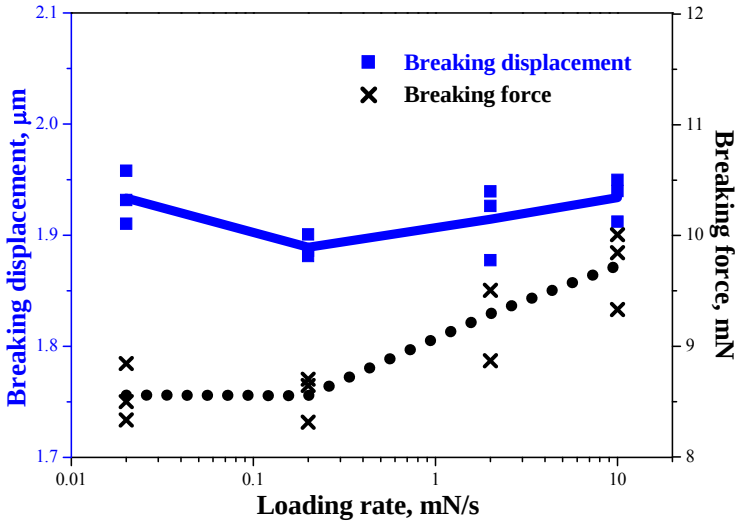

Fig. 4. Plots of particle breaking force and breaking displacement versus loading rate.

The mechanical behaviour of polymer materials is usually described with their viscoelastic characteristics, depending on the time and the temperature [13]. Therefore the acrylic particle behaviour is significantly time-dependent due to the fading memory effect of viscoelastic materials, which embodies that the force-displacement relationships of particles are strain rate dependent. Even though at same deformation levels, various loading rates of the particles induce different strain rates. Higher loading rates lead to the larger compression modulus due to the reduced time available for the stresses redistributing in terms of molecular chain rearrangement and reorientation within particles. This causes a more brittle behaviour of the particles with the higher loading rate. On the other hand, the fracture of particles is predominantly a function of energy losses to local plastic deformation [14]. The chemical units in strongly crosslinked acrylic particles reduce the probability of developing local plastic deformations in which plastic deformation may occur by induced elastic shear deformations with the formation of slippage bands or the formation of microcracks.

4. Conclusions

In summary, this study demonstrates a nanoindentation-based flat punch method for measuring mechanical properties of single acrylic particles with a narrow size distribution. The effect of loading rate on mechanical properties has been investigated and the results show that the loading rate strongly influences the particle deformation behaviour. Compression modulus *K*-value and breaking force are very sensitive to the variation in loading rate. With increasing loading rates, the *K*-value increases due to less time for the particle to recover. Breaking displacement at fracture point appears to be independent of loading rate, whereas breaking force is influenced by the loading rate. The results indicate that the particle fracture is controlled by the deformation degree and not the amount of force.

Acknowledgements

The authors gratefully appreciate the fund support from The Research Council of Norway via a NANOMAT KMB Project (Grant No. NANOMAT-169737/S10).

References

[1] Paik K W, Kwon W S, *Conduction mechanism of Anisotropic Conductive Adhesives (ACAs): Conductor ball deformation and build-up of contraction stresses*. Proceedings of 10th International Symposium on Advanced Packaging Materials, Processes, Properties and Interfaces, Irvine 2005, p214-220.

[2] Galloway J, Syed A, Kang W, Kim J Y, Cannis J, Ka Y H, et al., *Mechanical, thermal, and electrical analysis of a compliant interconnect*. IEEE Transactions on Components and Packaging Technologies, 2005; **28**: 297-302.

[3] Kwon W S, Paik K W, *Experimental analysis of mechanical and electrical characteristics of metal-coated conductive spheres for anisotropic conductive adhesives (ACAs) interconnection*. IEEE Transactions on Components and Packaging Technologies, 2006; **29**: 528-534.

[4] He J Y, Zhang Z L, Kristiansen H, *Mechanical properties of nanostructured polymer particles for anisotropic conductive adhesives*. International Journal of Materials Research, 2007; **98**: 389-392.

[5] Kim D O, Jin J H, *Investigation for surface morphology and mechanical property variations of single polymer particles*. Journal of Applied Polymer Science, 2007; **104**: 2350-2360.

[6] He J Y, Zhang Z L, Midttun M, Fonnum G, Modahl G I, Kristiansen H, Redford K, *Size effect on mechanical properties of micron-sized PS-DVB polymer particles*. Polymer, 2008; **49**: 3993-3999.

[7] Dou G, Whalley D C, Liu C, *Mechanical characterization of individual NiAu coated microsize polymer particles*. Applied Physics Letters, 2008; **92**: 104108.

[8] He J Y, Zhang Z L, Kristiansen H, *Nanomechanical characterization of Single Micron-Sized Polymer Particles*. Journal of Applied Polymer Science, 2009; **113**: 1398-1405.

[9] He J Y, Helland T, Zhang Z L, Kristiansen H, *Fracture of micrometre-sized Ni/Au coated polymer particles*. Journal of Physics D: Applied Physics, 2009; **42**: 085405.

[10] Ugelstad J, Berge A, Ellingsen T, Schmid R, Nilsen T N, Mor P C, et al., *Preparation and application of new monosized polymer particles*. Progress in Polymer Science, 1992; **17**: 87-161.

[11] Zhang Z L, Kristiansen H, Liu J, *A method for determining elastic properties of micron-sized polymer particles by using flat punch test*. Computational Materials Science, 2007; **39**: 305-314.

[12] Chow T S, *Fractal dynamic theory of glasses and physical aging. Linear and cross-linked polymers*. Macromolecules, 1992; **25**: 440-444.

[13] Choi S T, Lee S R, Earmme Y Y, *Flat indentation of a viscoelastic polymer film on a rigid substrate*. Acta Materialia, 2008; **56**: 5377-5387.

[14] Trostyanskaya E B, Babaevskii P G, Kulik S G, Stepanova M I, *Increasing the fracture viscosity of highly cross-linked composite polymer matrices*. Mechanics of Composite Materials, 1981; **16**: 509-514.

DEPARTMENT OF STRUCTURAL ENGINEERING
NORWEGIAN UNIVERSITY OF SCIENCE AND TECHNOLOGY

N–7491 TRONDHEIM, NORWAY
Telephone: +47 73 59 47 00 Telefax: +47 73 59 47 01

"Reliability Analysis of Structural Systems using Nonlinear Finite Element Methods",
C. A. Holm, 1990:23, ISBN 82-7119-178-0.

"Uniform Stratified Flow Interaction with a Submerged Horizontal Cylinder",
Ø. Arntsen, 1990:32, ISBN 82-7119-188-8.

"Large Displacement Analysis of Flexible and Rigid Systems Considering Displacement-Dependent Loads and Nonlinear Constraints",
K. M. Mathisen, 1990:33, ISBN 82-7119-189-6.

"Solid Mechanics and Material Models including Large Deformations",
E. Levold, 1990:56, ISBN 82-7119-214-0, ISSN 0802-3271.

"Inelastic Deformation Capacity of Flexurally-Loaded Aluminium Alloy Structures",
T. Welo, 1990:62, ISBN 82-7119-220-5, ISSN 0802-3271.

"Visualization of Results from Mechanical Engineering Analysis",
K. Aamnes, 1990:63, ISBN 82-7119-221-3, ISSN 0802-3271.

"Object-Oriented Product Modeling for Structural Design",
S. I. Dale, 1991:6, ISBN 82-7119-258-2, ISSN 0802-3271.

"Parallel Techniques for Solving Finite Element Problems on Transputer Networks",
T. H. Hansen, 1991:19, ISBN 82-7119-273-6, ISSN 0802-3271.

"Statistical Description and Estimation of Ocean Drift Ice Environments",
R. Korsnes, 1991:24, ISBN 82-7119-278-7, ISSN 0802-3271.

"Properties of concrete related to fatigue damage: with emphasis on high strength concrete",
G. Petkovic, 1991:35, ISBN 82-7119-290-6, ISSN 0802-3271.

"Turbidity Current Modelling",
B. Brørs, 1991:38, ISBN 82-7119-293-0, ISSN 0802-3271.

"Zero-Slump Concrete: Rheology, Degree of Compaction and Strength. Effects of Fillers as Part Cement-Replacement",
C. Sørensen, 1992:8, ISBN 82-7119-357-0, ISSN 0802-3271.

"Nonlinear Analysis of Reinforced Concrete Structures Exposed to Transient Loading",
K. V. Høiseth, 1992:15, ISBN 82-7119-364-3, ISSN 0802-3271.

"Finite Element Formulations and Solution Algorithms for Buckling and Collapse Analysis of Thin Shells",
R. O. Bjærum, 1992:30, ISBN 82-7119-380-5, ISSN 0802-3271.

"Response Statistics of Nonlinear Dynamic Systems",
J. M. Johnsen, 1992:42, ISBN 82-7119-393-7, ISSN 0802-3271.

"Digital Models in Engineering. A Study on why and how engineers build and operate digital models for decisison support",
J. Høyte, 1992:75, ISBN 82-7119-429-1, ISSN 0802-3271.

"Sparse Solution of Finite Element Equations",
A. C. Damhaug, 1992:76, ISBN 82-7119-430-5, ISSN 0802-3271.

"Some Aspects of Floating Ice Related to Sea Surface Operations in the Barents Sea",
S. Løset, 1992:95, ISBN 82-7119-452-6, ISSN 0802-3271.

"Modelling of Cyclic Plasticity with Application to Steel and Aluminium Structures",
O. S. Hopperstad, 1993:7, ISBN 82-7119-461-5, ISSN 0802-3271.

"The Free Formulation: Linear Theory and Extensions with Applications to Tetrahedral Elements with Rotational Freedoms",
G. Skeie, 1993:17, ISBN 82-7119-472-0, ISSN 0802-3271.

"Høyfast betongs motstand mot piggdekkslitasje. Analyse av resultater fra prøving i Veisliter'n",
T. Tveter, 1993:62, ISBN 82-7119-522-0, ISSN 0802-3271.

"A Nonlinear Finite Element Based on Free Formulation Theory for Analysis of Sandwich Structures",
O. Aamlid, 1993:72, ISBN 82-7119-534-4, ISSN 0802-3271.

"The Effect of Curing Temperature and Silica Fume on Chloride Migration and Pore Structure of High Strength Concrete",
C. J. Hauck, 1993:90, ISBN 82-7119-553-0, ISSN 0802-3271.

"Failure of Concrete under Compressive Strain Gradients",
G. Markeset, 1993:110, ISBN 82-7119-575-1, ISSN 0802-3271.

"An experimental study of internal tidal amphidromes in Vestfjorden",
J. H. Nilsen, 1994:39, ISBN 82-7119-640-5, ISSN 0802-3271.

"Structural analysis of oil wells with emphasis on conductor design",
H. Larsen, 1994:46, ISBN 82-7119-648-0, ISSN 0802-3271.

"Adaptive methods for non-linear finite element analysis of shell structures",
K. M. Okstad, 1994:66, ISBN 82-7119-670-7, ISSN 0802-3271.

"On constitutive modelling in nonlinear analysis of concrete structures",
O. Fyrileiv, 1994:115, ISBN 82-7119-725-8, ISSN 0802-3271.

"Fluctuating wind load and response of a line-like engineering structure with emphasis on motion-induced wind forces",
J. Bogunovic Jakobsen, 1995:62, ISBN 82-7119-809-2, ISSN 0802-3271.

"An experimental study of beam-columns subjected to combined torsion, bending and axial actions",
A. Aalberg, 1995:66, ISBN 82-7119-813-0, ISSN 0802-3271.

"Scaling and cracking in unsealed freeze/thaw testing of Portland cement and silica fume concretes",
S. Jacobsen, 1995:101, ISBN 82-7119-851-3, ISSN 0802-3271.

"Damping of water waves by submerged vegetation. A case study of laminaria hyperborea",
A. M. Dubi, 1995:108, ISBN 82-7119-859-9, ISSN 0802-3271.

"The dynamics of a slope current in the Barents Sea",
Sheng Li, 1995:109, ISBN 82-7119-860-2, ISSN 0802-3271.

"Modellering av delmaterialenes betydning for betongens konsistens",
Ernst Mørtsell, 1996:12, ISBN 82-7119-894-7, ISSN 0802-3271.

"Bending of thin-walled aluminium extrusions",

Birgit Søvik Opheim, 1996:60, ISBN 82-7119-947-1, ISSN 0802-3271.

"Material modelling of aluminium for crashworthiness analysis",
Torodd Berstad, 1996:89, ISBN 82-7119-980-3, ISSN 0802-3271.

"Estimation of structural parameters from response measurements on submerged floating tunnels",
Rolf Magne Larssen, 1996:119, ISBN 82-471-0014-2, ISSN 0802-3271.

"Numerical modelling of plain and reinforced concrete by damage mechanics",
Mario A. Polanco-Loria, 1997:20, ISBN 82-471-0049-5, ISSN 0802-3271.

"Nonlinear random vibrations - numerical analysis by path integration methods",
Vibeke Moe, 1997:26, ISBN 82-471-0056-8, ISSN 0802-3271.

"Numerical prediction of vortex-induced vibration by the finite element method",
Joar Martin Dalheim, 1997:63, ISBN 82-471-0096-7, ISSN 0802-3271.

"Time domain calculations of buffeting response for wind sensitive structures",
Ketil Aas-Jakobsen, 1997:148, ISBN 82-471-0189-0, ISSN 0802-3271.

"A numerical study of flow about fixed and flexibly mounted circular cylinders",
Trond Stokka Meling, 1998:48, ISBN 82-471-0244-7, ISSN 0802-3271.

"Estimation of chloride penetration into concrete bridges in coastal areas",
Per Egil Steen, 1998:89, ISBN 82-471-0290-0, ISSN 0802-3271.

"Stress-resultant material models for reinforced concrete plates and shells",
Jan Arve Øverli, 1998:95, ISBN 82-471-0297-8, ISSN 0802-3271.

"Chloride binding in concrete. Effect of surrounding environment and concrete composition",
Claus Kenneth Larsen, 1998:101, ISBN 82-471-0337-0, ISSN 0802-3271.

"Rotational capacity of aluminium alloy beams",
Lars A. Moen, 1999:1, ISBN 82-471-0365-6, ISSN 0802-3271.

"Stretch Bending of Aluminium Extrusions",
Arild H. Clausen, 1999:29, ISBN 82-471-0396-6, ISSN 0802-3271.

"Aluminium and Steel Beams under Concentrated Loading",
Tore Tryland, 1999:30, ISBN 82-471-0397-4, ISSN 0802-3271.

"Engineering Models of Elastoplasticity and Fracture for Aluminium Alloys",
Odd-Geir Lademo, 1999:39, ISBN 82-471-0406-7, ISSN 0802-3271.

"Kapasitet og duktilitet av dybelforbindelser i trekonstruksjoner",
Jan Siem, 1999:46, ISBN 82-471-0414-8, ISSN 0802-3271.

"Etablering av distribuert ingeniørarbeid; Teknologiske og organisatoriske erfaringer fra en norsk ingeniørbedrift",
Lars Line, 1999:52, ISBN 82-471-0420-2, ISSN 0802-3271.

"Estimation of Earthquake-Induced Response",
Símon Ólafsson, 1999:73, ISBN 82-471-0443-1, ISSN 0802-3271.

"Coastal Concrete Bridges: Moisture State, Chloride Permeability and Aging Effects"
Ragnhild Holen Relling, 1999:74, ISBN 82-471-0445-8, ISSN 0802-3271.

"Capacity Assessment of Titanium Pipes Subjected to Bending and External Pressure",
Arve Bjørset, 1999:100, ISBN 82-471-0473-3, ISSN 0802-3271.

"Validation of Numerical Collapse Behaviour of Thin-Walled Corrugated Panels",
Håvar Ilstad, 1999:101, ISBN 82-471-0474-1, ISSN 0802-3271.

"Strength and Ductility of Welded Structures in Aluminium Alloys",
Miroslaw Matusiak, 1999:113, ISBN 82-471-0487-3, ISSN 0802-3271.

"Thermal Dilation and Autogenous Deformation as Driving Forces to Self-Induced Stresses in High Performance Concrete",
Øyvind Bjøntegaard, 1999:121, ISBN 82-7984-002-8, ISSN 0802-3271.

"Some Aspects of Ski Base Sliding Friction and Ski Base Structure",
Dag Anders Moldestad, 1999:137, ISBN 82-7984-019-2, ISSN 0802-3271.

"Electrode reactions and corrosion resistance for steel in mortar and concrete",
Roy Antonsen, 2000:10, ISBN 82-7984-030-3, ISSN 0802-3271.

"Hydro-Physical Conditions in Kelp Forests and the Effect on Wave Damping and Dune Erosion. A case study on Laminaria Hyperborea",
Stig Magnar Løvås, 2000:28, ISBN 82-7984-050-8, ISSN 0802-3271.

"Random Vibration and the Path Integral Method",
Christian Skaug, 2000:39, ISBN 82-7984-061-3, ISSN 0802-3271.

"Buckling and geometrical nonlinear beam-type analyses of timber structures",
Trond Even Eggen, 2000:56, ISBN 82-7984-081-8, ISSN 0802-3271.

"Structural Crashworthiness of Aluminium Foam-Based Components",
Arve Grønsund Hanssen, 2000:76, ISBN 82-7984-102-4, ISSN 0809-103X.

"Measurements and simulations of the consolidation in first-year sea ice ridges, and some aspects of mechanical behaviour",
Knut V. Høyland, 2000:94, ISBN 82-7984-121-0, ISSN 0809-103X.

"Kinematics in Regular and Irregular Waves based on a Lagrangian Formulation",
Svein Helge Gjøsund, 2000-86, ISBN 82-7984-112-1, ISSN 0809-103X.

"Self-Induced Cracking Problems in Hardening Concrete Structures",
Daniela Bosnjak, 2000-121, ISBN 82-7984-151-2, ISSN 0809-103X.

"Ballistic Penetration and Perforation of Steel Plates",
Tore Børvik, 2000:124, ISBN 82-7984-154-7, ISSN 0809-103X.

"Freeze-Thaw resistance of Concrete. Effect of: Curing Conditions, Moisture Exchange and Materials",
Terje Finnerup Rønning, 2001:14, ISBN 82-7984-165-2, ISSN 0809-103X

"Structural behaviour of post tensioned concrete structures. Flat slab. Slabs on ground",
Steinar Trygstad, 2001:52, ISBN 82-471-5314-9, ISSN 0809-103X.

"Slipforming of Vertical Concrete Structures. Friction between concrete and slipform panel",
Kjell Tore Fosså, 2001:61, ISBN 82-471-5325-4, ISSN 0809-103X.

"Some numerical methods for the simulation of laminar and turbulent incompressible flows",
Jens Holmen, 2002:6, ISBN 82-471-5396-3, ISSN 0809-103X.

"Improved Fatigue Performance of Threaded Drillstring Connections by Cold Rolling",
Steinar Kristoffersen, 2002:11, ISBN: 82-421-5402-1, ISSN 0809-103X.

"Deformations in Concrete Cantilever Bridges: Observations and Theoretical Modelling",
Peter F. Takâcs, 2002:23, ISBN 82-471-5415-3, ISSN 0809-103X.

"Stiffened aluminium plates subjected to impact loading",
Hilde Giæver Hildrum, 2002:69, ISBN 82-471-5467-6, ISSN 0809-103X.

"Full- and model scale study of wind effects on a medium-rise building in a built up area",
Jónas Thór Snæbjørnsson, 2002:95, ISBN82-471-5495-1, ISSN 0809-103X.

"Evaluation of Concepts for Loading of Hydrocarbons in Ice-infested water",
Arnor Jensen, 2002:114, ISBN 82-417-5506-0, ISSN 0809-103X.

"Numerical and Physical Modelling of Oil Spreading in Broken Ice",
Janne K. Økland Gjøsteen, 2002:130, ISBN 82-471-5523-0, ISSN 0809-103X.

"Diagnosis and protection of corroding steel in concrete",
Franz Pruckner, 20002:140, ISBN 82-471-5555-4, ISSN 0809-103X.

"Tensile and Compressive Creep of Young Concrete: Testing and Modelling",
Dawood Atrushi, 2003:17, ISBN 82-471-5565-6, ISSN 0809-103X.

"Rheology of Particle Suspensions. Fresh Concrete, Mortar and Cement Paste with Various Types of Lignosulfonates",
Jon Elvar Wallevik, 2003:18, ISBN 82-471-5566-4, ISSN 0809-103X.

"Oblique Loading of Aluminium Crash Components",
Aase Reyes, 2003:15, ISBN 82-471-5562-1, ISSN 0809-103X.

"Utilization of Ethiopian Natural Pozzolans",
Surafel Ketema Desta, 2003:26, ISBN 82-471-5574-5, ISSN:0809-103X.

"Behaviour and strength prediction of reinforced concrete structures with discontinuity regions",
Helge Brå, 2004:11, ISBN 82-471-6222-9, ISSN 1503-8181.

"High-strength steel plates subjected to projectile impact. An experimental and numerical study",
Sumita Dey, 2004:38, ISBN 82-471-6282-2 (printed version), ISBN 82-471-6281-4 (electronic version), ISSN 1503-8181.

"Alkali-reactive and inert fillers in concrete. Rheology of fresh mixtures and expansive reactions",
Bård M. Pedersen, 2004:92, ISBN 82-471-6401-9 (printed version), ISBN 82-471-6400-0 (electronic version), ISSN 1503-8181.

"On the Shear Capacity of Steel Girders with Large Web Openings",
Nils Christian Hagen, 2005:9 ISBN 82-471-6878-2 (printed version), ISBN 82-471-6877-4 (electronic version), ISSN 1503-8181.

"Behaviour of aluminium extrusions subjected to axial loading",
Østen Jensen, 2005:7, ISBN 82-471-6873-1 (printed version), ISBN 82-471-6872-3 (electronic version), ISSN 1503-8181.

"Thermal Aspects of corrosion of Steel in Concrete",
Jan-Magnus Østvik, 2005:5, ISBN 82-471-6869-3 (printed version), ISBN 82-471-6868 (electronic version), ISSN 1503-8181.

"Mechanical and adaptive behaviour of bone in relation to hip replacement. A study of bone remodelling and bone grafting",
Sébastien Muller, 2005:34, ISBN 82-471-6933-9 (printed version), ISBN 82-471-6932-0 (electronic version), ISSN 1503-8181.

"Analysis of geometrical nonlinearities with applications to timber structures",
Lars Wollebæk, 2005:74, ISBN 82-471-7050-5 (printed version), ISBN 82-471-7019-1 (electronic version), ISSN 1503-8181.

"Pedestrian induced lateral vibrations of slender footbridges",
Anders Rönnquist, 2005:102, ISBN 82-471-7082-5 (printed version), ISBN 82-471-7081-7 (electronic version), ISSN 1503-8181.

"Initial Strength Development of Fly Ash and Limestone Blended Cements at Various Temperatures Predicted by Ultrasonic Pulse Velocity",

Tom Ivar Fredvik, 2005:112, ISBN 82-471-7105-8 (printed version), ISBN 82-471-7103-1 (electronic version), ISSN 1503-8181.

"Behaviour and modelling of thin-walled cast components",
Cato Dørum, 2005:128, ISBN 82-471-7140-6 (printed version), ISBN 82-471-7139-2 (electronic version), ISSN 1503-8181.

"Behaviour and modelling of selfpiercing riveted connections",
Raffaele Porcaro, 2005:165, ISBN 82-471-7219-4 (printed version), ISBN 82-471-7218-6 (electronic version), ISSN 1503-8181.

"Behaviour and Modelling og Aluminium Plates subjected to Compressive Load",
Lars Rønning, 2005:154, ISBN 82-471-7169-1 (printed version), ISBN 82-471-7195-3 (electronic version), ISSN 1503-8181.

"Bumper beam-longitudinal system subjected to offset impact loading",
Satyanarayana Kokkula, 2005:193, ISBN 82-471-7280-1 (printed version), ISBN 82-471-7279-8 (electronic version), ISSN 1503-8181.

"Control of Chloride Penetration into Concrete Structures at Early Age",
Guofei Liu, 2006:46, ISBN 82-471-7838-9 (printed version), ISBN 82-471-7837-0 (electronic version), ISSN 1503-8181.

"Modelling of Welded Thin-Walled Aluminium Structures",
Ting Wang, 2006:78, ISBN 82-471-7907-5 (printed version), ISBN 82-471-7906-7 (electronic version), ISSN 1503-8181.

"Time-variant reliability of dynamic systems by importance sampling and probabilistic analysis of ice loads",
Anna Ivanova Olsen, 2006:139, ISBN 82-471-8041-3 (printed version), ISBN 82-471-8040-5 (electronic version), ISSN 1503-8181.

"Fatigue life prediction of an aluminium alloy automotive component using finite element analysis of surface topography".
Sigmund Kyrre Ås, 2006:25, ISBN 82-471-7791-9 (printed version), ISBN 82-471-7791-9 (electronic version), ISSN 1503-8181.

"Constitutive models of elastoplasticity and fracture for aluminium alloys under strain path change",
Dasharatha Achani, 2006:76, ISBN 82-471-7903-2 (printed version), ISBN 82-471-7902-4 (electronic version), ISSN 1503-8181.

"Simulations of 2D dynamic brittle fracture by the Element-free Galerkin method and linear fracture mechanics",
Tommy Karlsson, 2006:125, ISBN 82-471-8011-1 (printed version), ISBN 82-471-8010-3 (electronic version), ISSN 1503-8181.

"Penetration and Perforation of Granite Targets by Hard Projectiles",
Chong Chiang Seah, 2006:188, ISBN 82-471-8150-9 (printed version), ISBN 82-471-8149-5 (electronic version), ISSN 1503-8181.

"Deformations, strain capacity and cracking of concrete in plastic and early hardening phases",
Tor Arne Hammer, 2007:234, ISBN 978-82-471-5191-4 (printed version), ISBN 978-82-471-5207-2 (electronic version), ISSN 1503-8181.

"Crashworthiness of dual-phase high-strength steel: Material and Component behaviour",
Venkatapathi Tarigopula, 2007:230, ISBN 82-471-5076-4 (printed version), ISBN 82-471-5093-1 (electronic version), ISSN 1503-8181.

"Fibre reinforcement in load carrying concrete structures",

Åse Lyslo Døssland, 2008:50, ISBN 978-82-471-6910-0 (printed version), ISBN 978-82-471-6924-7 (electronic version), ISSN 1503-8181.

"Low-velocity penetration of aluminium plates",
Frode Grytten, 2008:46, ISBN 978-82-471-6826-4 (printed version), ISBN 978-82-471-6843-1 (electronic version), ISSN 1503-8181.

"Robustness studies of structures subjected to large deformations",
Ørjan Fyllingen, 2008:24, ISBN 978-82-471-6339-9 (printed version), ISBN 978-82-471-6342-9 (electronic version), ISSN 1503-8181.

"Constitutive modelling of morsellised bone",
Knut Birger Lunde, 2008:92, ISBN 978-82-471-7829-4 (printed version), ISBN 978-82-471-7832-4 (electronic version), ISSN 1503-8181.

"Experimental Investigations of Wind Loading on a Suspension Bridge Girder",
Bjørn Isaksen, 2008:131, ISBN 978-82-471-8656-5 (printed version), ISBN 978-82-471-8673-2 (electronic version), ISSN 1503-8181.

"Cracking Risk of Concrete Structures in The Hardening Phase",
Guomin Ji, 2008:198, ISBN 978-82-471-1079-9 (printed version), ISBN 978-82-471-1080-5 (electronic version), ISSN 1503-8181.

"Modelling and numerical analysis of the porcine and human mitral apparatus",
Victorien Emile Prot, 2008:249, ISBN 978-82-471-1192-5 (printed version), ISBN 978-82-471-1193-2 (electronic version), ISSN 1503-8181.

"Strength analysis of net structures",
Heidi Moe, 2009:48, ISBN 978-82-471-1468-1 (printed version), ISBN 978-82-471-1469-8 (electronic version), ISSN1503-8181.

"Numerical analysis of ductile fracture in surface cracked shells",
Espen Berg, 2009:80, ISBN 978-82-471-1537-4 (printed version), ISBN 978-82-471-1538-1 (electronic version), ISSN 1503-8181.

"Subject specific finite element analysis of bone – for evaluation of the healing of a leg lengthening and evaluation of femoral stem design",
Sune Hansborg Pettersen, 2009:99, ISBN 978-82-471-1579-4 (printed version), ISBN 978-82-471-1580-0 (electronic version), ISSN 1503-8181.

"Evaluation of fracture parameters for notched multi-layered structures",
Lingyun Shang, 2009:137, ISBN 978-82-471-1662-3 (printed version), ISBN 978-82-471-1663-0 (electronic version), ISSN 1503-8181.

"Modelling of Dynamic Material Behaviour and Fracture of Aluminium Alloys for Structural Applications",
Yan Chen, 2009:69, ISBN 978-82-471-1515-2 (printed version), ISBN 978-82 471-1516-9 (electronic version), ISSN 1503-8181.